การสังเคราะห์ LLDPE/ZnO พอลิเมอร์นาโนคอมโพสิทด้วยวิธีพอลิเมอร์ไรเซชันแบบอินซิทู โดยใช้ตัวเร่งปฏิกิริยาเมทัลโลซีน

นายอภิวัตร โง้วธนะวัฒน์

วิทยานิพนธ์ฉบับนี้เป็นส่วนหนึ่งของการศึกษาตามหลักสูตรปริญญาวิศวกรรมศาสตรมหาบัณฑิต
สาขาวิศวกรรมเคมี ภาควิชาวิศวกรรมเคมี
คณะวิศวกรรมศาสตร์ จุฬาลงกรณ์มหาวิทยาลัย
ปีการศึกษา 2552

SYNTHESIS OF LLDPE/ZnO POLYMER NANOCOMPOSITES BY *IN SITU* POLYMERIZATION USING METALLOCENE CATALYST

Mr. Apiwat Ngowthanawat

A Thesis Submitted in Partial Fulfillment of the Requirements
for the Degree of Master of Engineering Program in Chemical Engineering
Department of Chemical Engineering
Faculty of Engineering
Chulalongkorn University
Academic Year 2009

Thesis Title	SYNTHESIS OF LLDPE/ZnO POLYMER NANOCOMPOSITES BY *IN SITU* POLYMERIZATION USING METALLOCENE CATALYST
By	Mr. Apiwat Ngowthanawat
Field of Study	Chemical Engineering
Thesis Advisor	Associate Professor Bunjerd Jongsomjit, Ph.D.

Accepted by the Faculty of Engineering, Chulalongkorn University in Partial Fulfillment of the Requirements for the Master's Degree

.... Dean of the Faculty of Engineering
(Associate Professor Boonsom Lerdhirunwong, Dr.Ing.)

Thesis Committee

Montree Wongsri .... Chairman
(Assistant Professor Montree Wongsri, D.Sc.)

.... Thesis Advisor
(Associate Professor Bunjerd Jongsomjit, Ph.D.)

.... Examiner
(Associate Professor ML. Supakanok Thongyai, Ph.D.)

Sirirat Wacharawichanant .... External Examiner
(Assistant Professor Sirirat Wacharawichanant, D.Eng)

อภิวัตร โจ้วธนะวัฒน์: การสังเคราะห์ LLDPE/ZnO พอลิเมอร์นาโนคอมโพสิทด้วยวิธีพอลิเมอร์ไรเซชันแบบอินซิทูโดยใช้ตัวเร่งปฏิกิริยาเมทัลโลซีน (SYNTHESIS OF LLDPE/ZnO POLYMER NANOCOMPOSITES BY *IN SITU* POLYMERIZATION USING METALLOCENE CATALYST) อ. ที่ปรึกษาวิทยานิพนธ์หลัก: รศ.ดร. บรรเจิด จงสมจิตร, 124 หน้า

พอลิเอทิลีนความหนาแน่นต่ำเชิงเส้นเป็นพลาสติกที่มีความสำคัญเป็นอย่างมากในปัจจุบัน โดยนิยมนำมาผลิตเป็นบรรจุภัณฑ์ประเภทถุงและฟิล์มที่ใช้ในทางเกษตรกรรม ซึ่งตัวเร่งปฏิกิริยาที่ถูกใช้ในการผลิตพอลิเมอร์ชนิดนี้ คือ ตัวเร่งปฏิกิริยาเมทัลโลซีน เนื่องจากมีค่าความว่องไวในการเกิดปฏิกิริยาสูง และพอลิเมอร์ที่ผลิตได้จากตัวเร่งปฏิกิริยาชนิดนี้จะมีค่าการกระจายตัวของน้ำหนักโมเลกุลสม่ำเสมอ แต่อย่างไรก็ตาม การที่จะนำตัวเร่งปฏิกิริยาเมทัลโลซีนมาใช้ในทางอุตสาหกรรมนั้น จะต้องสามารถใช้ได้กับกระบวนการผลิตที่มีอยู่เดิม คือ กระบวนการวัฏภาคแก๊ส และกระบวนการแบบสเลอรี ดังนั้น จึงมีความจำเป็นที่จะต้องนำตัวเร่งปฏิกิริยาเมทัลโลซีนมายึดเกาะลงบนตัวรองรับ ซึ่งมีข้อเสียคือจะทำให้ค่าความว่องไวในการเกิดปฏิกิริยาลดลง แต่วิธีดังกล่าวก็มีข้อดีหลายประการ คือ สามารถควบคุมสัณฐานของพอลิเมอร์ได้ ป้องกันการเกิดตะกรันในเครื่องปฏิกรณ์ และลดปริมาณการใช้ตัวเร่งปฏิกิริยาร่วมที่มีราคาแพง ดังนั้น จึงมีความจำเป็นที่จะต้องศึกษาวิธีการยึดเกาะตัวเร่งปฏิกิริยาเมทัลโลซีนลงบนตัวรองรับ โดยไม่ทำให้ค่าความว่องไวในการเกิดปฏิกิริยาลดลง ซึ่งในการพัฒนาตัวเร่งปฏิกิริยาเมทัลโลซีนนั้นสามารถทำได้ 3 ทาง คือ การพัฒนาที่โครงสร้างของตัวเร่งปฏิกิริยา ตัวรองรับ และสภาวะในการทำปฏิกิริยา ซึ่งในงานวิจัยนี้จะมุ่งเน้นไปที่การพัฒนาตัวรองรับ โดยตัวรองรับที่เลือกนำมาใช้ คือ ซิงค์ออกไซด์ เนื่องจากในทางพอลิเมอร์นาโนคอมโพสิท ซิงค์ออกไซด์จะช่วยทำให้พอลิเมอร์มีความทนทานต่อแสงแดดได้ดีขึ้น โดยในงานวิจัยนี้จะแบ่งการศึกษาออกเป็น 2 ส่วน ในส่วนแรกจะทำการศึกษาผลของวิธียึดเกาะตัวเร่งปฏิกิริยาเมทัลโลซีนบนตัวรองรับ ซึ่งพบว่าวิธีที่แตกต่างกันจะทำให้ได้ค่าความว่องไวในการเกิดปฏิกิริยาที่ต่างกัน ในส่วนที่สองจะทำการศึกษาผลของปริมาณโคมอนอเมอร์ที่ใช้ในการทำปฏิกิริยา ซึ่งพบว่าปริมาณโคมอนอเมอร์ส่งผลเป็นอย่างมากต่อค่าความว่องไวในการเกิดปฏิกิริยาและสัณฐานของพอลิเมอร์ นอกจากนี้ในงานวิจัยนี้ได้นำพอลิเมอร์ที่ได้มาวิเคราะห์คุณสมบัติอื่นๆ เพิ่มเติมด้วย

ภาควิชา............วิศวกรรมเคมี............ ลายมือชื่อนิสิต........อภิวัตร โจ้วธนะวัฒน์..................
สาขาวิชา...........วิศวกรรมเคมี.......... ลายมือชื่อ อ.ที่ปรึกษาวิทยานิพนธ์หลัก..........
ปีการศึกษา..........2552.....................

##5170645821: MAJOR CHEMICAL ENGINEERING

KEYWORDS: SUPPORTED METALLOCENE CATALYST / COPOLYMERIZATION OF ETHYLENE / POLYMER NANOCOMPOSITE / ZINC OXIDE

APIWAT NGOWTHANAWAT: SYNTHESIS OF LLDPE/ZnO POLYMER NANOCOMPOSITES BY *IN SITU* POLYMERIZATION USING METALLOCENE CATALYST. THESIS ADVISOR: ASSOC. PROF. BUNJERD JONGSOMJIT, Ph.D., 124 pp.

Linear low-density polyethylene (LLDPE) is very important plastic with many applications including package, agricultural film and cable cover. Nowadays, extensive studies have been focused on the use of metallocene as catalyst in the production of LLDPE because of its higher catalytic activity and more uniform molecular weight distribution (MWD) of polymer produced. To use metallocene catalysts used in industrial slurry and gas-phase processes, they have to be heterogenized on supports, which causes the catalytic activity lower than homogeneous metallocenes. As a result, it is important to find a way to attach the metallocene to the support without losing the performance of the homogeneous system. This effort can be achieved by the development of metallocene structure, support and polymerization conditions. In this study, zinc oxide (ZnO) nanoparticles, which are also used as photo-stabilizers in polymer nanocomposites, have been selected as the fillers. LLDPE/ZnO nanocomposites were synthesized via *in situ* polymerization of ethylene/1-octene with zirconocene/MAO catalyst and the effect of comonomer content on the catalytic activity was investigated and further discussed in more details. It was found that different impregnation methods can alter catalytic activity. In addition, comonomer content also affected polymerization activity. All polymers were further characterized using ^{13}C NMR to determine the polymer properties and polymer microstructure.

Department :........Chemical Engineering...... Student's Signature Apiwat Ngowthanawat
Field of Study :.....Chemical Engineering...... Advisor's Signature.........................
Academic Year :...2009...........................

ACKNOWLEDGEMENTS

The author would like to express my greatest gratitude and appreciation to Associate Professor Dr. Bunjerd Jongsomjit, my thesis advisor, for his invaluable suggestions, encouragement during my study and useful discussions throughout this research. His advice is always worthwhile and without him this work could not be possible.

I wish to thank Assistant Professor Dr. Montree Wongsri, as the chairman, Associate Professor Dr. ML. Supakanok Thongyai, and Assistant Professor Dr. Sirirat Wacharawichanant as the members of the thesis committee for their valuable guidance and revision throughout my thesis.

Many thanks for kind suggestions and useful help to Mr. Ekrachan Chaichana, Miss Mingkwan Wannaborworn, Miss Prae Rothakit, Mr. Somchart Amornlertpreecha, Miss Sasiradee Juntasee and many friends in the Center of Excellence on Catalysis and Catalytic Reaction Engineering, Department of Chemical Engineering, Chulalongkorn University for friendship and their assistance especially the members of ZM group. To the many others, not specifically named, who have provided me with support and encouragement, please be assured that I think of you.

Finally, I would like to express my highest gratitude to my family for their unconditional love and their support throughout this study.

CONTENTS

CONTENTS (CON.)

CONTENTS (CON.)

LIST OF TABLES

LIST OF FIGURES

LIST OF FIGURES (CON.)

Figure Page

LIST OF FIGURES (CON.)

LIST OF FIGURES (CON.)

LIST OF FIGURES (CON.)

CHAPTER I

INTRODUCTION

Copolymers of ethylene with higher α–olefins are very important commercial products classified as linear low-density polyethylene (LLDPE). The short branching coming from the incorporation of the α–olefins leads to the lower melting points, crystallinities and densities. Consequently, films made from these materials are more flexible and better suited to a variety of applications including packing, agricultural films and cable coatings [Van Grieken *et al.*, 2007].

Even though conventional Ziegler–Natta catalyst systems are still very widely used in the commercial production of LLDPE [Piel *et al.*, 2006; Smit *et al.*, 2006], extensive studies in copolymerization have also been directed at the use of metallocene and post-metallocene catalysts. Major producers of polyolefin, such as Exxon, Phillips, and Dow have entered the LLDPE market by using metallocene catalysts [Awudza and Tait, 2008].

While Ziegler-Natta catalysts produce copolymers with wide molecular weight distribution (MWD) and chemical composition distribution (CCD) because of multiple active sites [Park *et al.*, 2007; Kaminsky, 2004; Ewen, 1998], metallocenes are single-site catalysts and produce very uniform polymers with narrow MWD, polydispersity indexes close to two or slightly higher, and CCD [Paredes *et al.*, 2007; Van Grieken *et al.*, 2007]. They also provide higher catalytic activity as well as more natural and environmentally clean polymer than conventional Ziegler-Natta catalysts [Razavi, 2000]. In addition, the properties of polymer can be tailored to meet specific market demands with metallocene catalysts.

One of the major contributions of metallocene technology is the preparation of linear low-density polyethylene (LLDPE) resins with uniform molecular structures (narrow MWD and CCD) and desired physical properties [Hong et al., 2006]. It is well known that comonomers play a key role in the properties of LLDPE. As the comonomer content increases, both crystallinity and melting point of the copolymer decrease.

However, one of the main conditions for the commercial use of metallocene catalysts is that it should be possible to handle them in existing plants, gas-phase and slurry polymerization, and hence they need to be heterogenized on supports. This system can also resolve the main production problem of homogeneous catalysis, i.e. reactor fouling, poor morphology control of the obtained polymers and the requirement for large amounts of cocatalyst. However, when a metallocene catalyst is supported, its activity decreases. As a result, it is important to find a way to attach the metallocene to the support without losing this performance of the homogeneous system.

It is known that the nature of the support as well as the technique used to anchor the metallocene onto it play important roles on catalytic activity and the properties of the polymers produced with supported metallocenes [Hamielec and Soares, 1996]. There are three basic methods to prepare supported metallocene catalyst; (i) supporting the cocatalyst followed by reaction with the metallocene; (ii) supporting the metalloncene, then reacting with the cocatalyst; and (iii) reacting a metallocene-cocatalyst mixture with the support. Significant effort has focused on the heterogenization of metallocenes onto supports, such as silica, alumina, magnesium chloride, zeolites, polymers and mesoporous molecular sieves. Nevertheless, there is no paper that has discussed the heterogeneous metallocene system using zinc oxide as inorganic support.

With regard to polymer nanocomposites, they are a class of hybrid materials composed of an organic polymer matrix that incorporates inorganic particles having at least one dimension in the nanometre size range. Even though incorporated only a few weight percentage, these inorganic modifiers have a strong impact on the properties of polymer, such as higher heat distortion temperatures, enhanced flame resistance, increased modulus, decreased thermal expansion coefficient and altered electronic and optical properties. Due to the synergistic effects that result from adding a small amount of nanofillers, the synthesis and characterization of polymer nanocomposites have extensively been investigated in the last decade [Reddy *et al.*, 2008]. Basically, there are three methods used to produce the polymer nanocomposite: (i) melt mixing; (ii) solution blending; and (iii) *in situ* polymerization. Because of the direct synthesis via polymerization along with the presence of nanoscale fillers, the *in situ* polymerization is perhaps considered the most powerful technique to produce polymer nanocomposites with good distribution and dispersion of the fillers inside polymer matrix [Zou *et al.*, 2008].

For polymer with a significant portion of its applications being under outdoor environments, especially LLDPE, degradation of polymeric materials by ultraviolet (UV) irradiation and other high energy radiations is a frequently encountered problem, called photo-degradation, that leads to changes in their chemical, physical, and mechanical properties. A number of publications have dedicated to zinc oxide (ZnO) particles filled polymer nanocomposites, such as polyethylene [Tjong and Liang, 2006; Yang *et al.*, 2005], polypropylene [Zhao and Li, 2006], polyimide [Somwangthanaroj *et al.*, 2009; Somwangthanaroj *et al.*, 2008] and polyester [Peng *et al.*, 2008]. The results from these researches indicate that the incorporation of ZnO into polymer matrix can impart significant improvements on the photo-degradation resistance of polymer to UV-irradiation. Therefore, ZnO nanoparticles are highly attractive for using as photo-stabilizers of polymer, and at the same time they would be the effective support for metallocenes.

In the present work, LLDPE/ZnO nanocomposites were synthesized via *in situ* polymerization of ethylene/1-octene with zirconocene/MAO catalyst for the first time based on our best knowledge. Catalyst precursors were prepared via three different impregnation methods: (i) activation of ZnO support with MAO; (ii) impregnation of zirconocene onto ZnO; and (iii) introduction of both MAO and zirconocene to the ZnO support. The effect of catalyst preparation method on catalytic activities and properties of copolymer was investigated and further discussed in more details.

CHAPTER II

LITERATURE REVIEWS

2.1 Polyolefin Catalysts

Polyolefins are commercially produced using free-radical initiators, Phillips type catalysts, Ziegler-Natta catalysts and metallocene catalysts. In 1953, Karl Ziegler revealed that high density polyethylene was easily made at low pressure with binary mixture of metal alkyls and transition metal salts, and in the next year, Giulio Natta demonstrated the ability of the same type of catalysts to form isotactic polymers from α-olefins. Their discoveries have changed polymer chemistry and provoked a worldwide research and development that culminated in many new commercial plastics and elastomers. In 1963 Karl Ziegler and Giulio Natta were awarded the Nobel Prize for Chemistry for their landmark discoveries of the polymerization catalysts, named Ziegler-Natta catalysts [Kaminsky and Laban, 2001; Huang and Rempel, 1995].

The Ziegler-Natta catalyst is a complex formed by reaction of a transition metal compound (halide, or alkoxide, or alkyl or aryl derivative) of group IV-VIII transition metals with a metal alkyl or alkyl halide of Group I-III base metals [Sinn and Kaminsky, 1980]. The former component is usually called the catalyst and the latter the cocatalyst. There are a number of researches involving the combination of pure or mixed metal alkyls with transition metal compounds, each claiming particular advantages. In practice, only a few group I-III metal alkyls are effective. Aluminum alkyls such as $\mathrm{AlEt_3}$, $\mathrm{Al}\text{-}i\text{-}\mathrm{Bu_3}$, $\mathrm{AlEt_2Cl}$, $\mathrm{AlEtCl_2}$, and $\mathrm{AlEt_2OR}$ have been preferred. Also, transition metal compounds containing titanium (Ti), vanadium (V), chromium (Cr) and, in special case, molybdenum (Mo), cobalt (Co), rhodium (Rh) and nickel (Ni) are primarily used. For industrial use, most Ziegler-Natta catalysts are based on titanium compound and aluminum alkyls [Reddy and Sivaram, 1995].

Compared to conventional Ziegler-Natta catalysts, metallocene catalysts are generally called single-site catalysts because of the equality of each catalyst site. In addition, they are characterized by higher activity, narrow molecular weight distribution, uniform comonomer incorporation, outstanding ability to incorporate sterically demanding comonomers, narrow comonomer distribution, and the ability to vary the comonomer distribution over the entire polymer chain [Olabisi *et al.*, 1997]. This catalyst system produces new polyolefins with tailor-made microstructure and properties.

The first homogeneous metallocene catalysts were discovered in 1957 by Breslow and Newberg, who used bis(cyclopentadienyl)titanium derivatives, replacing the chloride ligand of the Ziegler-Natta transition metal catalyst system, together with alkylaluminum for ethylene polymerization [Hamielec and Soares, 1996]. Several other researchers including Natta followed this original work, using the same catalytic system or modifications of that system. However, these catalytic systems had low activities and stabilities for the polymerization of ethylene and produced only low molecular weight polymers. Additionally, they were not active for propylene polymerization. A breakthrough occurred when Kaminsky and his co-workers noticed that the addition of water to the trialkyl aluminum in a molar ratio of 1:1 during ethylene polymerization significantly improved the catalyst activity [Kaminsky and Arndt, 1996; Sinn and Kaminsky, 1980]. It was already known that trialkyl aluminum reacts with water to produce alkyl aluminoxane. Therefore, Kaminsky and his group decided to use alkyl aluminoxane oligomeric product as the cocatalyst with the metallocene catalyst. This combination made the breakthrough in the development of metallocene/aluminoxane catalyst systems for olefin polymerization. It produced a metallocene catalyst system whose activity is significantly higher than that of conventional Ziegler-Natta catalyst and is capable of producing stereoregular polyolefin with very narrow molecular weight distribution. The metallocene catalyst systems have sustained industrial and academic interests.

2.2 Metallocene Catalyst

Metallocene catalysts are organometallic compounds. The typical chemical structure consists of a transition metal atom that is essentially sandwiched between ligands such as cyclopentadienyl, fluorenyl, indenyl, or their substituted structures. It is schematically represented in Figure 2.1 where M is the group IV transition metal, normally Zr, Ti, and Hf; A is an optional bridging atom usually Si or C atom; R is a ligand substituent such as H, alkyl, or other hydrocarbon groups; and X is chlorine or other halogens from group VIIA or an alkyl group. These components together with the cocatalyst type determine the catalytic behavior of these organometallic compounds towards the polymerization of olefins. Structures of metallocenes that are widely used in the polymerization of olefins are shown in Figure 2.2. These polymerization catalysts have been used for the production of polymers with entirely novel properties.

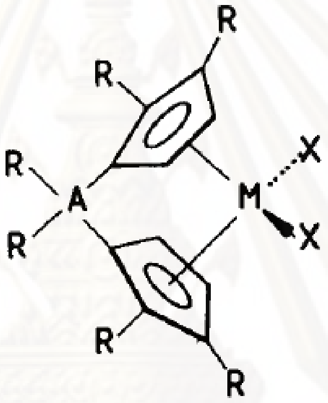

Figure 2.1 Typical chemical structure of a metallocene catalyst [Olabisi *et al.*, 1997]

According to the structure of metallocene catalyst, it is devided into five main symmetry categories as shown in Figure 2.3. Ewan was the first to link the symmetry at metallocene center to the microstructure of the resultant polymer. Catalysts that exhibit C_{2v} symmetry typically produce atactic polymers or moderately stereoregular polymers by chain-end control mechanisms. C_s symmetric catalysts that have mirror planes containing the two distereotopic coordination sites behave similarly. However, the C_s-symmetric catalysts that have a mirror plane reflecting two enantiomorphic coordination sites frequently produce syndiotactic polymers while C_2-symmetric complexes, both racemic and enantiomerically pure ones, typically form isotactic polymers via a site-control mechanism. Stereoselectivities of asymmetric (C_1) complexes are unpredictable and have been reported to produce polymer architectures ranging from highly isotactic to atactic, including hemiisotactic structure which is isotactic-atactic stereoblock [Coates, 2000; Schupfner and Kaminsky, 1995; Ewen, 1988]. Different polymer architectures relevant to this modification of ligands are shown in Figure 2.4 [Kaminsky and Laban, 2001].

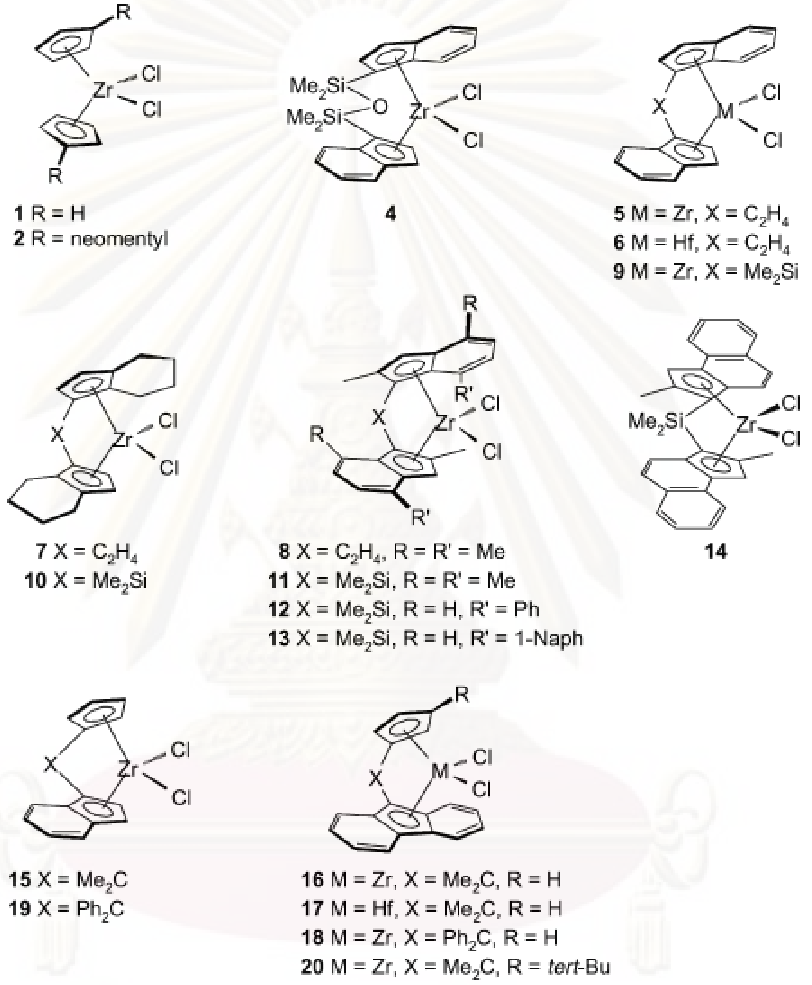

Figure 2.2 Structures of metallocenes that are used in the polymerization of olefins [Kaminsky and Laban, 2001]

It is generally assumed that the function of MAO is firstly to undergo a fast ligand exchange reaction with the metallocene dichloride, as a result, rendering the metallocene methyl and dimethylaluminum compounds. In a further step, either Cl^- or CH_3^- is abstracted from the metallocene compound by an Al-center in MAO, thus, forming a metallocene cation and a MAO anion. This mechanism is illustrated in Figure 2.5.

The zirconocene/MAO catalyst system is about 10-100 times more active for ethylene polymerization than the conventional Ziegler systems. Chien and Wang (1989) revealed that bis(cyclopentadienyl) zirconium dichloride (Cp_2ZrCl_2) and MAO can produce up to 39.8×10^3 kg of polyethylene/mol Zr.h and every zirconium atom formed an active complex and produced about 46,000 polymer chains per hour. Also, the time of insertion of one ethylene unit (turnover number) is only 3×10^{-5} seconds [Kaminsky and Arndt, 1997]. Generally, zirconium catalysts are more active than the hafnium or titanium systems [Chien and Wang, 1989]. In addition, among the different aluminoxane cocatalysts, methylaluminoxane is much more effective than ethyl- or isobutylaluminoxane [Chien and He, 1991].

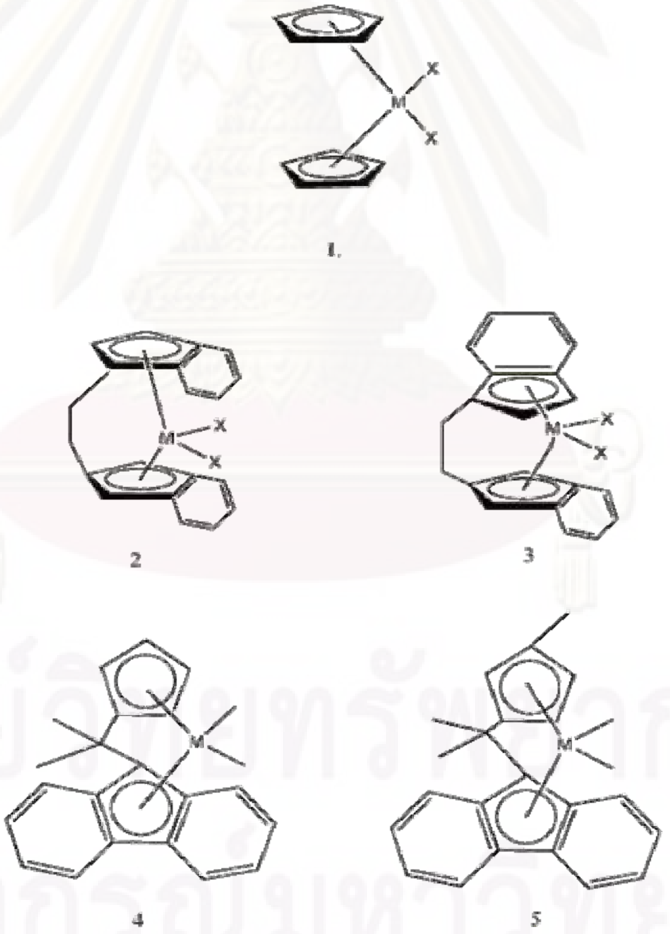

Figure 2.3 Schematic representations of metallocene symmetry (Type 1: C_{2v}-symmetric, Type 2: C_2-Symmetric, Type 3 and Type 4: C_s-symmetric, Type 5: C_1-symmtric) [Gupta *et al.*, 1994]

By altering the chemical environment around the central transition metal atom, it is possible to change considerably the behavior of the metallocene catalysts. For examples, Kaminsky *et al.* (1986) used bis(pentamethyl cyclopentadienyl)zirconium dichloride (($(Me_5Cp)_2ZrCl_2$) and MAO to catalyze ethylene polymerization. The catalyst was 5-10 times less active than Cp_2ZrCl_2/MAO, but it produced polymer with higher average molecular weight and much broader molecular weight distributions under the same polymerization conditions. This behavior was attributed to the presence of two active site types formed sequentially during the contact of metallocene and MAO.

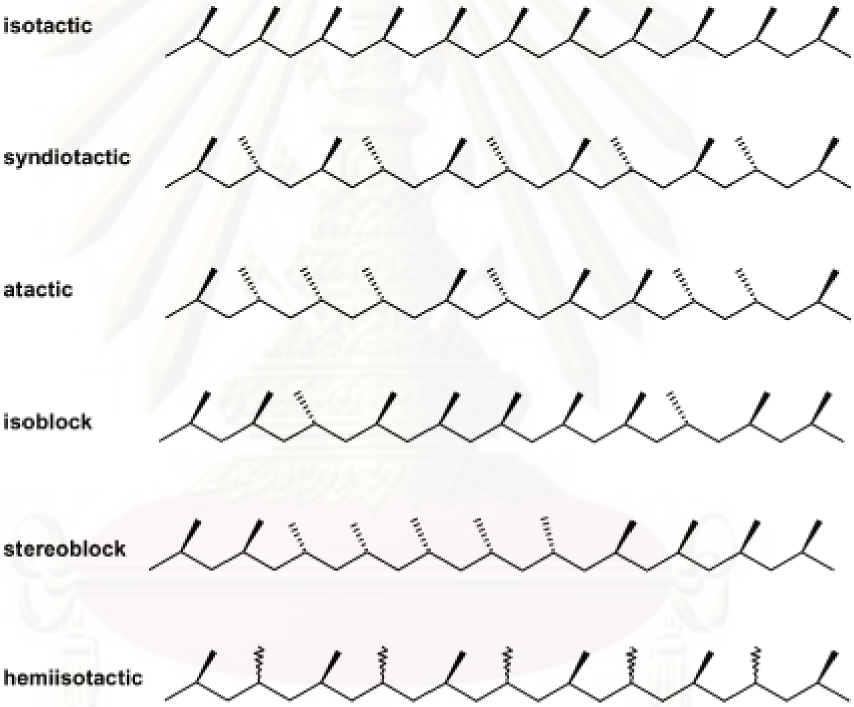

Figure 2.4 Different type of polymer tacticity [Kaminsky and Laban, 2001]

The fact that zirconocene dichloride systems are only active at high Al/Zr ratios (typically Al/Zr > 2000) led Pédeutour *et al.* (2001) to investigate the use of other zirconocene precursors. In particular, their study was extended to zirconocenes *rac*-$Et(Ind)_2ZrX_2$, bearing various extractable X ligands other than chloride. In their work, the activation process by methylaluminoxane (MAO) of various zirconocene precursors of the type *rac*-$Et(Ind)_2ZrX_2$, with different extractable X ligands (X = Cl, Me, NMe_2, CH_2Ph), was investigated both by means of UV–VIS spectroscopy and through 1-hexene polymerization kinetics. The different elementary steps yielding olefin polymerization active species, i.e. methylation and cationization of the transition metal could be readily discriminated. Unlike *rac*-Et(Ind)$_2$ZrCl$_2$ precursor for which high amount of MAO (Al/Zr = 2000) is required to form catalytic species active towards olefin polymerization, the complete activation of other *rac*-Et(Ind)$_2$ZrX$_2$ tested (with X = Me, NMe$_2$, CH$_2$Ph) is readily achieved at relatively low Al/Zr ratios (Al/Zr = 40–50). The corresponding zirconocenium species exhibit different catalytic activity according to the nature of the extracted X ligand, showing the important role of the formed [MAO-X]$^-$ counter-anion in the activation process and more particularly, its ability to still coordinate with the metal center and compete with the incoming olefin (Figure 2.6).

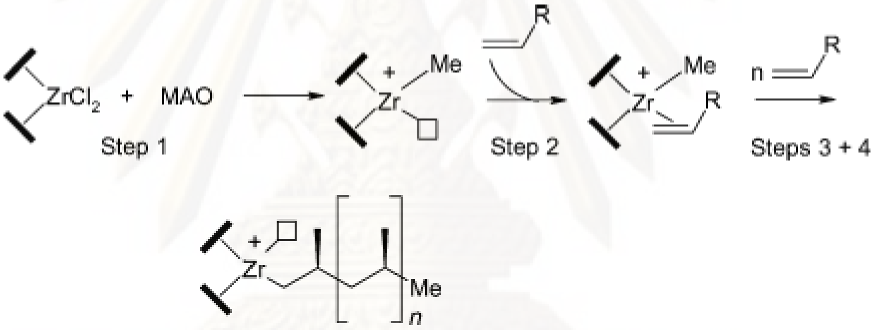

Figure 2.5 Mechanism of the polymerization of olefins by zirconocenes [Kaminsky and Laban, 2001]

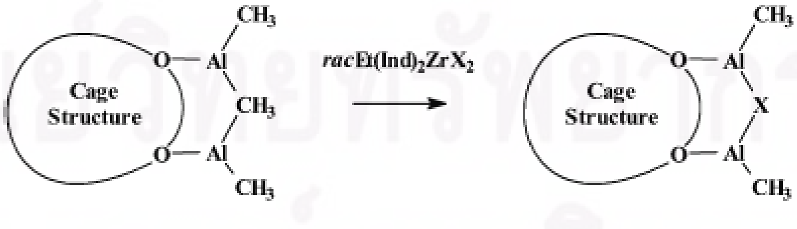

Figure 2.6 Schematic representation of MAO showing the substitution of one bridging methyl group by X ligand extracted from *rac*-Et(Ind)$_2$ZrX$_2$ (X = Cl, NMe$_2$, CH$_2$Ph) [Pédeutour *et al.*, 2001]

The degree of stereocontrol and the physical properties of polymers produced with stereorigid bridged homogeneous metallocene catalysts have been a point of much consideration. Schupfner and Kaminsky (1995) compared five different indenyl catalysts with respect to microstructure of the resulting polymers over a broad range of polymerization temperatures. Propylene bulk polymerization with *rac*-$Et(Ind)_2ZrCl_2$, *rac*-$Et(H_4\text{-}Ind)_2ZrCl_2$, $(CH_3)_2Si(Ind)_2ZrCl_2$, $(CH_3)_2Si(H_4\text{-}Ind)_2ZrCl_2$/MAO were carried out at polymerization temperatures from 0 to 60 °C. The regio-irregularities, racemic placements and their succession, which are known to cause depression of the melting point of isotactic polypropylene produced with homogeneous catalysts, were studied and compared. Only stereospecific 2,1-insertions were detectable and found to increase with temperature. 1,3-insertion showed up only for catalyst with tetrahydroindenyl ligands and replaced the 2,1-insertions at elevated polymerization temperatures. A racemic propylene placement occurring after a 2,1 -insertion sequence was found to a minor extent compared to regular meso enchainment.

Metallocenes are highly useful for the copolymerization of ethylene with other olefins. Propylene, 1-butene, 1-hexene, and 1-octene have been studied as comonomers, forming linear low density polyethylene (LLDPE). These copolymers have a great industrial potential and show a higher growth rate than the homopolymer. Due to the short branching from the incorporated α-olefin, the copolymers show a lower melting point, lower crystallinity, and a lower density, making films more flexible and easier processablity. Their applications can be found in packaging, shrink films with low steam permeation, elastic films, cable coating, etc.

The most remarkable property of metallocene catalysts is their ability to produce copolymers with narrower chemical composition distributions than those produced with heterogeneous Ziegler-Natta catalysts. This not only permits an improved control of copolymer composition but is also essential for the production of elastomers that is free of crystallinity. Moreover, metallocene catalysts can produce copolymers with an almost random incorporation of comonomers which results in a maximum decrease in polymer crystallinity for a given amount of comonomer incorporation. Bis(cyclopentadienyl)titanium dimethyl (CP_2TiMe_2) and MAO can produce random copolymers of ethylene with propylene, 1-butene or 1-hexene [Stadler *et al.*, 2006]. This catalyst can also be used for the copolymerization of ethylene and 1,3-butadiene and for the terpolymerization of ethylene-propylene-ethylidene norbornene [Hamielec and Soares, 1996].

When using C_2-symmetric metallocenes, comonomer is randomly distributed. Under the same conditions, C_s-symmetric metallocenes are more effective for inserting α-olefins into polymer chain than C_2-symmetric or unbridged metallocenes. Also, in this case, hafnocenes are more efficient than zirconocenes [Herfert and Fink, 1992]. An interesting effect is observed for the polymerization reaction with ethylene (bisindenyl)zirconium dichloride ($(Et(Ind)_2)ZrCl_2$). Although the activity of ethylene homopolymerization was very high, it increased when copolymerizing with propylene [Kaminsky and Arndt, 1997].

Kaminsky and Scholobohm (1986) copolymerized ethylene and 1-butene by Cp_2ZrCl_2/MAO. For the same degree of 1-butene incorporation, the melting point of the copolymer made with the zirconocene catalyst was lower than that made with the heterogeneous catalyst $TiCl_4$/triethylaluminum (TEA). This result indicates that the comonomer is more regularly distributed in the copolymer chain when the zirconocene catalyst is used.

The copolymerization of ethylene with other olefins is affected by the variation of Al/Zr ratio, temperature and catalyst concentration. These variations change the properties of the obtained copolymer. The effect of polymerization conditions and molecular structure of the catalyst on ethylene/α-olefin copolymerization have also been investigated extensively.

2.3 Heterogeneous Metallocene Catalyst

The development of metallocene technologies has led to the synthesis of new polymers with different structures and properties to feed up the progressive market demand. According to the olefin polymerization, metallocences are crucial since they can control the properties of polyolefins. Metallocene catalysts are often used in the heterogeneous form based on the most existent technologies such as gas phase and slurry polymerization. Therefore, they are supported on an insoluble carrier prior to the polymerization. The reasons for the heterogenization of the metallocene are to slower the deactivation of the metallocene, employ less cocatalyst required, protect the reactor fouling, control the polymer morphology and fulfill the requirements of the commercial polymerization processes [Chien, 1999; Ribeiro *et al.*, 1997].

It is known that the nature of the support as well as the technique used to anchor the metallocene onto it play important roles on catalytic activity and the properties of the polymers produced with supported metallocenes [Hamielec and Soares, 1996]. There are three basic methods to prepare supported metallocene catalyst; (i) supporting the cocatalyst followed by reaction with the metallocene; (ii) supporting the metalloncene, then reacting with the cocatalyst; and (iii) reacting a metallocene-cocatalyst mixture with the support. Significant effort has focused on the heterogenization of metallocenes onto supports such as silica, alumina, magnesium chloride, zeolites, polymers and mesoporous molecular sieves.

It is difficult to predict which catalyst preparation route to choose or start with for a particular catalyst. As a result, a considerable amount of investigative research will be needed to identify the optimum preparation for a particular catalyst. Method (ii) is usually avoided as it is difficult to predict how the various surface hydroxyl groups would interact with the metal center of metallocene, and how the resultants species would interact with the cocatalyst. In addition, close contact to the support surface may affect the local steric environment. Typically, the other two methods are employed. However, the catalyst/cocatalyst solution may be unstable or susceptible to over-reduction or any other common deactivation mechanism [Bochmann, 2004; Pédeutour *et al.*, 2001]. Thus, method (i), avoiding any MAO-complex precontacting stage, would most likely be the best starting point [Severn and Chadwick, 2008].

Dos Santos *et al.* (1999) investigated the effect of silica calcinations temperature and grafting reaction condition on the performance of the catalytic system. They dehydroxylated silica at various temperatures between room temperature and 450 °C, and reacted these with solutions of $(n\mathrm{BuCp})_2\mathrm{ZrCl}_2$ at different contact temperatures and times. Silica pretreated at a higher temoerature led to lower catalyst loadings, but when contacted with MAO it afforded catalyst systems with higher activities and produced resins of higher molecular weight and narrower molecular weight distributions. High grafting temperatures and long contact times led to higher metal contents, but reduced the activity of the system.

Dos Santos and colleagues also studied the grafting reaction of several other metallocenes on silica dehydroxylated at 450 °C. The metal contents were found to depend on the metal center of metallocene (Ti<Hf<Zr) and the support. Alkyl substitution of the cyclopentadienyl ligand had no significant effect on the metal loadings of the catalyst. Furthermore, the ethyl-bridged indenyl derivatives gave higher metal contents than the more bulky dimethylsilyl-bridged analogues. [Guimarães *et al.*, 2003]

Precontacting a toluene or aliphatic hydrocarbon solution of MAO with a calcined silica followed by reaction with an appropriate catalyst is one of the earliest and most frequently used and commercially available methods to facilitate the immobilization of single-site α-olefin polymerization catalysts. Welborn (1989) and Takahashi (1991) were among the first to disclose the contacting of silica with a toluene solution of MAO. In both cases, the treatment of MAO-immobilized silica with various metallocene catalysts yielded supported single-site catalysts that were effective in the homopolymerization and copolymerization of ethylene.

Employing a heat-treatment regime in a particular step of the supportation procedure has been reported to improve not only the fixation of MAO onto the silica surface but also the performance of the finished catalyst. Razavi (1998), Gauthier and coworkers (2003) found that refluxing the silica/MAO toluene suspension prior to contact with a C_2- or C_1- symmetric metallocene can improve the stereoselectivity and activity of the finished catalyst and yielded polymer resins with good bulk density and morphology. Higher Al contents of the finished catalysts were observed with high contact and washing temperature (115 °C). In addition, Gauthier and coworkers revealed that at different loadings of $Me_2Si(2\text{-}Me\text{-}4\text{-}PhInd)_2ZrCl_2$ on the MAO/SiO_2, the catalytic activity of the finished catalyst was changed. At a 2 wt% loading, the catalyst performance was apparently higher than the performance obtained with 1 wt% loading. Interestingly, it was proposed that a large critical pore diameter (CPD), which is defined as the pore volume after contacting the silica pore with MAO and complex, is crucial to achieve high activity, and that the appropriate CPD is facilitated by a combination of heat fixation of MAO and an appropriate support [Severn and Chadwick, 2008].

Moreover, for metallocene, the introduction of substituents at certain positions of the two aromatic ligands and/or the bridge modifies not only the steric and electronic conditions in the molecule but also the symmetry of such a metallocene complex. A systematic study employing 18 different kinds of substituted metallocenes in ethylene polymerization activated by MAO was performed evaluating the influence of the nature and of the size of the substituents on catalyst activity and on polymer properties [Tian and Huang, 1994]. However, a few work dealt with such effect involving supported metallocenes. For instance, Sacchi *et al.* (1995) did a comparative study on propylene polymerization stereochemistry using $Et(Ind)_2ZrCl_2$ (Et: Ethylene, Ind: Indenyl) and $(Ind)_2ZrCl_2$, both homogenous and supported on silica. Both supported systems produced isospecific polymers, suggesting that only isospecific centers are formed independently of the metallocene stereochemical structure. A recent review was published by Alt and Köppl (2000) comparing the behavior of more than 90 metallocene complexes in catalyst activity and in the resulting molecular weight, considering ethylene and propylene homopolymerization.

Guimarães *et al.* (2003) aimed at studying the effect of the ligand hindrance in supported metallocene on the immobilized metal content, on catalyst activity and on polymer properties. A series of metallocenes differing in the metal center (M = Zr, Ti, Hf), in the coordination sphere (RCp with R = H, Me, *i*Bu, *n*Bu and Indenyl) and the bridge (Et, Me_2Si) were studied as homogeneous systems and supported on silica and MAO-mediated (2 wt% Al/SiO_2) silica. The effect of these parameters was evaluated in the grafted metal content, catalyst activity and polymer properties. In supported metallocenes, the final grafted content depends on the metal center (Ti < Hf < Zr), on the coordination sphere and on the support. In the case of Cp ligands the presence of alkyl substituent does not impinge a significant effect. However, indenyl derivatives lead to higher metal content. The presence of Me_2Si bridge reduced the final grafted content in comparison to ethylene one. Higher metal contents were achieved in the case of MAO-mediated systems. In this case, two surface species were observed by XPS analysis probably one resulting from the reaction between metallocene and surface silanol groups and other from the reaction with immobilized MAO. In homogeneous systems the inductive effect from alkyl groups can be observed, but this effect is reduced in supported systems probably due to the steric effect played by the silica surface, which seems to be much more important than the metallocene coordination sphere itself. Besides, a reduction in catalyst activity itself is observed in all the supported systems in comparison to the homogeneous counterpart. Concerning polymer properties, the supported systems presented higher molecular weight in comparison to those obtained with the homogeneous counterpart.

An important aspect of olefin polymerization using heterogeneous catalysts, concerns the characteristics of polymer growth and catalyst particle fragmentation during the course of polymerization. As polymerization proceeds, the catalyst support becomes fragmented and dispersed within the growing polymer matrix and, therefore the morphology of the starting support is replicated in the final polymer. Various models describing particle growth during olefin polymerization have been developed. The morphology of the polymer particle is a complex function of the polymer type, polymerization conditions, catalysts heterogeneization method and support properties as morphology and friability. To provide true replication, the catalyst particle must meet some requirements, summarized as follows: (i) high surface area, (ii) high porosity, (iii) mechanical strength high enough to withstand mechanical processing, but low enough to allow the forces developed by the growing polymer to break down the initial catalyst particle into the microscopic particles that remain entrapped and dispersed in the expanding polymer, (iv) homogeneous distribution of the active centers and (v) free access of the monomers to the active centers. When monomer contacts the active sites on the surface of the catalyst, polymer formation takes place and the fast-forming chains will be growing on the catalyst surface and pores, filling them up and leading to the support fragmentation. The monomer must diffuse through the boundary layer around the catalyst particle and through its pores to reach the active sites, where polymerization occurs. In ethylene polymerization, it is frequently observed that polymer growth starts at and near the particle surface, leading to the formation of a shell of polyethylene around the catalyst particle. This involves the diffusion limitation, preventing free access of the monomer to active sites within the particle. Polymerization then takes place layer by layer, as the monomer gradually diffuses through the outer layers to the core. This mechanism of particle growth is associated with a kinetic profile in which an initial induction period is followed by an acceleration period, after which, in the absence of chemical deactivation, a stationary rate is obtained. As known, the addition of a comonomer such a 1-hexene changes the properties of the polymer layer around the catalyst particle which affects catalyst particle fragmentation and kinetic profiles.

The enhancement of ethylene polymerization rate by α-olefin (comonomer) is a well-known phenomenon of considerable technological and scientist interest, called “comonomer effect”. Several possible causes had been proposed to explain this fact, but the most supported is the easier monomer diffusion due to crystallinity reduction of the growing polymer when a small amount of comonomer is added. In ethylene homopolymerization, the monomer diffusion is very slow through the highly crystalline polymer formed around the catalyst particle until sufficient polymer has formed to allow particle fragmentation. The comonomer addition leads to less crystalline polymer formation, which makes the diffusion of ethylene easier, and thus favors extended particle fragmentation.

Van Grieken *et al.* (2007) have investigated the synthesis of ethylene/1-hexene copolymers with $(n\mathrm{BuCp})_2\mathrm{ZrCl}_2/\mathrm{MAO}/\mathrm{SiO}_2\text{-}\mathrm{Al}_2\mathrm{O}_3$ catalytic system and studied the influence of 1-hexene concentration on catalytic activity and polymer properties. In their research, the activity of $(n\mathrm{BuCp})_2\mathrm{ZrCl}_2/\mathrm{MAO}/\mathrm{SiO}_2\text{-}\mathrm{Al}_2\mathrm{O}_3$ catalytic system in the ethylene/1-hexene copolymerization increased with comonomer concentration up to

0.194 mol/L. The initial enhancement in the catalyst activity is related with better monomer diffusion. At higher concentrations of 1-hexene, the activity decreased due to the lower insertion rate of the larger comonomer in the polymer chain. The 1-hexene incorporation increased with the concentration in the polymerization reactor, obtaining ethylene/1-hexene copolymers with broader chemical composition distributions, lower molecular weights and crystallinity than ethylene homopolymer. The percentages of 1-hexene in the copolymers obtained at different reaction times revealed that 1-hexene incorporation decreased at polymerization time above 20 minutes because mass transfer limitations are less pronounced in the initial stages of polymerization. For this reason, the copolymer chemical composition distribution (CCD) during the first minutes of reaction is broader with a maximum placed at lower temperatures than homopolymer, corresponding to 1-hexene rich fractions. As polymerization time increases, the CCD curves become narrower with a maximum placed at higher temperatures as a result of the gradual formation of an ethylene-rich fraction in addition to the main copolymer fraction. Furthermore, the presence of 1-hexene helps the fragmentation process, which could be related with the filter effect which proposes that the formation of an ethylene-rich fraction arises from easier diffusion of ethylene, with respect to 1-hexene, through a copolymer envelope formed in the outer regions of the catalyst particle.

The other researchers that studied about “comonomer effect” are Awudza and Tait (2007). Their study was concerned with a comparison of the comonomer effects in ethylene/α-olefin copolymerization using homogeneous system and silica-supported Cp_2ZrCl_2/MAO catalyst systems. 1-butene, 1-hexene, 4-methylpentene-1 (4-MP-1), and 1-octene were used as the comonomers for this study. The results obtained indicated that at 70 °C there was general rate depression with the homogeneous catalyst system whereas rate enhancement occurred in all copolymerization carried out with the silica-supported catalyst system. Rate enhancement was observed for both the homogeneous and the silica-supported catalyst systems when ethylene/4-MP-1 copolymerization was carried out at 50 °C. Active center studies during ethylene/4-MP-1 copolymerization indicated that the rate depression during copolymerization using the homogeneous catalyst system at 70 °C was due to a reduction in the active center concentration. However, the increase in polymerization rate when the silica-supported catalyst system was used at the same temperature resulted from an increase in the propagation rate coefficient.

Hong *et al.* (2006) extended the composition of linear low-density polyethylene (LLDPE) resins to that containing 1-decene comonomer units, and examined the effects of comonomer (type and concentration) to copolymerization and physical properties of LLDPE resins. CGC metallocene technology, under high temperature and high pressure (industrial reaction condition), was used to prepare three types of well-defined LLDPE copolymers containing 1-hexene, 1-octene, and 1-decene units. They showed high molecular weight with narrow molecular weight and composition distributions, comparative catalyst activities, and similar comonomer effects. However, 1-decene seemed to exhibit significantly the higher comonomer incorporation than 1-hexene and 1-octene, which may be associated with its high boiling point (171 °C), maintaining liquid phase during the polymerization. The resulting LLDPE copolymers showed a clear structure–property relationship. Melting temperature and crystallinity of the copolymer were governed by comonomer content whereas the density of the copolymer decreased with the increase of comonomer content. The tensile properties of 1-decene-based LLDPE are very comparative with those of the commercial LLDPE resins with similar compositions

As well known, the mesoporous silica tube-like materials designated as MCM-41 was first introduced in 1992. The MCM-41 is recognized as a well-defined as mesoporous material with narrow pore size distribution, large internal surface area, distinct adsorption properties and hexagonal arrangement of uniformly sized cylindrical pore. It has the possibility to control the internal diameter of mesopores between 15 and 100 Å by varying the chain length of the micellar surfactant template. In fact, its pore diameter can enable large metallocene molecules to be immobilized onto both the surface and inside the pore. These excellent properties of this material essentially emulate researchers to use the MCM-41 as the support for metallocene catalysts for olefin polymerization. As mentioned before, a support with distinct bimodal structure has a number of excellent advantages. In particular, the large pores provide rapid transportation of reactant and product molecules whereas the small pores render a large surface area. Moreover, the geometrical shape of the nano-channels of MCM-41 can serve as polymerization reactors to affect the pattern and activity of monomer insertion. Thus, the arrangement of polymer chain and polymer morphology can be controlled. Bunchongturakarn *et al.* (2008) studied the bimodal MCM-41-supported zirconocene/dMMAO catalyst exhibited higher catalytic activity for ethylene/1-octene copolymerization and compared to the unimodal one. The higher activity can be attributed to lesser support interaction. The copolymer having broader MWD was obtained with the bimodal support without any significant changes in MW and polymer microstructure as seen by ^{13}C NMR.

Many scientists have investigated MCM-41 materials in which a catalytically active component was introduced. Several elements, such as aluminium and boron have been incorporated into the catalyst structure in order to generate potential catalytic activity. Therefore, modification of the MCM-41 may provide an alternative strategy to obtain suitable supports to maintain high activity as in the homogeneous system for the supported metallocene catalysts. Jiamwijitkul *et al.* (2007) studied the effect of boron (B)-modification on the MCM-41-supported dMMAO/zirconocene catalyst during ethylene/1-octene copolymerization. It showed a promising increase (almost twice) in catalytic activity. The enhanced activity can be attributed to the decreased interaction between the support and dMMAO with boron modification as was proved by TGA. It was proposed that boron acted as a spacer anchoring the support and dMMAO. However, at high boron loading (ca. 5 wt%), the activity slightly decreased due to the migration of dMMAO into boron layer resulting in less surface concentration of $[Al]_{dMMAO}$ which was measured by XPS. The inhibition of chain transfer reaction during polymerization apparently occurred upon the boron modification providing higher MW polymer. It was also suggested that boron modification has rendered more uniform catalytic sites which was leading to narrower MWD of the polymer observed. Based on ^{13}C NMR, boron modification did not affect the microstructure of copolymers obtained. However, the insertion of 1-octene ncreased with boron modification probably due to decreased steric hindrance of the MCM-41 support.

Silveira *et al.* (2007) comparatively investigated the effect of different supports. A series of hybrid supported catalysts was prepared by sequentially grafting Cp_2ZrCl_2 and $(n\text{BuCp})_2ZrCl_2$ (1:3 ratio) onto alumino-silicates (MCM-41, SBA-15, MCM-22, ITQ-2), alumina and chrysotiles (native and leached). ITQ-2 is a zeolitic material described as a delaminated zeolite. Supports and catalysts were characterized by Rutherford backscattering spectrometry (RBS), atomic force microscopy and nitrogen adsorption. Grafted metal content laid between 0.2 and 0.8 wt% Zr/SiO_2 and 0.9 wt% Zr/Al_2O_3. All the systems were shown to be active in ethylene polymerization with methylaluminoxane as the cocatalyst. Catalyst activity and molecular weight were shown to depend on the textural characteristic of the silicas, namely grain size and pore diameter. The highest activity in ethylene polymerization (ca. 3200 kg PE mol Zr^{-1} h^{-1}) was obtained with the supported catalyst using SBA-15 with average particle size around 0.21 mm. Resulting polymers were characterized by gel permeation chromatography and differential scanning calorimetry.

In addition, Paredes *et al.* (2007) used two types of silica, mesostructured MCM-41 and SBA-15, to immobilize $(n\text{BuCp})_2ZrCl_2$/MAO for copolymerization of ethylene and 1-hexene. Also, commercial carriers such as silica and silica-alumina have been investigated for comparison. They found that all copolymers produced with these supports had narrow molecular weight distribution (MWD) while chemical composition distribution (CCD) varied from narrow and unimodal to board and bimodal. The CCDs of copolymers made with $(n\text{BuCp})_2ZrCl_2$/MAO supported on SiO_2 and SiO_2/Al_2O_3 were always unimodal, but those made with MCM-41 and SBA-15 became bimodal with increasing 1-hexene content. This bimodality may be related to the presence of two catalyst site types on the surface of the support.

Li *et al.* (2006) compared the catalytic behavior between nano-sized and micro-sized silica particles which are used to support Cp_2ZrCl_2/MAO catalyst for ethylene polymerization. They revealed that nano-sized catalyst exhibited much better ethylene polymerization activity than micro-sized catalyst. At the optimum temperature of 60 °C, nano-sized catalyst’s activity was 4.35 times the micro-sized catalyst’s activity, which was attributed to the large specific external surface area, the absence of internal diffusion resistance, and the better active site dispersion for the nano-sized catalyst. For support having size in micrometers, most active sites for polymerization were located inside fine pores, and strong internal diffusion resistance might occur inside the pores of the micro-sized catalysts. Nanoparticles have a characteristic of very large external specific surface areas. In addition, in their study, they found that nano-sized silica supported rac-ethylenebis(1-indenyl)zirconium (IV) dichloride/methylaluminoxane (*rac*-Et[Ind]$_2$ZrCl$_2$/MAO) catalyst had better activity for propylene polymerization than micro-sized silica supported *rac*-Et[Ind]$_2$ZrCl$_2$/MAO catalyst.

Chaichana *et al.* (2007) synthesized the LLDPE/nano-SiO$_2$ via the *in situ* polymerization with zirconocene/MAO catalyst. The effect of nano-SiO$_2$ particle size on characteristics and catalytic properties was investigated. In this experiment, SiO$_2$ with different particle size (10 and 15 nm) was first impregnated with MAO. Then, copolymerization of ethylene/1-hexene was performed in the presence of nano-SiO$_2$/MAO to produce LLDPE/nano-SiO$_2$ composites. It was found that the larger particle exhibited higher polymerization activity due to fewer interactions between SiO$_2$ and MAO. The larger particle also rendered higher insertion of 1-hexene leading to decreased melting temperature (T_m). There was no significant change in the LLDPE molecular structure by means of ^{13}C NMR. In addition, in order to give a better understanding, they developed a conceptual model for impact of nano-SiO$_2$ particle size on the steric hindrance, interaction, and comonomer insertion as shown in Figure 2.7.

It has been reported that a new immobilization method of introducing a spacer group such as polysiloxane between the support and metallocene resulted in higher catalytic activity. However, it should be noted that the absorption of MAO on a support prior to immobilizing the metallocene catalysts is one of the possible ways to form a heterogeneous catalytic system. The use of $Cl_2Si(CH_3)_2$-modified SiO$_2$ before treatment with MAO and used this modified support with Cp_2ZrCl_2 for ethylene polymerization was studied by Soga *et al.* (1993). They found that with the modified SiO$_2$, the activity increased with the addition of trimethylaluminum (TMA) as cocatalyst.

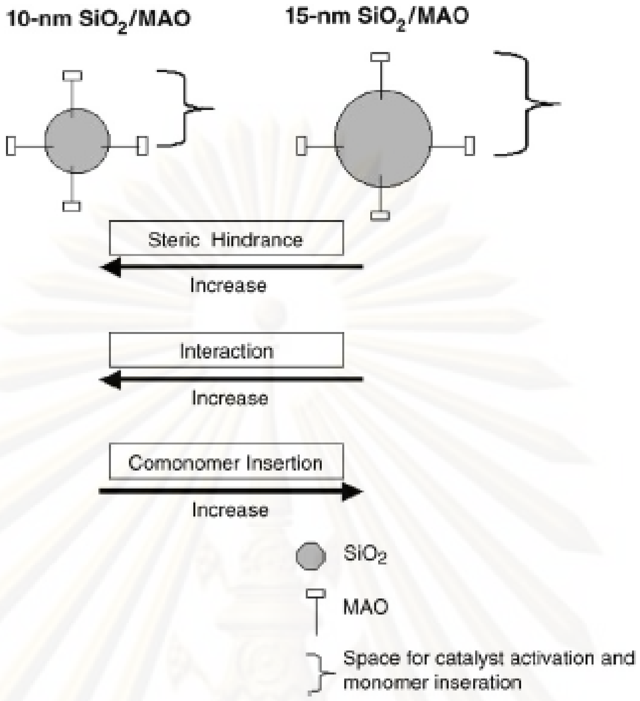

Figure 2.7 Conceptual model for impact of nano-SiO_2 particle size on steric hindrance, interaction, and comonomer insertion [Chaichana *et al.*, 2007]

Jongsomjit *et al.* (2004) investigated the effect of $SiCl_4$-modified silica/MAO-supported $Et[Ind]_2ZrCl_2$ metallocene catalyst on copolymerization of ethylene with α-olefins. Effect of $SiCl_4$ on activities was diminished with higher α-olefins. Molecular weights of copolymers decreased with $SiCl_4$ modification. $SiCl_4$ modification also resulted in a lower molecular weight distribution. ^{13}C NMR showed that ethylene incorporation in all systems gave copolymers with similar triad distribution. In addition, a narrow branching distribution can be achieved with $SiCl_4$ modification.

Generally, the activity and selectivity of polymerization catalyst are markedly dependent on their pore structure of support. In the slurry polymerization, effects of the support pore size have been studied. The support with large surface area, however, usually contains small pore size, which results in poor intra-pellet diffusion efficiency of reactants and products, slow transportation of reactants and products. Nevertheless, a catalyst with large pore size has a small specific surface area and is not beneficial to disperse support metal, leading to low metal dispersion. The distinct bimodal pore structure support, which contains large pores and small pores at the same time, provides pathways for rapid molecular transportation contributing to high diffusion efficiency as theoretically expressed by Levenspiel (1972) by the large pores and contributes to higher dispersion of supported metal by the small pores, which enlarged the surface area of the support. Furthermore, it is able to diminish the diffusion resistance by its large pores. In polymerization, the geometrical shapes of the nano-channels of support affect the pattern and activity of monomer insertion. Thus, the arrangement of polymer chain and polymer morphology can be controlled.

Wongwaiwattanakul and Jongsomjit (2008) focused on effect of different pore sizes of silica supports used for the supported dMMAO with zirconocene catalyst for copolymerization of ethylene/1-octene. The different silica supports having large pore, small pore and bimodal pore of silica–alumina were studied. They revealed that the large pored silica exhibited the highest polymerization activity due to both highest amount of available active sites present along with the moderate interaction between dMMAO and the support. The strong interaction between dMMAO and the support as proven by TGA analysis apparently resulted in dramatically decreased polymerization activity for the bimodal pored silica–alumina. The copolymers produced were further characterized by means of DSC and ^{13}C NMR. Although they exhibited the similar triad distribution, the degree of 1-octene insertion was different.

As known, beside silica, many inorganic supports such as Al_2O_3, TiO_2 and $MgCl_2$ have been used to immobilize metallocene catalyst. It has been reported that silica is perhaps the most attractive support employed for supported metallocene catalysts. However, the properties of silica itself may not be completely satisfied for all purposes based on the polymerization activity and properties of the obtained polymers. In order to increase an efficiency of supported metallocene catalysts, the modification of silica can be made or alternative supports would be further investigated. Owpradit and jongsomjit (2008) studied the effect of different TiO_2 nanoparticles employed on catalytic and characteristic properties of LLDPE/TiO_2 nanocomposites synthesized by the *in situ* polymerization with zirconocene/dMMAO catalyst. It was found that the presence of rutile phase in titania apparently resulted in decreased activities due to low intrinsic activity of active sites being present. Based on ^{13}C NMR results, all LLDPE/TiO_2 samples exhibited the random copolymer having different degree of 1-hexene insertion. The highly dispersion of titania can enhance the degree of 1-hexene insertion resulting in decreased crystallinity.

Desharun *et al.* (2008) synthesized LLDPE/Al_2O_3 nanocomposites synthesized by the *in situ* polymerization with dried-modified methylaluminoxane (dMMAO)/ zirconocene catalyst. The effect of Al_2O_3 content on catalytic activities and properties of polymer produced was examined.The enhancement of catalytic activity was observed with increased $[Al]_{dMMAO}/[Zr]_{cat}$ ratios. It was found that the melting temperature of LLDPE/Al_2O_3 nanocomposites apparently increased with the addition of the Al_2O_3 nanofiller. The addition of the Al_2O_3 nanofiller presumably inhibited the chain transfer reaction leading to the higher molecular weight of samples. In addition, the Al_2O_3 nanofiller was well distributed (based on the distribution of the secondary particles) inside the polymer matrix, but was poorly dispersed (based on the dispersion of primary particles) due to agglomeration of Al_2O_3 particles.

Another support used to immobilize cocatalyst in heterogeneous metallocene system is zirconia (ZrO_2). Jongsomjit *et al.* (2006) synthesized linear LLDPE/ZrO_2 nanocomposites via *in situ* polymerization with *rac*-Et(Ind)$_2$ZrCl$_2$/MAO catalyst. The amounts of nano-ZrO_2 filler employed were varied at 0.1 and 0.3 g corresponding to $[Al]_{MAO}/[Zr]_{Cat}$ ratios = 1135 and 3405, respectively. It can be observed that the polymer yield increased with increasing the ratios of $[Al]_{MAO}/[Zr]_{Cat}$. However, the observed polymer yields were much lower (about 5-30 times) compared to the yield with no filler addition. The filler contents in polymer were in the range of 23-25 wt%. Moreover, from differential scanning calorimetry (DSC), it was observed that the LLDPE/ZrO_2 nanocmposites exhibited slightly lower melting temperature (T_m) and crystallization temperature (T_c). In their work, Jongsomjit *et al.* have also proposed conceptual model for polymer forming on the nano-ZrO_2-filler via *in situ* polymerization by a metallocene catalyst as shown in Figure 2.8.

Pothirat *et al.* (2008) have compared the use of silica and zirconia as a support for zirconocene/MAO catalyst for copolymerization of ethylene/1-olefin (1-hexene, 1-octene, and 1-decene). First, MAO as the cocatalyst was impregnated onto the support. Then, copolymerization of ethylene/1-olefin was performed. It was found that the use of zirconia support showed promising activities compared to those of the silica. An increase in catalytic activities can be attributed to higher amount of $[Al]_{MAO}$ present on the zirconia support coupled with strong interaction between the $O_{support}$–$Al_{cocatalyst}$ linkage. In addition, the use of zirconia also resulted in higher degree of 1-olefin insertion and decreased melting temperature of copolymers produced.

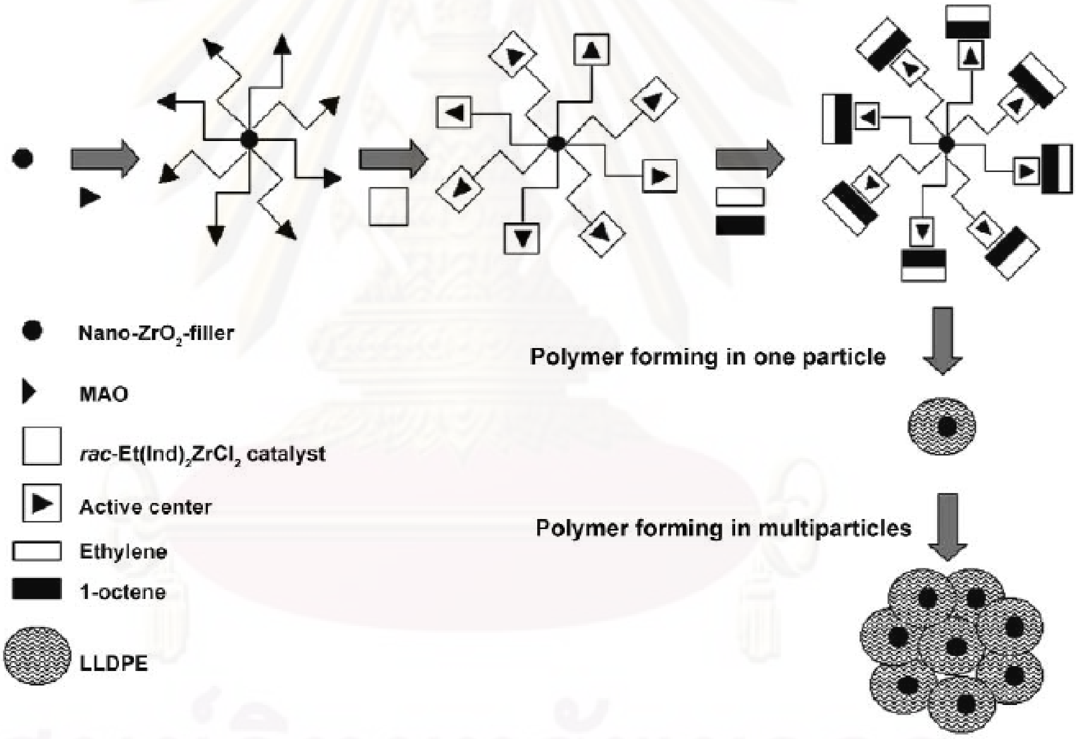

Figure 2.8 Conceptual model for polymer forming on the nano-ZrO_2-filler via *in situ* polymerization by a metallocene catalyst [Jongsomjit *et al.*, 2006]

Much of current research related to the development of *in situ* nanocomposites of olefins by polymerizing them with metallocenes in the presence of surface-treated fillers is carried out in the slurry phase. In slurry-phase methods, a large amount of solvent is required and there is always a need of purification of the final product due to the possibility of traces of solvents present in the product. To overcome these drawbacks, to perform solvent-free metallocene-catalyzed polymerizations with *in situ* incorporation of inorganic nanoparticles, Reddy *et al.* (2008) have used a gas-phase polymerization technique as this does not require solvents and also utilizes monomer feed stocks efficiently. The catalyst used for the synthesis of *in situ* polyethylene nanocomposites by gas-phase polymerization was nanosilica-supported zirconocene. The fillers used were Cloisite-20A, kaolin and nanosilica. Three different *in situ* polyethylene nanocomposites, i.e. Cloisite-20A-filled polyethylene (CFPE), kaolin-filled polyethylene (KFPE) and nanosilica-filled polyethylene (SFPE), were prepared by gas-phase polymerization. The nanocomposites were obtained in the form of fine powder. Using their approach, it is observed that the nanofillers are completely encapsulated by a thin layer of polyethylene. Significantly higher molecular weight polyethylene was formed in the case of KFPE in comparison to CFPE and SFPE. The thermal decomposition temperature, melting temperature and enthalpy are also observed to be higher for KFPE.

In previous studies, a unique catalyst type called constrained geometry catalyst (CGC) using half-sandwich titanocenes has been found. Such catalysts can give high activity and can incorporate a large amount of a-olefin into a copolymer. Research revealed that [*t*-BuNSiMe$_2$Flu]TiMe$_2$ complex could be employed to polymerize propylene, norbornene and ethylene. Several papers reported [*t*-BuNSiMe$_2$Flu]TiMe$_2$ catalyst was suitable for the propylene polymerization in various polymerization conditions due to the effects of activators and solvents used. They found that the kind of activators and the polarity of solvents played important roles on the catalytic activities and microstructure of polymer as well [Nishii *et al.*, 2004a; Nishii *et al.*, 2004b; Ioku *et al.*, 2002a; Shiono *et al.*, 2000]. Only few papers, however, have discussed the copolymerization of ethylene with α-olefins [Intaragamjon *et al.*, 2006; Hagihara *et al.*, 1998] and only one reported the supporting system [Ioku *et al.*, 2002b].

Ketloy *et al.* (2007) studied the characteristics and catalytic properties of [*t*-BuNSiMe$_2$Flu]TiMe$_2$/dMMAO catalyst dispersed on various supports towards ethylene/1-octene copolymerization were investigated. First, the dMMAO was impregnated onto various supports, such as SiO_2, SiO_2–TiO_2, and TiO_2. Then, copolymerization of ethylene/1-octene was conducted with and without the presence of supports in different solvent mediums. The SiO_2–TiO_2 support exhibited the highest activity among all the supports. The high activity observed for the SiO_2–TiO_2 support can be attributed to fewer interactions between the support and dMMAO, as confirmed by XPS and TGA results. The different solvents can alter the nature of the catalyst in two ways: (i) changing the interactions between the support and cocatalyst and/or (ii) changing the form of active species i.e., active ion-pair and solvent-separated ion-pair, as seen in the homogeneous system. However, there was no effect with regards to activity of the solvent mediums employed for the homogeneous system. It is worth noting that the Ti-complex made possible high incorporation of 1-octene having the triblock (OOO) and diblock (EOO) copolymers.

2.4 Zinc oxide (ZnO) nanoparticle filled polymer nanocomposites

Polymer nanocomposites are a class of hybrid materials that is composed of an organic polymer matrix that incorporates inorganic particles having at least one dimension in the nanometre size range. Even though incorporated only a few weight percentage, these inorganic modifiers have a strong impact on the properties of polymer such as higher heat distortion temperatures, enhanced flame resistance, increased modulus, decreased thermal expansion coefficient and altered electronic and optical properties. Due to the synergistic effects that result from adding a small amount of nanoparticles, the synthesis and characterization of polymer nanocomposites have extensively been investigated in the last decade [Reddy *et al.*, 2008]. Basically, there are three methods used to produce the polymer nanocomposite: (i) melt mixing; (ii) solution blending; and (iii) in situ polymerization. Because of the direct synthesis via polymerization along with the presence of nanoscale fillers, the *in situ* polymerization is considered the most powerful technique to produce polymer nanocomposites with good distribution and dispersion of the fillers inside polymer matrix [Zou *et al.*, 2008].

The nanosize fillers can be generally any filler or combination of fillers having at least one dimension (length, width, or thickness) from about 1 to about 30 nm. When only one dimension is in the nanometer range, the filler is present in the form of sheets of one to a few nanometers thick to hundreds or thousands nanometers long, such as platelet clays and layered silicates (phylosilicates). When the two dimensions are in the nanometer scale and the third is larger, the filler forms an elongated structure, such as carbon nanotubes. When the three dimensions are in the order of nanometers, the filler is present in the form of spherical nanoparticles, such as silica and zeolite.

Despite the efforts that have been directed towards the preparation of polymer nanocomposites and the unique properties of these materials, there are some aspects associated with their structure and mechanisms of reinforcement that remain unclear. For instances, in mechanical reinforcement, the major issues are the homogeneous dispersion of nanofillers in the polymeric matrix and the development of chemical bonding or strong interactions between nanofiller and interface of matrix.

Regarding polyethylene, the dispersion quality of inorganic nanofillers is one of the main difficulties. This is due to the hydrophobic nature of polyethylene, which gives rise to a significant problem in enhancing adhesion between the hydrophilic nanofiller and the matrix creating poor bond strength between the polymer matrix and filler. The problem of poor dispersibilty of nanofillers in a polyethylene matrix can be solved by a number of techniques including *in situ* polymerization of monomers in the presence of nanoparticles [Owpradit and jongsomjit, 2008; Chaichana *et al.*, 2007; Desharun *et al.*, 2007; Jongsomjit *et al.*, 2006], use of compatibilizers [Tjong and Liang, 2006; Hotta and Paul, 2004; Wang *et al.*, 2003], and modification of the nanoparticles with coupling agents (e.g. silane coupling) [Peng *et al.*, 2008; Zhao and Li, 2006; Hua *et al.*, 2005; Huang *et al.*, 2004; Huang *et al.*, 2003]. Although most of these techniques provide satisfactory dispersion of the nanoparticles, nevertheless, they are synthesized by complex polymerization and processing conditions, which add to the high cost of the polymer nanocomposites [Alexandre and Dubois, 2000]. Therefore, it can be concluded that the conventional techniques, such as melt mixing and solution blending, are still the most convenient candidates for the preparation of polymer nanocomposites.

Zinc oxide (ZnO) is an important II–VI semiconductor material with a wide band gap of 3.37 eV and a large exciton binding energy of 60 meV. Due to the excellent chemical and thermal stability of ZnO and its specific optoelectronic properties, a variety of applications including photonic crystals, photodetectors, photodiodes, light emitting diodes, varistors, gas sensors, solar cells, field emission and photocatalysis have been reported [Tang *et al.*, 2009; Kale *et al.*, 2007]. Many studies have shown that the size, shape, and properties of ZnO nanoparticles depend strongly on the preparation method and conditions. As a result, it is very important to find a way to synthesize ZnO with desired properties via a simplest method.

Many researchers have studied the synthesis of polymer nanocomposites using ZnO as inorganic fillers. Tjong and Liang (2006) prepared low-density polyethylene (LDPE)/ZnO composites via melt mixing process. ZnO powders with sizes of 200 nm and 2 μm were used. The dielectric and conductivity properties of the LDPE/ZnO composites as a function of ZnO volume fraction were investigated. The results showed that the dielectric constant of the composites reinforced with micro- and nanoparticles increases almost linearly with increasing ZnO volume content. However, the resistivity of the microcomposites showed a sharp decrease when the ZnO content was higher than18 vol% and the resistivity of nanocomposites started to decrease at lower ZnO content, i.e. 2.8 vol%.

Carrión *et al.* (2007) prepared polycarbonate (PC)/ZnO nanocomposites containing 0.1, 0.5, 1 and 5 wt% nanoparticles using simple conventional methods and determined the influence of ZnO nanoparticles on the thermal, mechanical and tribological properties of polycarbonate. Increasing the concentration of ZnO nanoparticles reduced the glass transition temperature and the degradation temperature of the nanocomposites with respect to neat PC. Then, the nanocomposites containing 0.5 and 1 wt% ZnO were selected for mechanical studies. PC with 0.5 wt% ZnO presented a higher modulus and similar tensile strength compared to neat PC, while a 74% reduction in the elongation at break. A ZnO concentration of 1 wt% dramatically reduced both the tensile strength and the elongation at break of PC. A 0.5 wt% proportion of ZnO nanoparticles increased hardness and reduced the wear rate with respect to neat PC, probably due to the effect of the filler agglomeration.

Zhao and Li (2006) studied the photo-degradation characteristics for ZnO nanoparticle filled polypropylene (PP) nanocomposites. Their research indicated that the incorporation of ZnO into PP matrix can impart significant improvements on the photo-degradation resistance of PP to UV irradiation. This performance was in accordance with the increase in nanoparticle content. Tensile test measurements indicated that the ZnO/PP nanocomposites remained ductile, with elongation at break values to be more than 500%, even with the incorporation of up to 5 wt% of ZnO nanoparticles. For UV irradiation treated nanocomposites, it was also observed that elongation at break values for UV-PP was only 4%, and increased in a proportional manner to the increase in ZnO nanoparticle content. This indicates that the presence of ZnO nanoparticles in the polymer composites can help to reduce the extent of photo-oxidation. Also, TGA measurements on unfilled PP and the PP/ZnO nanocomposites showed that, after UV irradiation, the ZnO/PP nanocomposites can maintain better thermal stability.

Another research that investigated photo-degradation properties of polymer composite was studied by Peng *et al.* (2008). In this experiment, ZnO-glass fiber-unsaturated polyester composites were prepared and, on exposure to the metal halide lamp, their resistance to UV degradation was evaluated. The results showed that ZnO can reduce the UV degradation of the unsaturated polyester matrix. ZnO can significantly retard the UV degradation process of the matrix resin, and can also increase the impact strength of the composites under the experimental conditions. Differential scanning calorimetry (DSC) analyses also indicated that the addition of ZnO to unsaturated polyester may retard the crosslink process and catalyzes the decomposition of the resin. When the content of ZnO reaches 6 wt%, the impact fracture mechanism changed abruptly and plastic deformation appeared, which indicated that 6 wt% for ZnO in unsaturated polyester could be considered as the critical content. The results also indicated that the proper content of ZnO added into the unsaturated polyester could prolong the durability and lessen the reject rate of transparent glass fiber-polyester composites.

Compared to other inorganic nanoparticles, ZnO is the best fillers to be used as photo stabilizer in polymer nanocomposites. Yang *et al.* (2005) confirmed this result. They study the photo-degradation of LLDPE modified with different nanofillers and/or light stabilizers, i.e. Al_2O_3, SiO_2 and ZnO. The experimental results indicated that all the nanofillers had positive effect on the photo-stabilization of LLDPE. Nevertheless, among them, ZnO had the best effect, while Al_2O_3 the least. In addition, the combination of two fillers had worse stabilization effect compared to a single nano-particle, which means unsynergism between fillers.

2.5 Linear Low Density Polyethylene (LLDPE) Nanocomposites

Linear low density polyethylene is one of the most versatile polymers, mainly due to its low density, good processability and low cost. However, its use is restricted because of several drawbacks, including lower strength and poor heat resistance. To overcome these drawbacks and to prepare materials with enhanced properties, in the past years LLDPE nanocomposites with several inorganic nanofilllers were prepared. An attractive feature of polymer nanocomposites is the promise of significantly improved stiffness and tensile strength, for a minor increase in specific gravity over the unmodified polymer. One of the few disadvantages associated with the use of nanofillers is their high cost. However, this negative effect is counterbalanced as only relatively small amounts (2–5%) of nanofillers are needed.

LLDPE is used extensively as packaging film due to its excellent mechanical properties, such as tear and impact strength as well as high tensile strength. LLDPE is a copolymer of ethylene and α-olefin, such as butene, hexene and octene. LLDPE consists of a linear backbone structure with little or no long chain branching as opposed to LDPE, which has a significant inclusion of long chain branches. However, despite all its attributes, LLDPE is not an ideal material even for films, where it is most commonly used. LLDPE polymerized by Ziegler–Natta catalysts contain a significant low molecular weight and n-hexane extractable constituent. In addition, they yield films which have low clarity and low gloss. LLDPE polymerized by metallocene catalysts have several advantages over that synthesized by Ziegler–Natta catalysts, such as strength, optical properties, narrow molecular weight distribution and low extractables, but are more difficult to process into films [Niaounakis and Kontou, 2005]. In general, the incorporation of fillers in LLDPE increases the elastic modulus of the material and can increase its tensile strength, but it almost invariably decreases the elongation at break [Osman *et al.*, 2005].

Kontou and Niaounakis (2006) prepared two series of linear low density polyethylene (LLDPE)/SiO_2 nanocomposites. They were based on two types of commercial LLDPE, one prepared by metallocene (mLLDPE) and the other by traditional Ziegler–Natta (zLLDPE) catalysts, and silica nanoparticles surface treated with dimethyldichlorosilane. The silica nanonparticles used have an average diameter of 16 nm, and their weight fraction varied from 2 up to 10%. The structure and thermal-mechanical features of the nanocomposites were characterized by scanning electron microscopy (SEM), differential scanning calorimetry (DSC), dynamic mechanical spectroscopy (DMA) as well as tensile tests. The effect of nanoparticles on crystallinity, and hence to the morphology of the materials was studied. The secondary transitions were also affected by the filler presence, while the tensile properties were reinforced with varying the nanoparticle weight fraction. The addition of the nanofillers brought up an increase in the elastic modulus and the tensile strengt of mLLDPE accompanied by an unusual dramatic increase in the elongation at break. The same trend, although to a lesser extent, was observed for the zLLDPE/SiO_2 composites. The increment of the elastic modulus of the composites with increasing filler content was simulated with three micromechanical models developed in previous works. The model which assumes an effective interface between the matrix and the nanoparticles provided the best fitting with the experimental data of mLLDPE/SiO_2.

The incorporation of nanosized fillers has been shown to have significant effects not only on some mechanical and thermo-mechanical properties, e.g. elastic modulus, heat distortion temperature (HDT), but also on the transparency and haze characteristics of LLDPE films. The possible use of these materials, i.e. polyolefin-based nanocomposites, as films for packaging and agriculture warrants a careful study of the nanoparticles effect on the polymer matrix UV stability. La Mantia *et al.* (2006) investigated the photo-oxidation of some polyolefin-based nanocomposites exposed to accelerated ageing in the absence and in the presence of different UV stabilizers. Benzotriazoles seem to provide the best stabilization. Interestingly, addition of a metal deactivator results in a more effective light stabilisation than that provided by the best UV stabilizer. Combination of a metal deactivator and UV absorber provides a synergistic effect.

In addition to inorganic materials, organic fillers, including carbon nanotube and clay, have been widely used in LLDPE nanocomposites. Carbon nanotubes (CNT) are a new class of materials that are known to possess excellent mechanical, electrical and thermal properties. Carbon nanotubes comprise a single sheet or sheets of graphite rolled into a cylinder several microns in length and a few nanometers in diameter. According to the number of graphite layers forming the tubes, carbon nanotubes are termed as single-walled (SWNT) or multiwalled (MWNT). MWNT are electrically conductive due to the graphite lattice whereas SWNT behave as conductors or semiconductors depending on the chirality of the graphite sheets. CNTs possess a very high aspect ratio up to 100–1000 and higher. It has been reported that CNTs are extremely strong with the strength of tens of GPa and exceptionally stiff with Young's modulus in TPa range, yet remarkably flexible with the breaking strain larger than 5%. These properties makes them promising as a reinforcement for composites. In addition, CNTs have excellent conductivity that makes them an ideal material for the production of conductive polymer composites, capable of dissipating the electrostatic charge or as shielding devices from the electromagnetic radiation. As in most fiber or particle reinforced materials, the effective utilization of nanotubes in the composite applications depends strongly on the ability to disperse the CNTs homogeneously throughout the matrix without destroying their integrity. Carbon nanotubes are strongly affected by Van der Waals forces due to their small size and large surface area. These forces give rise to the formation of aggregates, which in turn make dispersion of CNTs in polymers difficult.

Aalaie *et al.* (2007) prepared LLDPE/multiwalled carbon nanotube (MWNT) nanocomposites via melt blending. The morphology and degree of dispersion of nanotubes in the polyethylene matrix were investigated using scanning electron microscopy (SEM). Both individual and agglomerates of MWNTs were evident. The rheological behavior and mechanical and electrical properties of the nanocomposites were studied using a capillary rheometer, tensile tester, and Tera ohm-meter, respectively. Both polyethylene and its nanocomposites showed non- Newtonian behavior in almost the whole range of shear rate. Addition of carbon nanotubes increased shear stress and shear viscosity. It was also found that the materials experience a fluid-solid transition below 1 wt% MWNT. Flow activation energy for the nanocomposites was calculated using an Arrhenius type equation. With increasing nanotube content, the activation energy of flow increases. A decrease of about 7 orders of magnitude was obtained in surface and volume resistivity upon addition of 5 wt% MWNT. In addition, a difference between electrical and rheological percolation thresholds was observed. The results confirm the expected nucleant effect of nanotubes on the crystallization process of polyethylene. A slight increase in Young’s modulus was also observed with increasing MWNT content.

Polymer–clay nanocomposites are known to display awide range of improved properties. Incorporation of nanosized fillers in thermoplastics results in significant effects not only on thermomechanical properties but also on transparency and film barrier properties. The photochemical behaviour of polyolefin–clay nanocomposites is of prime importance as the durability is the key factor for outdoor applications such as films for packaging and agriculture. Morlat-Therias *et al.* (2008) studied the chemical modifications of LLDPE/organo-clay nanocomposites that were exposed to UV light in conditions of artificially accelerated aging and natural weathering. Analysis by infrared spectroscopy of the chemical modifications produced by photo-aging showed that the presence of an organo-clay led to the decrease of the oxidation induction time of the polymer (LLDPE), which resulted in lower durability of the nanocomposites.

Protection against photo-oxidation was tested with different kinds of UV stabilizers and with a metal deactivator. It was shown that the metal deactivator was very efficient in stabilizing the nanocomposite since it totally canceled the prodegradant effect of the organo-clay. This confirms the role played by iron impurities in natural clays. The use of a metal deactivator offers a new insight into the stabilization strategy for polymer nanocomposites.

CHAPTER III

EXPERIMENTAL

3.1 Research objectives

- To synthesize and characterize LLDPE/ZnO nanocomposites using metallocene catalyst via *in situ* polymerization of ethylene/1-octene
- To investigate the effect of catalyst preparation method on catalytic activities and properties of polymer nanocomposites

3.2 Research scopes

- Characterization of ZnO nanoparticles by X-ray diffraction (XRD), scanning electron microscopy (SEM) and transmission electron microscopy (TEM)
- Calcination of ZnO nanoparticles
- Preparaion of catalyst precursors via 3 different methods; (i) impregnation of MAO onto ZnO support; (ii) activation of ZnO support with zirconocene; and (iii) introduction of both MAO and zirconocene to the ZnO support.
- Characterization of the catalyst precurors using scanning electron microscopy (SEM), energy dispersive X-ray spectroscopy (EDX), and thermogravimetric analysis (TGA)
- Synthesis of LLDPE/ZnO nanocomposites with *rac*-$Et(Ind)_2ZrCl_2$/MAO catalysts by *in situ* polymerization of ethylene/1-octene at T = 70 °C; [ethylene] = 0.018 mol; $[Al]_{MAO}/[Zr]_{zirconocene} = 1135$; $[Al]_{TMA}/[Zr]_{zirconocene} = 2500$; in toluene with total volume of 30 ml
- Characterization of the LLDPE/ZnO nanocomposites with scanning electron microscopy (SEM), ^{13}C nuclear magnetic resonance spectrometer (^{13}C NMR) and X-ray diffraction (XRD)

3.3 Research methodology

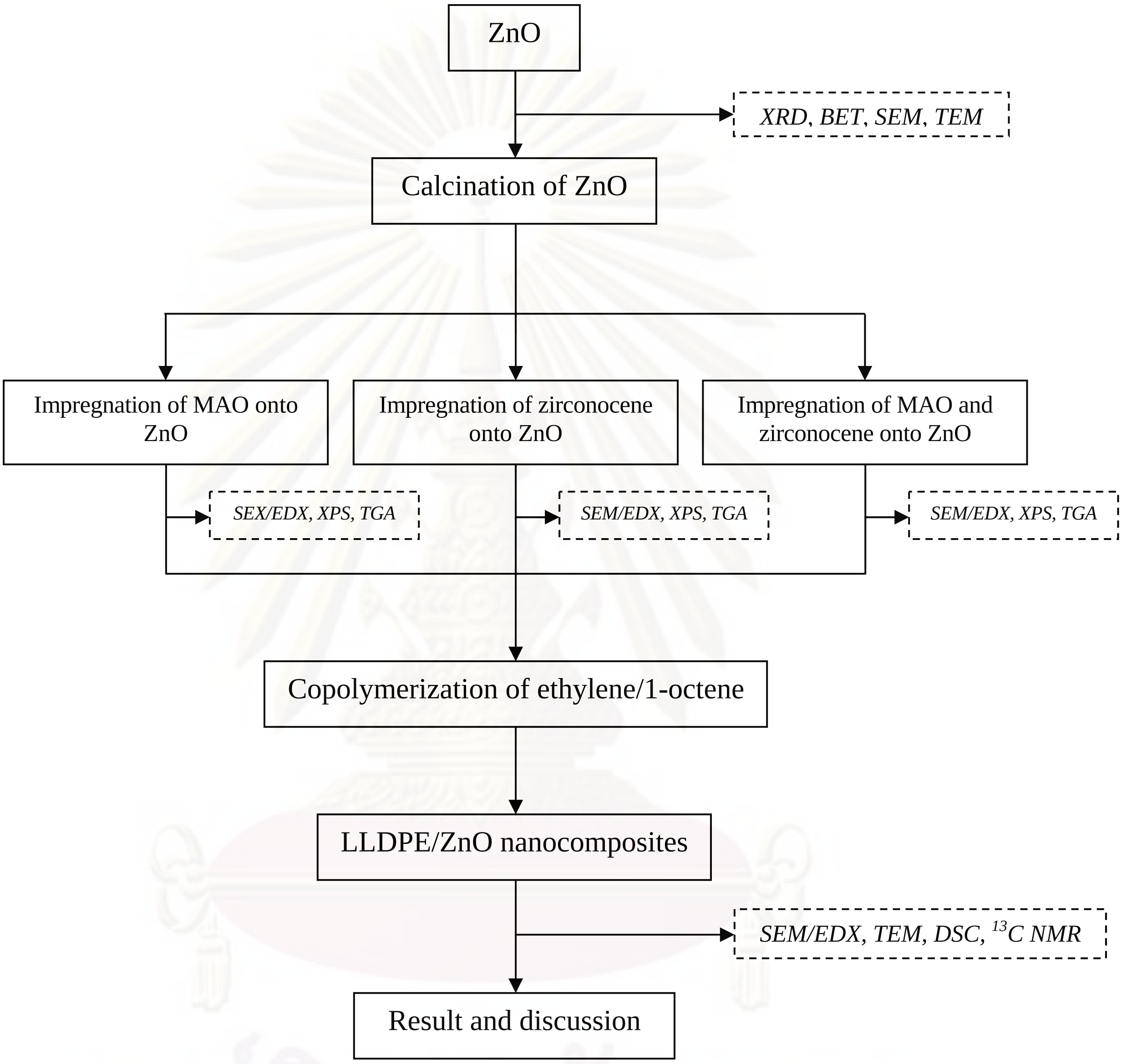

Figure 3.1 Flow diagram of research methodology

3.4 Chemicals

The chemicals that were used in this work are list as follows:

- Ethylene gas (99.96%) was donated from PTT Chemical Plc., Thailand and used as received.
- 1-Octene (97%) was purchased from Aldrich Chemical Company, Inc. and purified by distilling over sodium under argon atmosphere before use.
- 1-Hexane (95%) was purchased from Aldrich Chemical Company, Inc. and purified by distilling over sodium under argon atmosphere before use.
- Toluene (Commercial grade) was purchased from SR lab. This solvent was dried over dehydrated $CaCl_2$ and distilled over sodium/benzophenone under argon atmosphere before use.
- Methylaluminoxane (MAO) 2.0 M in toluene was donated from PTT Chemical Plc., Thailand and used without further purification.
- Trimethylaluminum (TMA) 2.0 M in toluene was supplied from Nippon aluminum Alkyls Ltd., Japan and used without further purification.
- Zinc oxide was purchased from Aldrich Chemical Company, Inc. and used as received
- Methanol (Commercial grade) was purchased from SR lab and used as received.
- Sodium lump (99%) in kerosene was purchased from Aldrich Chemical Company, Inc. and used as received.
- Benzophenone (99%) was purchased from Aldrich Chemical Company, Inc. and used as received.
- Calcium hydride (99%) was purchased from Fluka Chemie A.G. Switzerland and used as received.
- Ultra high purity argon gas (99.999%) was purchased from Thai Industrial Gas Co., Ltd., (TIG) and further purified by passing through columns packed with molecular sieve 3A, BASF Catalyst R3-11G, sodium hydroxide (NaOH) and phosphorus pentaoxide (P_2O_5) to remove traces of oxygen and moisture.

3.5 Equipments

Because metallocene system is extremely sensitive to the oxygen and moisture, the special equipments were required for the preparation and polymerization process. For example, glove box equipped with the oxygen and moisture protection system will be used to produce the inert atmosphere. Schlenk techniques (vacuum and purge with inert gas) are the others set of equipment that will be used to handle air-sensitive product.

- Inert gas supply

The inert gas (argon) was passed through columns of BASF catalyst R3-11G as oxygen scavenger, molecular sieve 3×10^{-10} m to remove moisture. The BASF catalyst was regenerated by treatment with hydrogen at 300 °C overnight before flowing of the argon gas through all of the columns mentioned above.

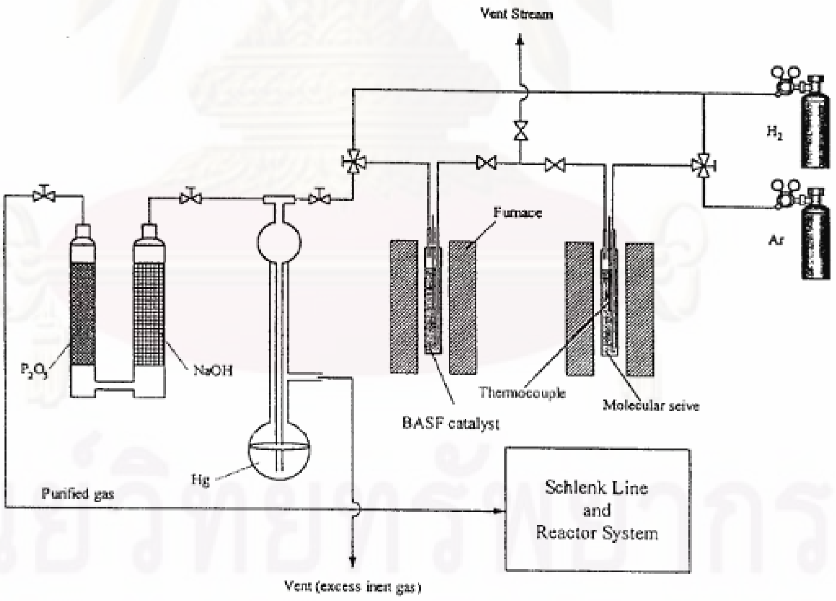

Figure 3.2 Inert gas supply system

- Cooling system

The cooling system is used in the solvent distillation in order to condense the evaporated solvent.

- Schlenk tube

Schlenk tube is a tube with a ground glass joint and side arm, which is three-way glass valve. Schlenk tubes having size of 50, 100 and 200 ml were used to prepare catalyst and store materials which are sensitive to oxygen and moisture

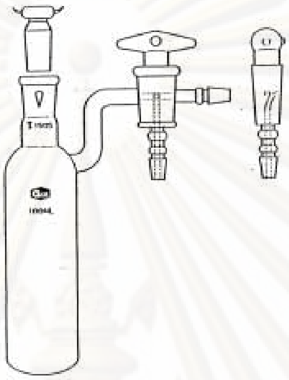

Figure 3.3 Schlenk tube

- Schlenk line

Schlenk line consists of vacuum and argon lines. The vacuum line was equipped with the solvent trap and vacuum pump, respectively. The argon line was connected with the trap and the mercury bubbler which is a manometer tube and contains enough mercury to provide a seal from the atmosphere when argon line was evacuated.

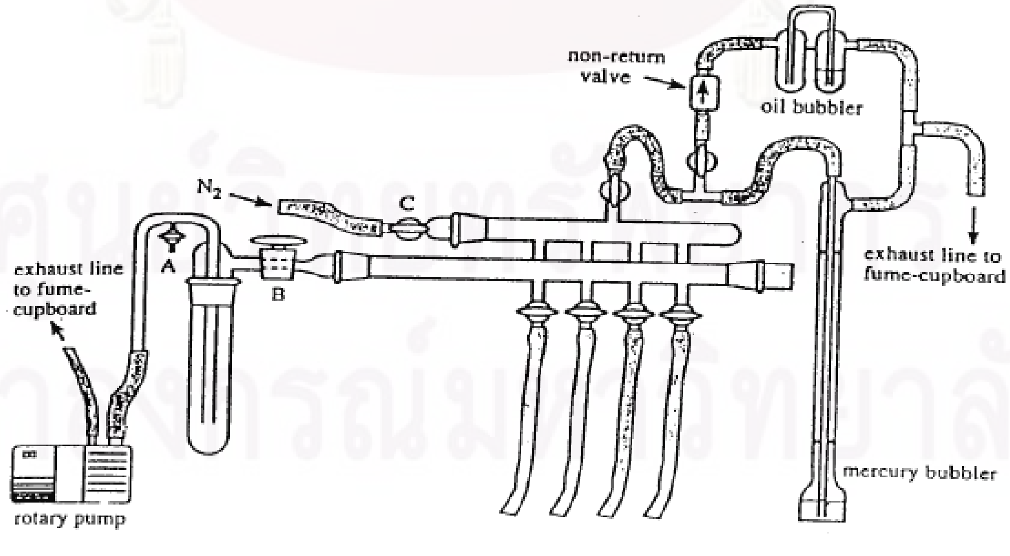

Figure 3.4 Schlenk line

- Magnetic stirrer and heater

The magnetic stirrer and heater model RTC basis from IKA Labortechnik were used.

- Reactor

A 100 ml semi-batch stainless steel autoclave equipped with magnetic stirrer was used as the copolymerization reactor for high pressure systems.

- Vacuum pump

The vacuum pump model 195 from Labconco Corporation was used. A pressure of 10^{-1} to 10^{-3} mmHg is adequate for the vacuum supply to the vacuum line of Schlenk line.

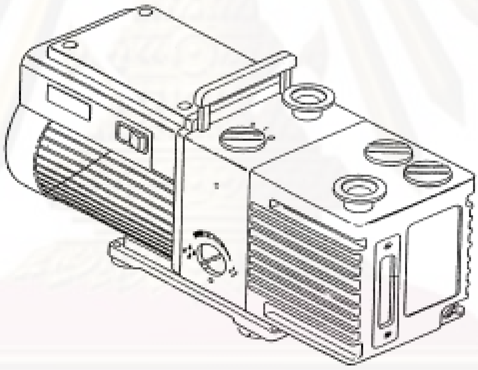

Figure 3.5 Vacuum pump

- Polymerization line

Polymerization line is composed of ethylene storage tank, pressure regulator for ethylene consumption, mass flow meter, 100 ml semibatch stainless steel autoclave reactor equipped with magnetic stirrer, thermometer, water bath, hot plate and other fittings. This system is schematically represented in Figure 3.6.

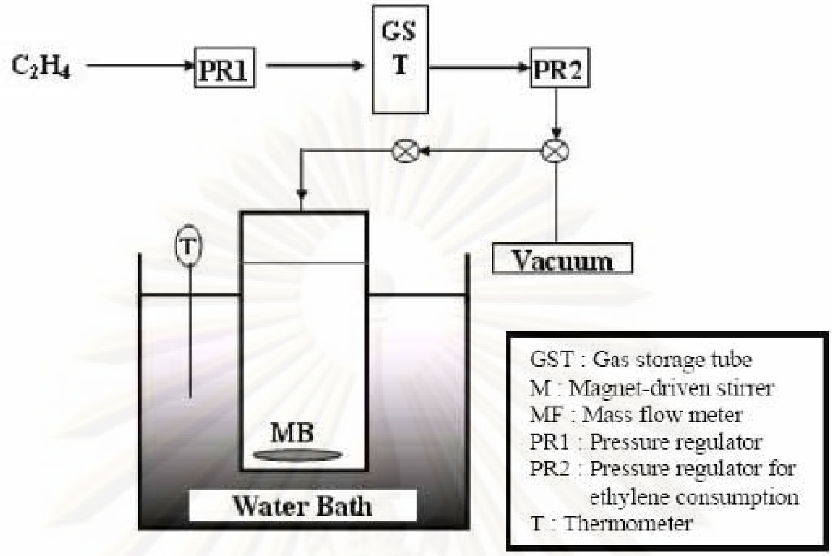

Figure 3.6 Diagram of system used in slurry phase polymerization

3.6 Characterization instruments

- X-ray diffraction analysis (XRD)

The X-ray diffraction (XRD) patterns of zinc oxide were performed using an X-ray diffractometer SIEMENS D5000 connected to a personal computer with Diffract AT version 3.3 program for fully control of the XRD analyzer at Center of Excellence on Catalysis and Catalytic Reaction Engineering, Chulalongkorn university. The experiments were carried out by using CuK_α radiation with Ni filter and the operating conditions for measurement is shown below.

2θ range of detection : 20 – 80°
Resolution : 0.04°
Number of scan : 10

The functions of based line subtraction and smoothing will be used in order to get the well formed XRD spectra.

- Scanning electron microscopy (SEM) and energy dispersive X-ray spectroscopy (EDX)

The morphology and crystallite size of secondary particles of zinc oxide were observed on a JEOL JSM6400 Scanning Electron Microscopy (SEM) at Scientific and Technological Research Equipment Center (STREC), Chulalongkorn University.

- Transmission electron microscopy (TEM)

Morphology of LLDPE/ZnO nanocomposites, and crystallite size and shape of primary particles of zinc oxide were observed by using a JEOL JEM1220 transmission electron microscopy (TEM) operated at 80 kV at Kasetsart University Research and Development Institute.

The specimens for TEM were prepared by putting the as-grown products in ethanol and immersing them in an ultrasonic bath for 15 minutes, then dropping a few drops of the resulting suspension containing the synthesized materials onto a TEM grid.

- Thermogravimetric analysis (TGA)

TGA was used to determine interaction between MAO as well as zirconocene and support in term of weight loss of catalyst precursors after impregnation. About 2 – 3 mg of each sample was analyzed by thermogravimetric and differential thermal analysis, PerkinElmer Thermal Analysis Diamond TG/DTA at Center of Excellences on Catalysis and Catalytic Reaction Engineering, Chulalongkorn University. The furnace was heated from 50 °C to 800 °C at a constant rate of 10 °C min^{-1} and then cooled naturally. The whole TG/DTA measurements were made under nitrogen gas at gas flow rate of 100 mL min^{-1}.

- Differential scanning calorimetry (DSC)

The melting temperature of ethylene/1-octene copolymers was determined with a Perkin-Elmer diamond DSC from MEKTEC, at the Center of Excellence on Catalysis and Catalytic Reaction Engineering, Chulalongkorn University. The analyses were performed at the heating rate of 20 °C min^{-1} in the temperature range of 50 – 150 °C. The heating cycle was run twice. In the first scan, sample was heated and the cooled to room temperature and then samples was reheated at the same rate in the second scan. However, only the results of the second scan were reported because the first scan was influenced by the mechanical and thermal history of samples.

- ^{13}C nuclear magnetic resonance spectrometer (^{13}C NMR)

The ^{13}C NMR spectra were recorded at 100 °C using JEOL JNM-A500 operating at 125 MHz. The copolymer solutions were prepared by using 1,2,4-trichlorobenzene as solvent and chloroform-d for internal lock.

3.7 Catalyst preparation method

The catalyst precursors were prepared by drying ZnO nanoparticles *in vacuo* to remove the physically absorbed water and then suspended in toluene to react with methylaluminoxane (MAO) for 30 min at room temperature. Then, it was washed three times with toluene to remove the unreact MAO. A solution of zirconocene, *rac*-Et[Ind]$_2$ZrCl$_2$, in toluene was added to the treated ZnO and the mixture was stirred for 30 min at room temperature. Then, the mixture was dried *in vacuo* after being washes three times with toluene. For comparative study, the sequence of support impregnation was changed in order to examine the effect of different catalyst preparation methods on the catalytic activities and properties of copolymer; namely, (i) impregnation of MAO onto ZnO; (ii) activation of ZnO with zirconocene; and (iii) introduction of both MAO and zirconocene to the ZnO support. The diagram of catalyst preparation procedure is shown on Figure 3.7.

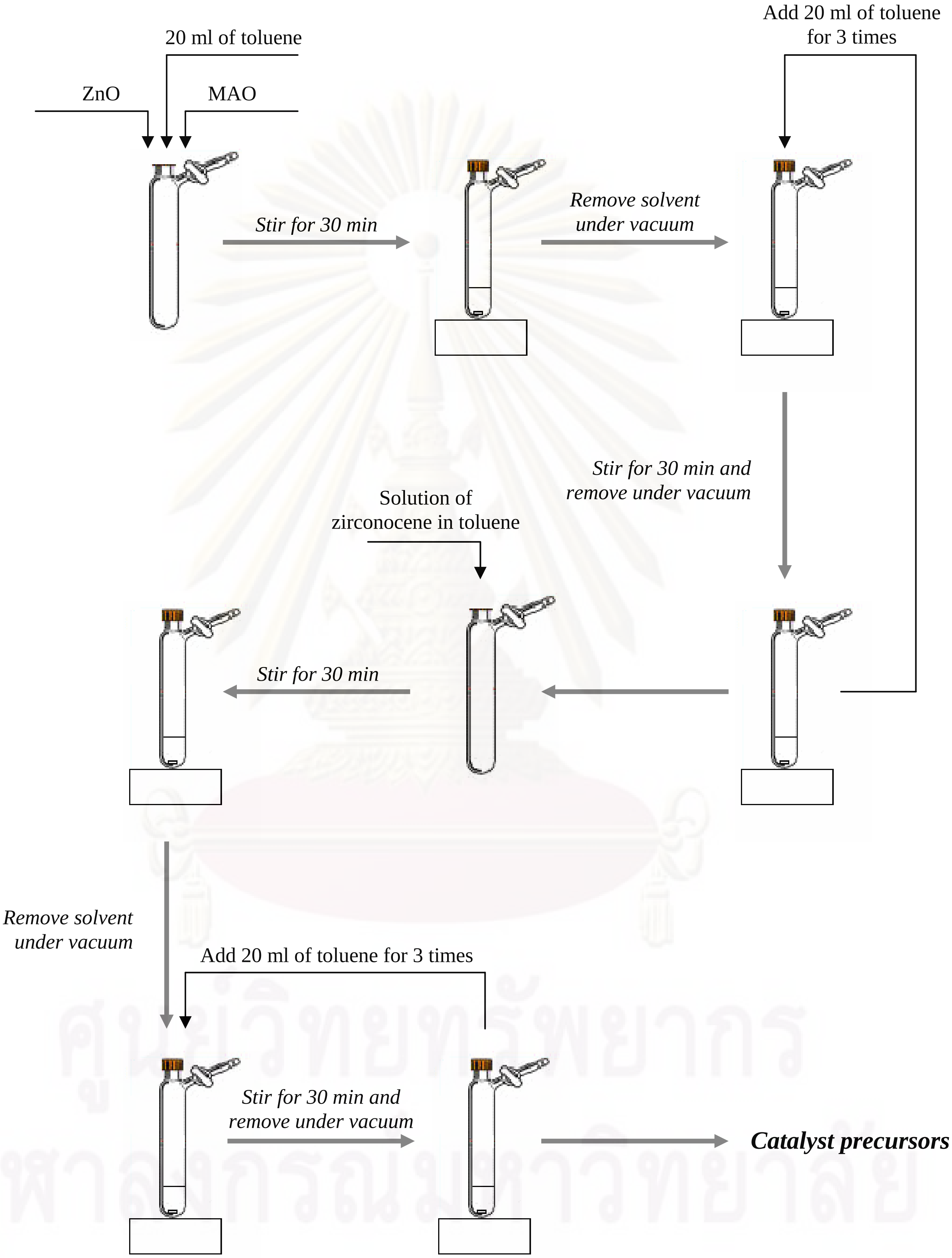

Figure 3.7 Diagram of catalyst preparation procedure

3.8 Polymerization procedure

The copolymerization of ethylene/1-olefin was carried out in a 100 ml semibatch stainless steel autoclave reactor equipped with magnetic stirrer. The desired amount of catalyst precursors prepared in the preceding step was introduced into the reactor. Then, toluene (to make a total volume of 30 ml) and TMA was injected into the reactor. The reactor was frozen in liquid nitrogen to stop reaction and then the appropriate amount of mol of 1-olefin was injected into the reactor. The autoclave was evacuated to remove the argon. After that, the reactor was heated up to polymerization temperature (70 °C) and the reaction was started by feeding ethylene gas (total pressure of 50 psi in the reactor) until the consumption of ethylene at 0.018 mol (a decrease in ethylene pressure of 6 psi was observed) was reached. The polymerization reaction was terminated by addition of acidic methanol (0.1% HCl in methanol). The reaction time was recorded for purpose of calculating the activity. The precipitated polymer was washed with methanol and dried at room temperature for further characterization. The polymerization procedure is diagrammatically represented in Figure 3.8.

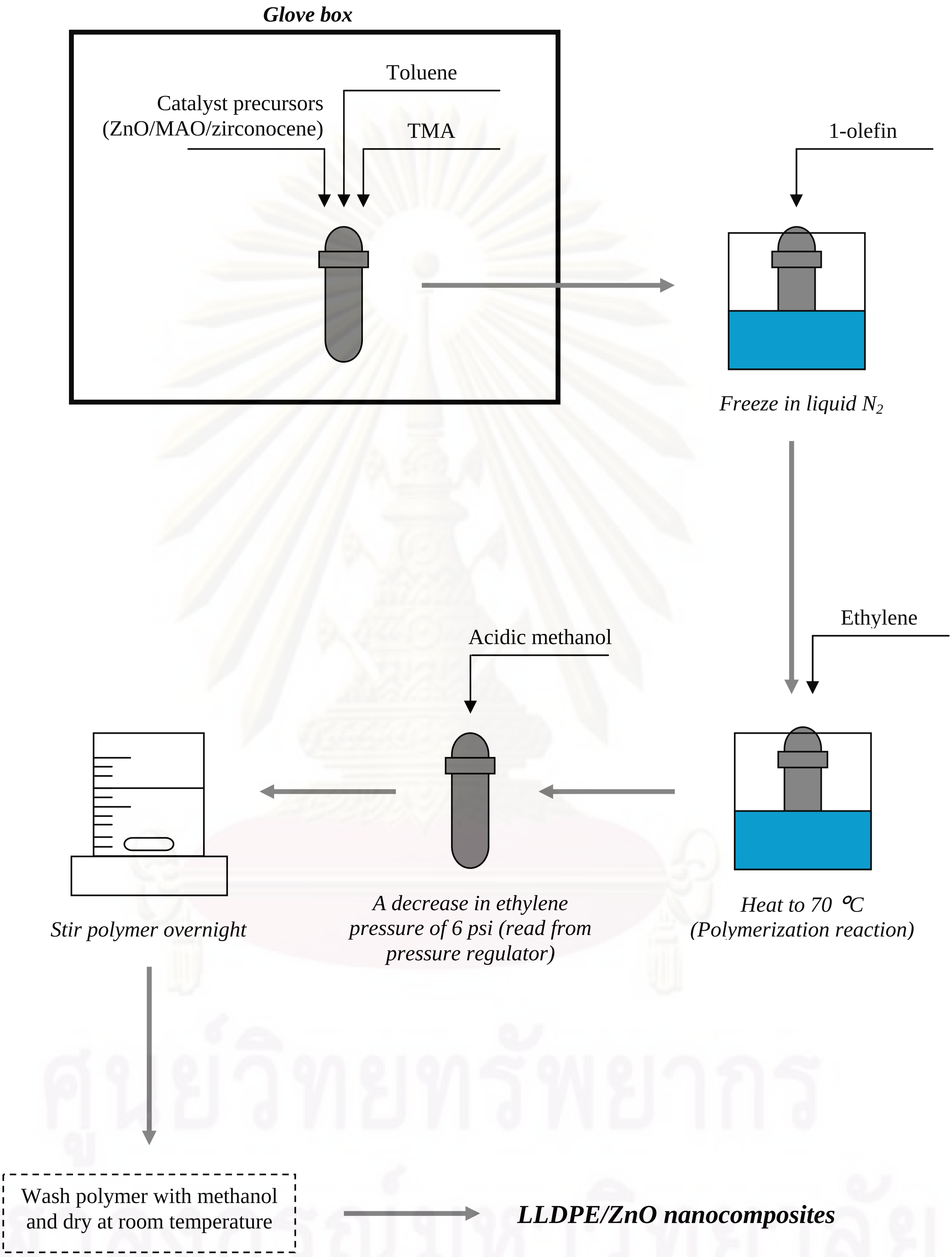

Figure 3.8 Diagram of polymerization procedure

CHAPTER IV

RESULTS AND DISCUSSION

In the present study, LLDPE/ZnO polymer nanocomposites were synthesized via *in situ* polymerization of ethylene/1-octene with zirconocene/MAO catalyst. The catalyst precursors were prepared via three different impregnation methods. The effect of catalyst preparation method on catalytic activities and properties of copolymer was investigated. In addition, the effect of initial comonomer content in ethylene/1-octene copolymerization was investigated to determine both the catalyst performance and the properties of LLDPE/ZnO polymer nanocomposites.

In this chapter, the results and discussion are divided into 3 sections. First, the characterization of ZnO nanofillers is presented in section 4.1. Next, the characterization of catalyst precursors prepared via different methods is present and discussed in section 4.2. LLDPE/ZnO nanocomposites synthesized by *in situ* polymerization of ethylene/1-octene with various initial contents of 1-octene are discussed in section 4.3. Finally, LLDPE/ZnO polymer nanocomposites using ZnO prepared via different impregnation methods are present and discussed in section 4.3.

4.1 Characterization of zinc oxide (ZnO) nanoparticles

In this research, ZnO was used as an inorganic supports for heterogeneous metallocene system. First of all, the XRD pattern of ZnO nanopowders is shown in Figure 4.1. All peaks of the sample (approximately indexed to 2θ values of 32°, 34°, 36°, 47°, 57°, 63°, 66°, 68° and 69°) are corresponding to the hexagonal wurtzite structure of ZnO with lattice parameters a and c of 3.24 and 5.19 Å, respectively. No peak from either ZnO in other phases or impurities is observed.

Figure 4.2 shows SEM image of the ZnO nanoparticles. It is observed that morphology of particles is nearly spherical ZnO with particle size of approximately 100 nm. However, from TEM image of ZnO nanoparticles as shown in Figure 4.3, it is obvious that the primary particles of ZnO are in various sizes and shapes. In addition, the result form N_2 physisorption technique (BET) indicated that ZnO has surface area of 19.34 m^2/g.

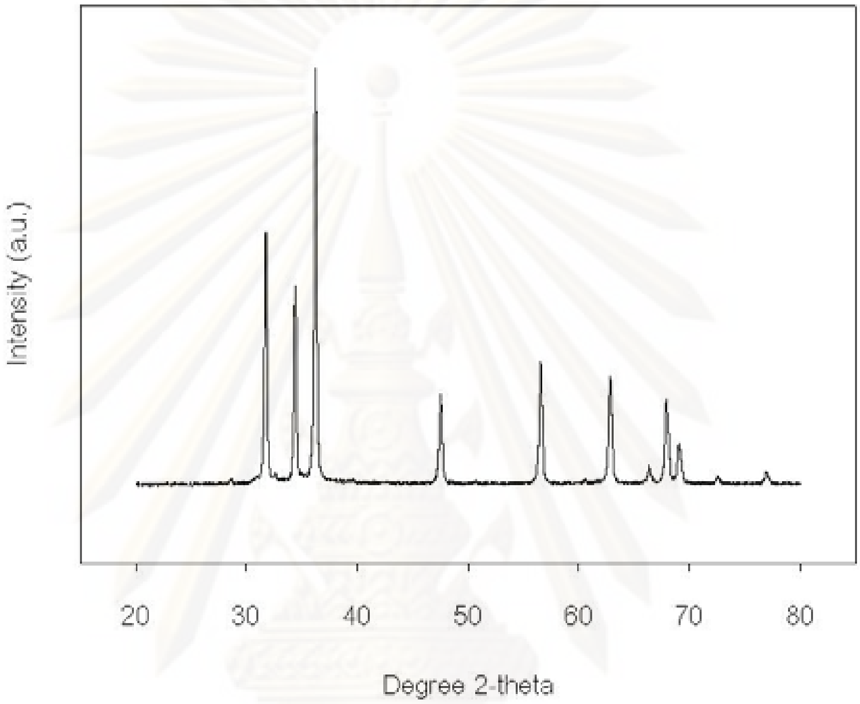

Figure 4.1 XRD patterns of ZnO nanoparticles

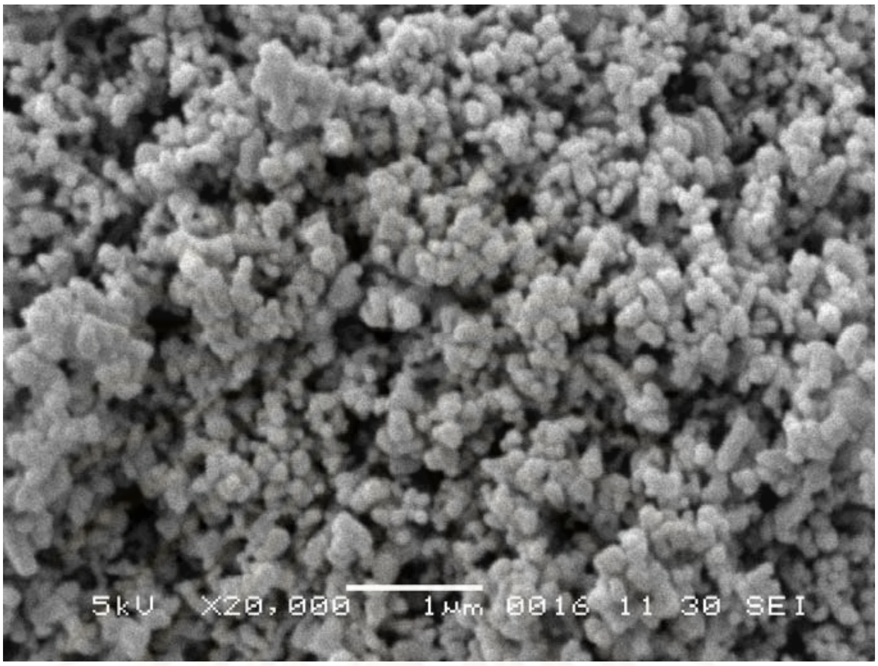

Figure 4.2 SEM images of ZnO nanoparticles

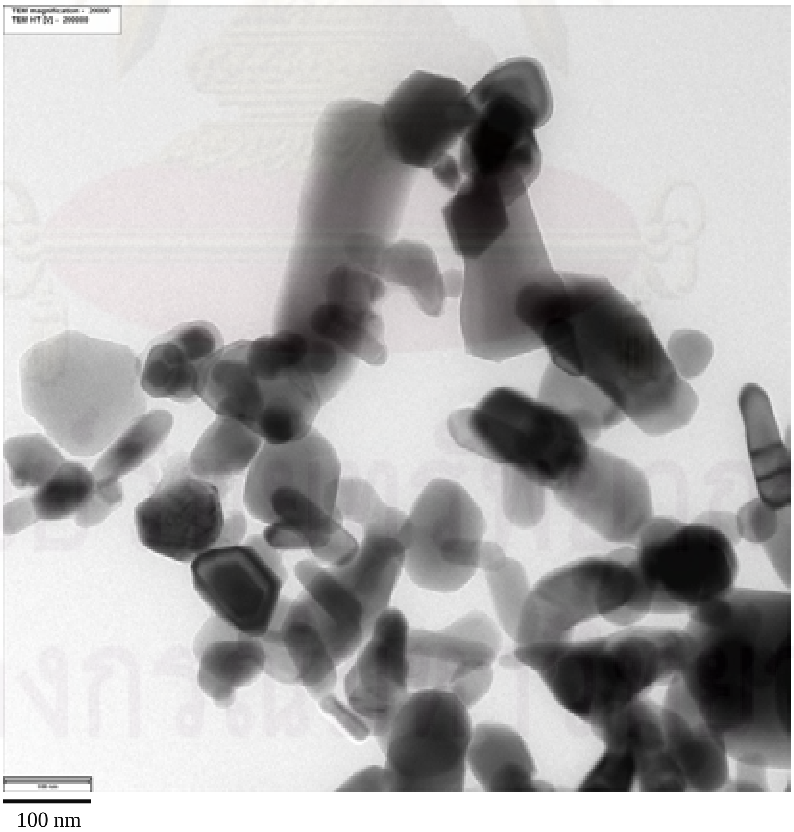

Figure 4.3 TEM images of ZnO nanoparticles

4.2 Characterization of catalyst precursors

After the characteristics of ZnO nanoparticles were determined, the catalyst precursors were prepared via three different impregnation methods as follows: (i) activation of ZnO support with MAO, designated as ZnO/Al; (ii) impregnation of zirconocene onto ZnO, designated as ZnO/Zr; and (iii) introduction of both MAO and zirconocene to the ZnO support, designated as ZnO/Al/Zr. Thereafter, the catalyst precursors were characterized using various techniques to determine morphology of catalyst precursors, the amount of $[Al]_{MAO}$ and $[Zr]_{zirconocene}$ present on the ZnO support, the distribution of MAO and zirconocene onto the different catalyst precursors and the interaction between catalyst and ZnO support.

4.2.1 Characterization of catalyst precursors using transmission electron microscopy (TEM)

In order to determine the dispersion of ZnO before and after impregnation, a more powerful technique such as transmission electron microscopy (TEM) was applied. The TEM micrographs of ZnO nanoparticles before and after impregnation with MAO and zirconocene are shown in Figure 4.4. It can be observed that all ZnO nanoparticles exhibit agglomeration and present as a group of secondary particles. There was also no significant change upon the particle morphology after impregnation. Furthermore, it is apparent that the crystallite size of primary particles examined using TEM was 100 nm, approximately.

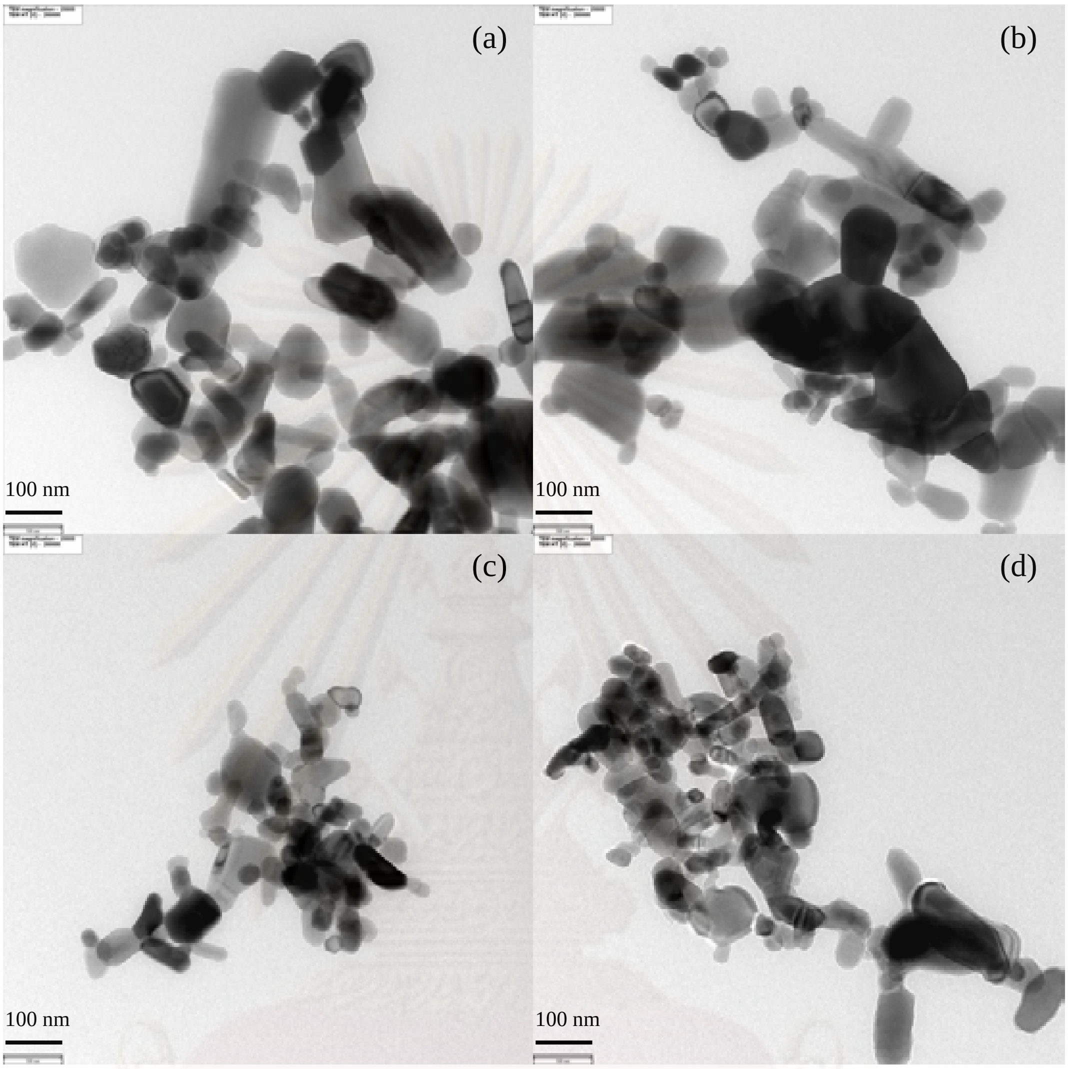

Figure 4.4 TEM micrographs of different catalyst precursors: (a) ZnO nanoparticles before impregnation; (b) ZnO/Al; (c) ZnO/Zr; and (d) ZnO/Al/Zr

4.2.2 Characterization of catalyst precursors using scanning electron microscopy (SEM) and energy dispersive X-ray spectroscopy (EDX)

SEM and EDX were performed to study the morphology and distribution of MAO or zirconocene onto the catalyst precursors, respectively. All samples apparently exhibited the similar morphologies. It can be observed that both MAO and zirconocene were well distributed over the ZnO support. Based on the EDX measurement, the amounts of $[Al]_{MAO}$ and $[Zr]_{zirconocene}$ present on catalyst precursors were determined as shown in Table 4.1

Table 4.1 Average amount of $[Al]_{MAO}$ and $[Zr]_{zirconocene}$ present in catalyst precursors prepared via different impregnation methods

Catalyst precursors	Average weight % of $[Al]_{MAO}$	Average weight % of $[Zr]_{zirconocene}$
ZnO/Al	17.97	-
ZnO/Zr	-	2.42
ZnO/Al/Zr	22.96	2.17

Besides the content of $[Al]_{MAO}$ and $[Zr]_{zirconocene}$ in supports, the distribution of $[Al]_{MAO}$ and $[Zr]_{zirconocene}$ on supports should be considered. The elemental distribution was also performed using EDX mapping. The distribution of $[Al]_{MAO}$ and $[Zr]_{zirconocene}$ in the various supports is shown in Figure 4.5. As seen, all samples exhibited good distributions of Al and Zr without any changes in the support morphology.

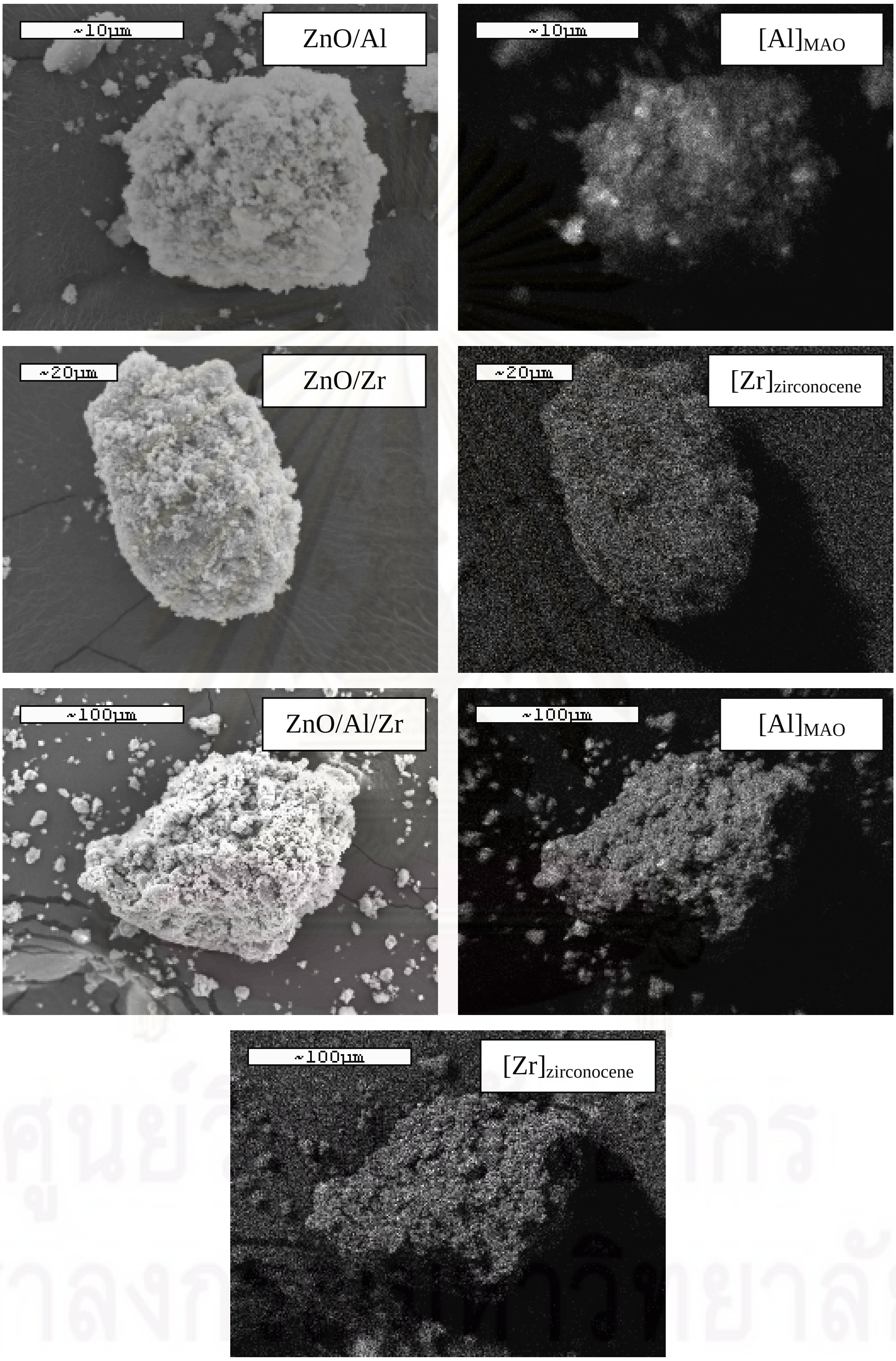

Figure 4.5 SEM micrographs and EDX mappings of different catalyst precursors

4.2.3 Characterization of catalyst precursors using X-ray photoelectron spectroscopy (XPS)

XPS is one of the most powerful techniques used for many applications in surface analysis, so it is also interesting to extend the use of XPS to determine the structure of catalyst precursors and the amounts of $[Al]_{MAO}$ and $[Zr]_{zirconocene}$ present on these catalyst precursors. The binding energy (BE) as well as the atomic and mass concentrations of $[Al]_{MAO}$ and $[Zr]_{zirconocene}$ at surface (the penetration depth for XPS is ca. 5 nm) are shown in Table 4.2.

Table 4.2 Elemental distribution on the surface of catalyst precursors and the binding energy measured using XPS

Catalyst precursors	Peak	B.E. (eV)	Atomic conc. (%)	Mass Conc. (%)
ZnO/Al	Zn 2p	1022.6	2.71	8.70
	Zn 2p (2)	1045.5	1.24	3.99
	O 1s	532.1	74.10	58.22
	Al 2p	74.6	21.95	29.09
ZnO/Zr	Zn 2p	1022.5	15.03	36.67
	Zn 2p (2)	1045.3	6.85	16.72
	O 1s	530.9	22.75	13.58
	O 1s (2)	532.6	55.36	33.04
ZnO/Al/Zr	Zn 2p	1022.8	0.66	2.16
	Zn 2p (2)	1045.9	0.36	1.18
	O 1s	531.7	67.84	54.48
	Al 2p	74.4	31.14	42.18

The XPS measurements shows that all the catalyst precursors exhibit two peaks of Zn $2p_{3/2}$ and Zn $2p_{1/2}$ around 1022.8 and 1045.7 eV, respectively, which are assigned to the lattice zinc in zinc oxide. The peak separation between these two peaks is 22.9 eV. These values correspond to the binding energy of Zn (II) ion. The small shift in peak position indicates a change of microenvironments for zinc [Wang *et al.*, 2010]. From Table 4.2, the O 1s peak at about 531.8 eV is due to the ZnO crystal lattice oxygen [Koudelka *et al.*, 1984]. However, the O 1s peak split into two peaks at 530.9 and 532.6 eV assigned to an oxygen deficiency of ZnO crystal lattice. These results form XPS technique led to the conclusion that impregnation of MAO and zirconocene onto ZnO nanoparticles did not alter the structure of ZnO. In addition, the binding energy of Al 2p core-level of $[Al]_{MAO}$ was measured. A typical XPS profile of Al 2p exhibits the BE of 74.6–74.8 eV. These values were also in accordance with the MAO present on the silica support, as reported by Hagimoto *et al.* (2004). Such results suggested that there is no significant change in the oxidation state of $[Al]_{MAO}$ occurred upon the impregnation procedure. Surprisingly, from this technique, there is no XPS spectra of Zr which is probably due to $[Zr]_{zirconocene}$ being present more deep into catalyst particles. As a result, it cannot be detected by XPS technique which the penetration depth is ca. 5 nm. Nevertheless, $[Zr]_{zirconocene}$ can be measured using EDX measurement which is more bulk technique.

Besides the BE obtained from XPS, the amounts of $[Al]_{MAO}$ and $[Zr]_{zirconocene}$ atomic and mass concentrations at surface (the penetration depth for XPS is ca. 5 nm) were also determined as shown in Table 4.2. It can be seen that a small amount of Zn is present on the surface of both ZnO/Al and ZnO/Al/Zr, which is much smaller than Al and O. This is due to the fact that MAO is a compound in which aluminum and oxygen atoms are arranged alternately. The basic units, -[Al(CH_3)-O-]-, join together forming cluster and cage structure of MAO [Kaminsky and Laban 2001; Reddy and Sivaram, 1995]. As a result, MAO locates at the majority of surface. Moreover, there is an interaction between MAO and zirconocene in ZnO/Al/Zr resulting in the lower amount of Zn at the surface of ZnO/Al/Zr compared with ZnO/Al.

4.2.4 Characterization of catalyst precursors using thermogravimetric analysis (TGA)

Besides the amount of $[Al]_{MAO}$ and $[Zr]_{zirconocene}$ being present on the ZnO nanoparticles, the interactions between them are also important to consider. In fact, the strong interaction of the active species with ZnO nanoparticles employed in this study is essentially referred to the interactions between the ZnO nanoparticles and the MAO cocatalyst as well as zirconocene. Based on this study, MAO and zirconocene were impregnated onto the ZnO support prior to polymerization. The degree of interactions between them can be possibly determined by the TGA measurement. In particular, the TGA can only provide useful information on the degree of interactions for the MAO and zirconocene that were bound to the ZnO nanoparticles in terms of the weight loss and removal temperature. The stronger interaction, in case of ZnO/Al, can result in the more difficulty for the MAO to react with Zr-complex during activation processes, leading to lower catalytic activity for polymerization [Ketloy *et al.*, 2007]. The TGA measurement was performed in order to examine the interaction between the $[Al]_{MAO}$ as well as $[Zr]_{zirconocene}$ and ZnO support. The TGA profiles of all catalyst precursors are shown in Figure 4.6, indicating that ZnO/Al and ZnO/Al/Zr have similar profiles while TGA profile of ZnO/Zr differs from the others. It is observed that the weight losses of catalyst present on various supports are in the order of ZnO/Al/Zr (16%) > ZnO/Al (14%) > ZnO/Zr (2%). The species having strong interaction with the support were removed at ca. 310 °C for ZnO/Al and ZnO/Al/Zr. However, from derivative weight profile, there were two peaks that overlapped between ca. 310 and 400 °C for ZnO/Al indicating that more species were removed at higher temperature. On the other hand, ZnO/Al/Zr did not show this overlap peak which pointed out that zirconocene may inhibit some species to be removed. In case of ZnO/Zr, the weight loss was only 2 wt%. This result is because $[Zr]_{zirconocene}$ was present deep into the catalyst particles, therefore, it is difficult to be removed. This characteristic was confirmed by EDX and XPS measurements. It should be noted that the weight losses at ca. 100 °C for all the catalyst precursors is due to the loss of sample humidity and organic solvent.

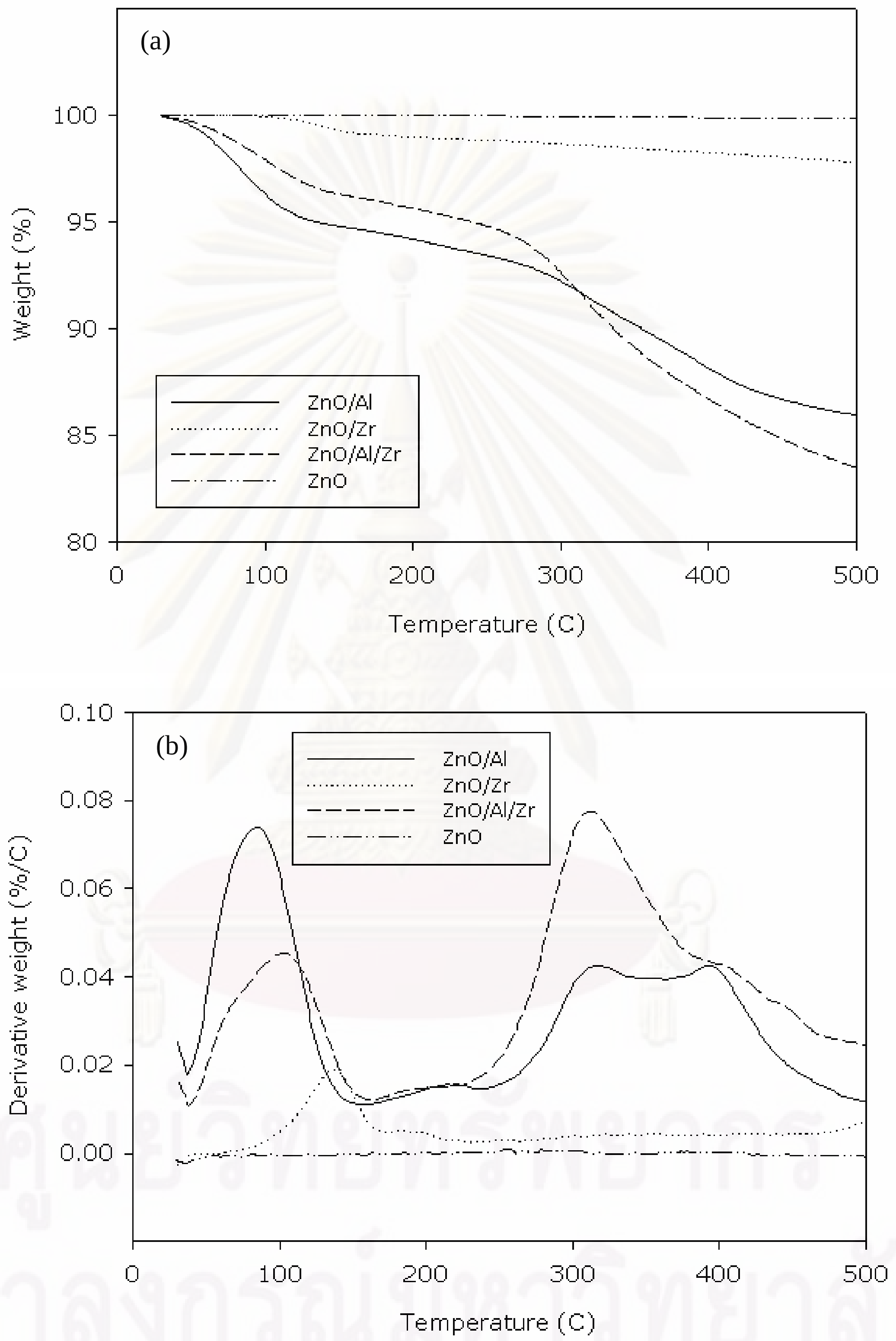

Figure 4.6 TGA profiles of various catalyst precursors: (a) weight; and (b) derivative weight

4.3 LLDPE/ZnO nanocomposites synthesized by *in situ* polymerization of ethylene/ 1-octene with various initial contents of 1-octene

LLDPE/ZnO nanocomposites were synthesized by *in situ* polymerization using ZnO prepared via three different impregnation methods as support for heterogeneous metallocene system. As mentioned earlier, these impregnation procedures includes: (i) activation of ZnO support with MAO; (ii) impregnation of zirconocene onto ZnO; and (iii) introduction of both MAO and zirconocene to the ZnO support. Each catalyst precursor is designated as ZnO/Al, ZnO/Zr and ZnO/Al/Zr, respectively. Based on EDX measurements, the amounts of $[Al]_{MAO}$ and $[Zr]_{zirconocene}$ present on each catalyst precursor can be determined as shown in Table 4.1.

After impregnation with MAO and zirconocene to obtain the catalyst precurcors, the *in situ* polymerization of ethylene/1-octene was performed with the presence of these catalyst precursors in order to produce the LLDPE/ZnO nanocomposites. As well-known, the properties of polymer nanocomposites strongly depend on the filler content, so it is reasonable to fix the amount of catalyst precursors at 0.1 g. Based on the impregnation method and the EDX measurement, the amounts of $[Al]_{MAO}$ and $[Zr]_{zirconocene}$ were varied on each sample. Therefore, the amount of additional MAO and zirconocene used for polymerization reaction were also not equal in order to keep the $[Al]_{MAO}/[Zr]_{zirconocene}$ ratio being constant at 1135 during each run. In this section, the effect of the initial comonomer content in ethylene/1-octene copolymerization was investigated to determine both the catalytic performance and the specification of the obtained copolymers. In addition, for comparative study, copolymerization reaction with ZnO-supported catalyst prepared by the in situ impregnation method was also conducted.

4.3.1 *In situ* polymerization of ethylene/1-octene with catalyst precurcors prepared via the in situ impregnation method

In situ polymerization of ethylene/1-octene with catalyst precurcors prepared via the in situ impregnation method was also carried out. In this system, the ZnO support was reacted with the desired amount of MAO at room temperature for 30 min, which allow the preparation of the catalysts in the form of suspensions. The catalytic activities obtained with different initial amounts of 1-octene are shown in Table 4.3.

Table 4.3 Polymerization activities of LLDPE/ZnO nanocomposites synthesized using catalyst precursors prepared via the in situ impregnation method with various initial contents of 1-octene

1-Octene (mol)	Time[a] (s)	Polymer yield[b] (g)	Catalytic activity (kg of polymer/ mol Zr.h)
0	92	0.6538	17056
0.0045	104	0.8071	18625
0.009	122	1.0362	20384
0.0135	167	1.6924	24321
0.018	147	1.3472	21995

[a] A period of time used for ethylene comsumption of 0.018 mol

[b] Measured at polymerization temperature of 70 °C; ethylene consumption = 0.018 mol; $[Al]_{TMA}/[Zr]_{zirconocene} = 2500$; in toluene with total volume = 30 ml; and $[Zr]_{zirconocene} = 5\times10^{-5}$ M

Form Table 4.3, the introduction of 1-octene into copolymerization enhanced catalytic activity higher than that of system without 1-octene in the first range. The enhancement of polymerization rate by 1-octene (comonomer) is called "comonomer effect". The most supported cause is the easier monomer diffusion due to crystallinity reduction of the growing polymer when a small amount of comonomer is added. In ethylene homopolymerization, the monomer diffusion is very slow through the highly crystalline polymer formed around the catalyst particle. The comonomer addition leads to less crystalline polymer formation, which makes the diffusion of ethylene easier, and thus favors extended ethylene insertion [Van Grieken *et al.*, 2007]. However, at 0.018 mol of 1-octene content, polymerization activity decreased due to an increase of the comonomer fraction in the polymeric growing chain leading to a decrease in the propagation rate, and hence a reduction in activity. High excess of 1-octene obstructed active sites of catalyst from reacting with ethylene monomer, and consequently reduce rate of ethylene insertion into the chain of growing polymer [Chaichana *et al.*, 2010]. The activity profile can be illustrated in Figure 4.7.

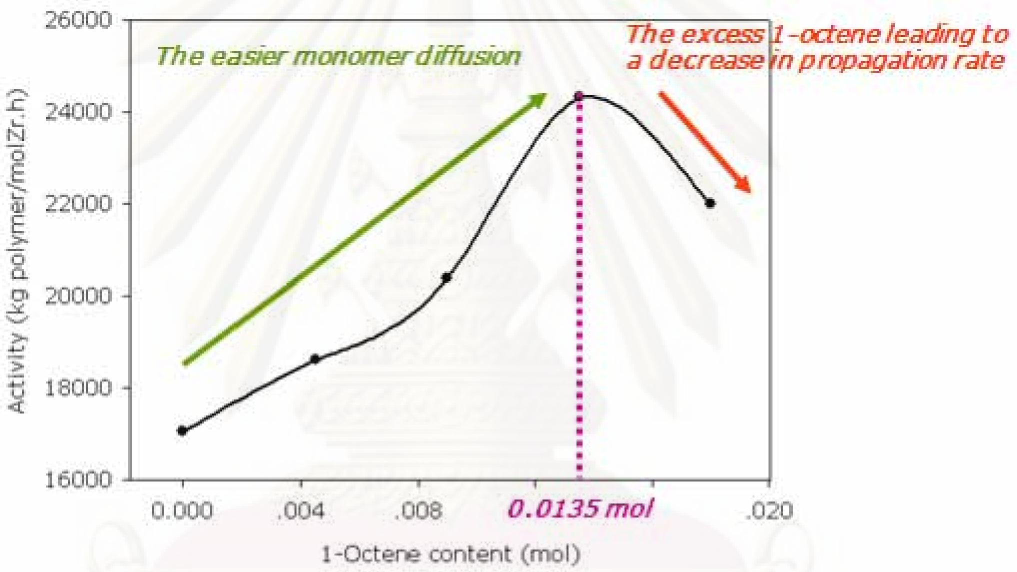

Figure 4.7 Activity profile of polymerization system using the catalyst precuesors prepared via in situ impregnation method

The various LLDPE/ZnO nanocomposites obtained were further characterized by means of ^{13}C NMR. The quantitative analysis of triad distribution for all copolymers was conducted on the basis assignment of the ^{13}C NMR spectra of ethylene/1-octene (EO) copolymer [Randall, 1989]. The characteristics of ^{13}C NMR spectra (as shown in Appendix A) for all copolymers were similar indicating the copolymer of ethylene/ 1-octene. The triad distribution of all LLDPE/ZnO is shown in Table 4.4. Ethylene incorporation in all systems gave copolymers with similar triad distribution.

Table 4.4 Triad distribution of LLDPE/ZnO nanocomposites synthesized using catalyst precursors prepared via the in situ impregnation method with various initials contents of 1-octene

1-Octene (mol)	Triad distribution						1-Octene insertion (%)
	OOO	EOO	EOE	EEE	OEO	OEE	
0.0045	0.026	-	0.117	0.331	0.071	0.455	14.3
0.009	0.048	-	0.152	0.539	0.035	0.226	20.0
0.0135	-	-	0.183	0.573	-	0.244	18.3
0.018	-	-	0.219	0.444	0.079	0.258	21.9

4.3.2 *In situ* polymerization of ethylene/1-octene with catalyst precurcors prepared by impregnation of MAO onto ZnO nanoparticles

In this section, the catalyst precursors were prepared by impregnation of MAO onto ZnO nanoparticles. The catalytic activities based on polymer product are shown in Table 4.5.

Table 4.5 Polymerization activities of LLDPE/ZnO nanocomposites synthesized using catalyst precursors prepared by impregnation of MAO onto ZnO nanoparticles with various 1-octene contents

Initial content of 1-octene (mol)	Time[a] (s)	Polymer yield[b] (g)	Catalytic activity (kg of polymer/ mol Zr.h)
0	72	0.0361	3645
0.0045	60	0.0371	4496
0.009	83	0.0592	5186
0.0135	63	0.0928	10710
0.018	92	0.1620	12802

[a] A period of time used for ethylene comsumption of 0.018 mol

[b] Measured at polymerization temperature of 70 °C; ethylene consumption = 0.009 mol; $[Al]_{TMA}/[Zr]_{zirconocene} = 2500$; in toluene with total volume = 30 ml; and $[Zr]_{zirconocene} = 1.65\times10^{-5}$ M

As seen form Table 4.5, the catalyst activity systematically increased with the increase of comonomer content in all cases, which is known as the comonomer effect. This result was relative to a physical phenomenon with the improvement of monomer diffusion in the lower crystalline copolymer structures. A monomer diffusion limitation occurs when the monomer polymerization rate is high in comparison to the diffusion rate to the catalyst particle [Hong *et al.*, 2006]. The activity profile can be illustrated in Figure 4.8.

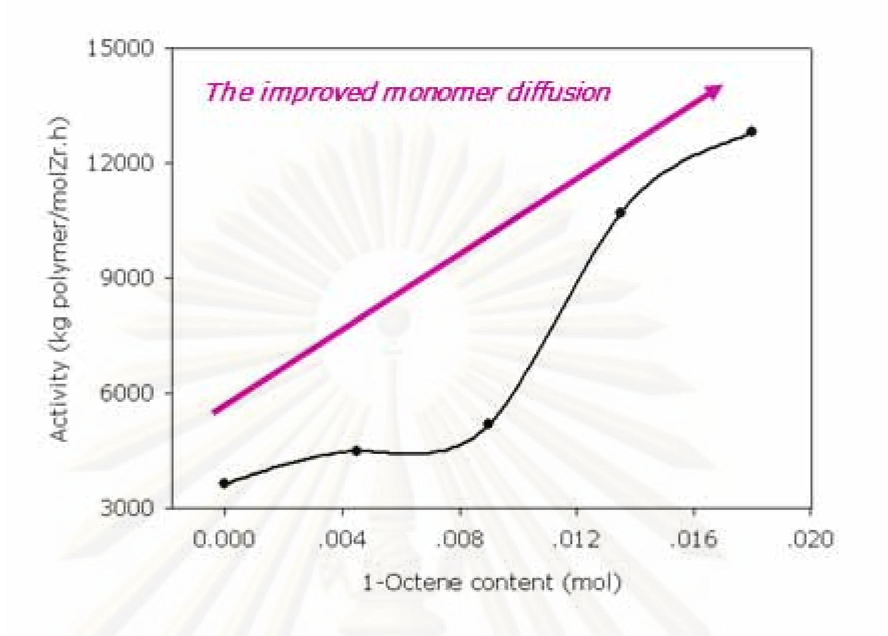

Figure 4.8 Activity profile of polymerization system using the catalyst precursors prepared via impregnation of MAO onto ZnO nanoparticles

The obtained LLDPE/ZnO nanocomposites were further characterized using XRD technique. Figure 4.9 shows the XRD patterns of LLDPE/ZnO nanocomposites synthesized with different initial content of 1-octene. In general, the XRD patterns of polyethylene (PE) exhibit two characteristic peaks at 2θ of 21.8 and 24.3°. It can be seen that LLDPE still exhibited two characteristic peaks at around 2θ of 21.8 and 24.3° although ZnO nanoparticles were incorporated into polymer matrix. Moreover, the intensity of LLDPE systems was lower than PE due to 1-octene insertion and it decreased with increasing of 1-octene content indicating a reduction in crystallinity of LLDPE/ZnO produced.

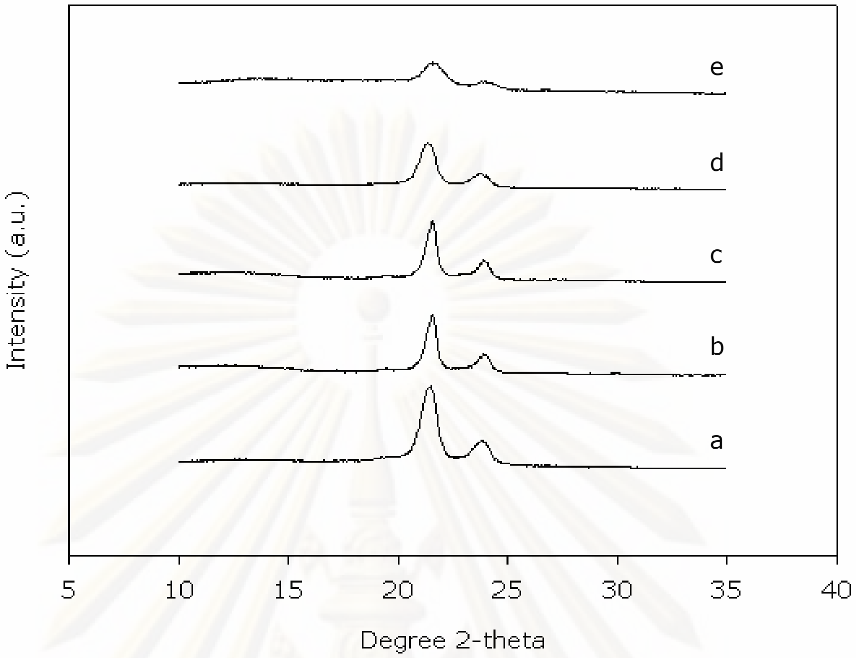

Figure 4.9 XRD patterns of LLDPE/ZnO nanocomposites synthesized using catalyst precursors prepared via impregnation of MAO onto ZnO nanoparticles with initial 1-octene content of: (a) no 1-octene added; (b) 0.0045 mol; (c) 0.009 mol; (d) 0.0135 mol; and (e) 0.018 mol

4.3.3 *In situ* polymerization of ethylene/1-octene with catalyst precurcors prepared by impregnation of both MAO and zirconocene onto ZnO nanoparticles

In this section, the catalyst precursors were prepared by impregnation of both MAO and zirconocene onto ZnO nanoparticles. The results of polymerization activities obtained from this system are shown in Table 4.6.

Table 4.6 Polymerization activities of LLDPE/ZnO nanocomposites synthesized using catalyst precursors prepared by impregnation of MAO and zirconocene onto ZnO nanoparticles with various 1-octene contents

Initial content of 1-octene (mol)	Time[a] (s)	Polymer yield[b] (g)	Catalytic activity (kg of polymer/ mol Zr.h)
0	166	1.1362	803
0.0045	157	1.1560	863
0.009	178	0.9576	631
0.0135	168	0.8437	589
0.018	211	0.9603	534

[a] A period of time used for ethylene comsumption of 0.018 mol

[b] Measured at polymerization temperature of 70 °C; ethylene consumption = 0.018 mol; $[Al]_{TMA}/[Zr]_{zirconocene} = 2500$; in toluene with total volume = 30 ml; and $[Zr]_{zirconocene} = 1.02\times10^{-3}$ M

Form Table 4.6, it can be observed that polymerization activity first increased and then decreased with the increasing 1-octene content, reaching maximum values at 0.0045 mol. The addition of a comonomer such a 1-octene changes the properties of the polymer layer around the catalyst particle, which affects the monomer diffusion to the catalyst particle. When monomer contacts the active sites on the surface of the catalyst, polymer formation takes place and the fast-forming chains will be growing on the catalyst surface. The monomer must diffuse through the boundary layer around the catalyst particle to reach the active sites, where polymerization occurs [Kittilsen *et al.*, 2001; McKenna and Soares, 2001]. In ethylene polymerization, it is frequently observed that polymer growth starts at and near the particle surface, leading to the formation of a shell of polyethylene around the catalyst particle. This results in the diffusion limitation, preventing free access of the monomer to active sites [Przybyla *et al.*, 1999]. As a result, the addition of a small amount of a comonomer decreases the crystallinity of the polymer envelope, thus enhancing activity.

At higher 1-octene concentrations the polymerization activity decreased. This is associated with an increase of the comonomer fraction in the polymeric growing chain leading to a reduction in activity because of a decrease in the propagation rate with the comonomer content. The activity profile of this polymerization system can be illustrated in Figure 4.10.

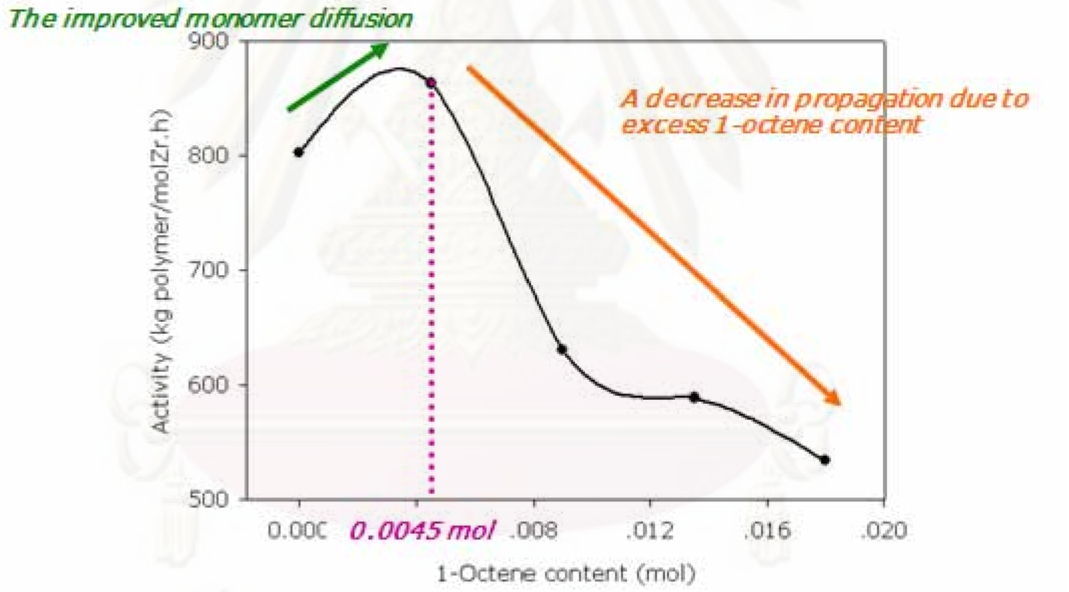

Figure 4.10 Activity profile of polymerization system using catalyst precursors prepared via impregnation of MAO and zirconocene onto ZnO nanoparticles

The quantitative analysis of triad distribution for all copolymers produced has been conducted on the assignment basis of the ^{13}C NMR spectra [Randall, 1989]. The triad distributions for all copolymers are shown in Table 4.7. Based on ^{13}C NMR, measurements, only LLDPE/ZnO produced with 0.018 mol of 1-octene content can be determined, exhibiting the majority of triad distribution of EEE.

Table 4.7 Triad distribution of LLDPE/ZnO nanocomposites synthesized using catalyst precursors prepared by impregnation of MAO and zirconocene onto ZnO nanoparticles with various initial contents of 1-octene

1-Octene (mol)	Triad distribution						1-Octene insertion (%)
	OOO	EOO	EOE	EEE	OEO	OEE	
0.0045	n.o.	n.o.	n.o.	n.o.	n.o.	n.o.	n.o.
0.009	n.o.	n.o.	n.o.	n.o.	n.o.	n.o.	n.o.
0.0135	n.o.	n.o.	n.o.	n.o.	n.o.	n.o.	n.o.
0.018	-	-	0.039	0.818	-	0.143	3.9

In addition, the DSC analysis was also used to measure the thermal properties of LLDPE/ZnO nanocomposites obtained. The DSC results are shown in Table 4.8.

Table 4.8 Thermal properties of LLDPE/ZnO nanocomposites synthesized using catalyst precursors prepared by impregnation of MAO and zirconocene onto ZnO nanoparticles with various initial contents of 1-octene

1-Octene (mol)	T_m (°C)	T_c (°C)	ΔH_m (J/g)	Crystallinity (%)
0.0045	115.46	100.77	24.8332	8.68
0.009	106.05	90.43	16.3253	5.71
0.0135	92.58	76.42	4.3714	1.53

DSC measurement indicated that both melting temperature and crystallinity of LLDPE/ZnO nanocomposites reduced with an increase in 1-octene content.

The XRD patterns of LLDPE/ZnO nanocomposites are shown in Figure 4.11. The XRD patterns of polyethylene (PE) show two characteristic peaks at 2θ of 21.8 and 24.3° corresponding to the orthorhombic crystalline form of PE.

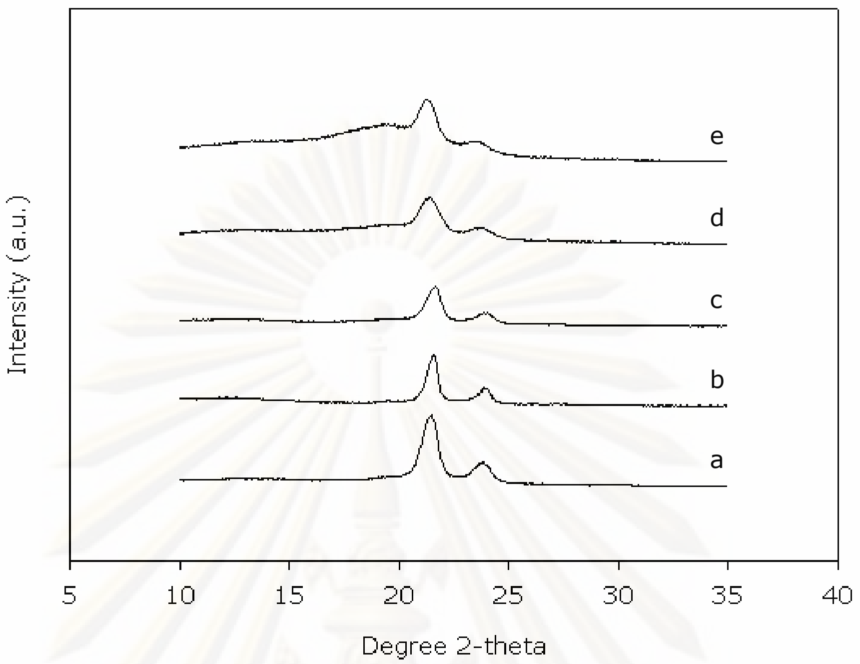

Figure 4.11 XRD patterns of LLDPE/ZnO nanocomposites systhesized using catalyst precursors prepared via impregnation of MAO and zirconocene onto ZnO nanoparticles with initial 1-octene content of: (a) no 1-octene added; (b) 0.0045 mol; (c) 0.009 mol; (d) 0.0135 mol; and (e) 0.018 mol

It is seen that while ZnO nanoparticles were incorporated into LLDPE metrix all LLDPE/ZnO nanocomposites exhibited two characteristics peaks at around 2θ of 21.8 and 24.3°. However, the intensity of LLDPE/ZnO nanocomposites decreased with increasing of 1-octene content indicating the lower crystallinity of polymer produced, which were consistent with results obtained from DSC analysis.

In summary, the results from this investigation indicated that the factors responsible for the comonomer effect may differ from one reaction system to another. The magnitude of the effect depends on the catalyst system and the comonomer employed.

4.4 LLDPE/ZnO polymer nanocomposites using zinc oxide prepared via different impregnation methods

In this section, the effect of catalyst preparation method was examined in terms of catalytic performance and polymer properties. The catalyst preparation method used in this experiment is the in situ impregnation and the ex situ impregnation method. In addition, the ex situ method was divided into three methods: (1) Impregnation of MAO onto ZnO; (2) Impregnation of zirconocene onto ZnO; and (3) Impregnation of both MAO and zirconocene onto ZnO. Copolymerization reactions were run by fixing initial content of 1-octene at 0.018 mol. For comparative study, copolymerization with the absence of ZnO nanoparticles (homogeneous metallocene system) was also carried out. The polymerization activity of various supporting system are shown in Table 4.9 and Figure 4.12.

Table 4.9 Polymerization activities of LLDPE/ZnO nanocomposites synthesized via various impregnation methods

System		Time[a] (s)	Polymer yield[b] (g)	Catalytic activity (kg of polymer/ mol Zr.h)
Homogeneous		101	1.9503	46343
In situ impregnation		147	1.3472	21995
Ex situ impregnation	ZnO/Al	92	0.1620	12802
	ZnO/Al/Zr	211	0.9603	534
	ZnO/Zr	n.o.	n.o.	n.o.

[a] A period of time used for ethylene comsumption of 0.018 mol, except for ZnO/Al which ethylene comsumption was 0.009 mol

[b] Measured at polymerization temperature of 70 °C; $[Al]_{TMA}/[Zr]_{zirconocene} = 2500$; initial content of 1-octene = 0.018 mol; in toluene with total volume = 30 ml; and $[Zr]_{zirconocene} = 5\times10^{-5}$ M for homogeneous and in situ impregnation system, 1.65×10^{-5} M for ZnO/Al system, 1.02×10^{-3} M for ZnO/Al/Zr system

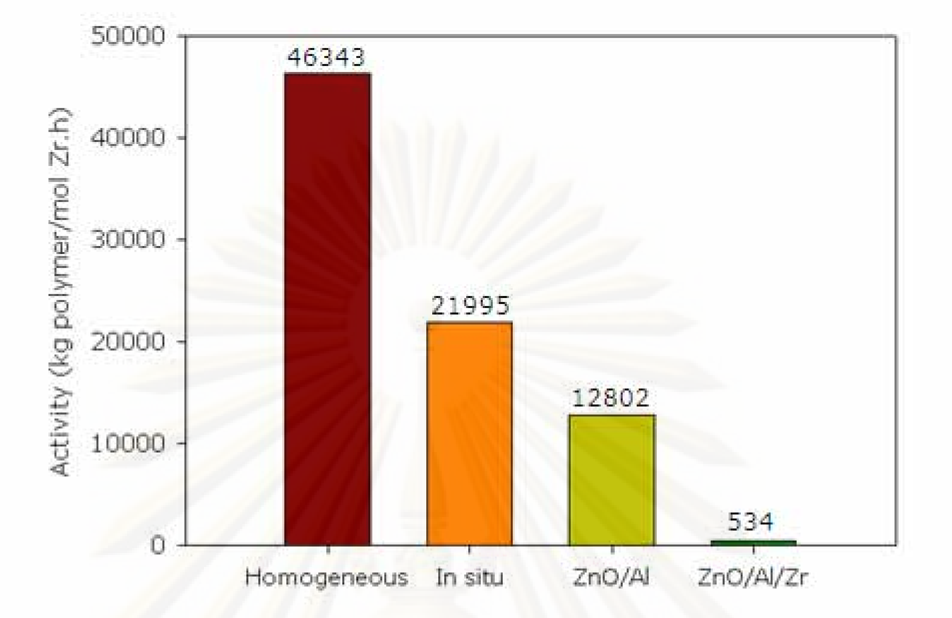

Figure 4.12 Activity profile of polymerization system using the catalyst precursors prepared via different impregnation methods with initial 1-octene content of 0.018 mol

From table 4.8, it is obvious that homogeneous system exhibited polymerization activity higher than other heterogeneous systems. This is due to the more active species present in the homogeneous system. This effect is apparently observed in the in situ impregnation system. Even though the amounts of [Zr] present in both catalytic systems were quite similar, the catalytic activities were different. This result indicated that not all of Zr species present in the catalytic system were active, especially for the supported system [Jongsomjit *et al.*, 2004b]. Moreover, the more steric hindrance in the heterogeneous system is another factor that causes a decrease in activity because this steric hindrance renders difficult accessibility to the catalyst sites [Franceschini *et al.*, 2009; Chaichana *et al.*, 2007]. This phenomenon is known as the supporting effect.

A comparative study of two supporting systems as shown in Table 4.8 indicated that the in situ-immobilized catalytic system exhibited higher activities compared with the ex situ systems (ZnO/Al and ZnO/Al/Zr). This is due to the more active catalytic species present in the in situ-immobilized catalytic system. For polymerization system using ZnO/Al and ZnO/Al/Zr as catalyst precursors, the amounts of $[Al]_{MAO}$ present on this catalyst precursors was lower than those present in the in situ-immobilized catalytic system. In addition, for the in situ method, MAO or zirconocene can be present in the bulk, which differs from the ex situ one that is only present at the surface of support. This makes the in situ method similar to homogeneous system. As a result, the catalytic activities obtained with the ex situ-impregnated systems were lower. Moreover, the impregnation of both MAO and zirconocene onto ZnO support may cause MAO and zirconocene to react with each other, and then deactivate prior to the polymerization, leading to lower activity than impregnation of only MAO. Another reason is that impregnation of both MAO and zirconocene onto ZnO causes more steric hindrance in the polymerization system.

From this experiment, the ZnO/Zr prepared by impregnation of zirconocene onto ZnO was not active for polymerization. This is because immobilization of only zirconocene onto support may render the formation of $ZrCH_2CH_2Zr$ species, which can be prevented by MAO. It is obviously observed in polymerization system using ZnO/Al/Zr which polymer can be produced because MAO was also immobilized together with zirconocene preventing the formation of $ZrCH_2CH_2Zr$ species. In addition, from TGA, EDX, and XPS measurements, it is apparently that $[Zr]_{zirconocene}$ was present deep into the catalyst particles and, therefore, resulting in ZnO/Zr being inactive for polymerization.

Moreover, polymerization system carried out with other initial content of 1-octene, i.e. 0.0135 mol, was considered. The activity profile of this polymerization system is shown in Figure 4.13. It is apparent that, at 1-octene content of 0.0135 mol, the activity obtained from in situ impregnation system was similar to homogeneous system. This condition would be an alternative to synthesize LLDPE/ZnO polymer nanocomposites with polymerization activity competitive to homogeneous system.

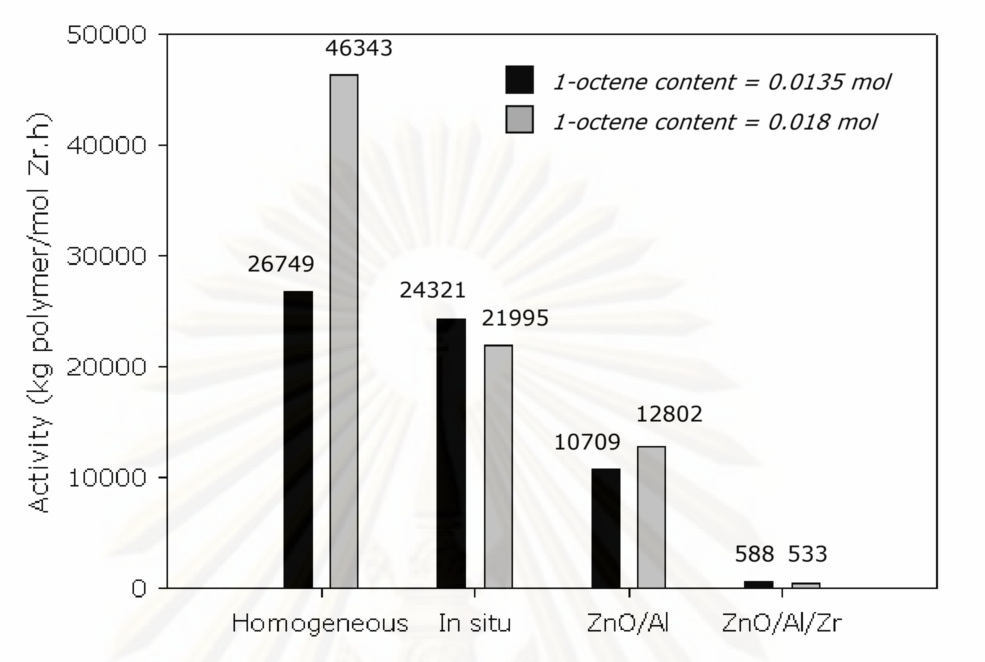

Figure 4.13 Activity profiles of polymerization system using the catalyst precursors prepared via different impregnation methods with various initial content of 1-octene

The obtained LLDPE/ZnO nanocomposites were further characterized using ^{13}C NMR measurements. The quantitative analysis of triad distribution for all polymers produced was conducted on the basic assignment of the ^{13}C NMR spectra as shown in Appendix A. The ^{13}C analysis indicated that LLDPE/ZnO nanocomposites synthesized via homogeneous and in situ impregnation system had similar triad distribution and 1-octene incorporation while most of triad distribution for LLDPE/ZnO synthesized with ZnO/Al/Zr was EEE with 1-octene insertion of only 3.9%. In case of ZnO/Al, triad distribution cannot be determined. Thus, it should be further characterized using XRD.

Table 4.10 Triad distribution of LLDPE/ZnO nanocomposites synthesized via various impregnation methods

System	Triad distribution						1-Octene insertion (%)
	OOO	EOO	EOE	EEE	OEO	OEE	
Homogeneous	-	-	0.212	0.550	0.071	0.167	21.2
In situ impregnation	-	-	0.219	0.444	0.079	0.258	21.9
Ex situ impregnation							
ZnO/Al	n.o.	n.o.	n.o.	n.o.	n.o.	n.o.	n.o.
ZnO/Al/Zr	-	-	0.039	0.818	-	0.143	3.9

SEM analysis was performed on the LLDPE/ZnO nanocomposites to compare the morphology of polymer synthesized using different impregnation methods. It can be seen from Figure 4.14 that LLDPE/ZnO nanocomposites synthesized using different catalyst precursors have the same morphology. This result indicated that the catalyst preparation method did not affect the morphology of polymer. In addition, the visual inspection of these polymer nanocomposites shows that the PE/ZnO nanocomposites (synthesized with the absence of 1-octene) consist of powdery particles while LLDPE/ ZnO nanocomposites are clearly more fiber-like products.

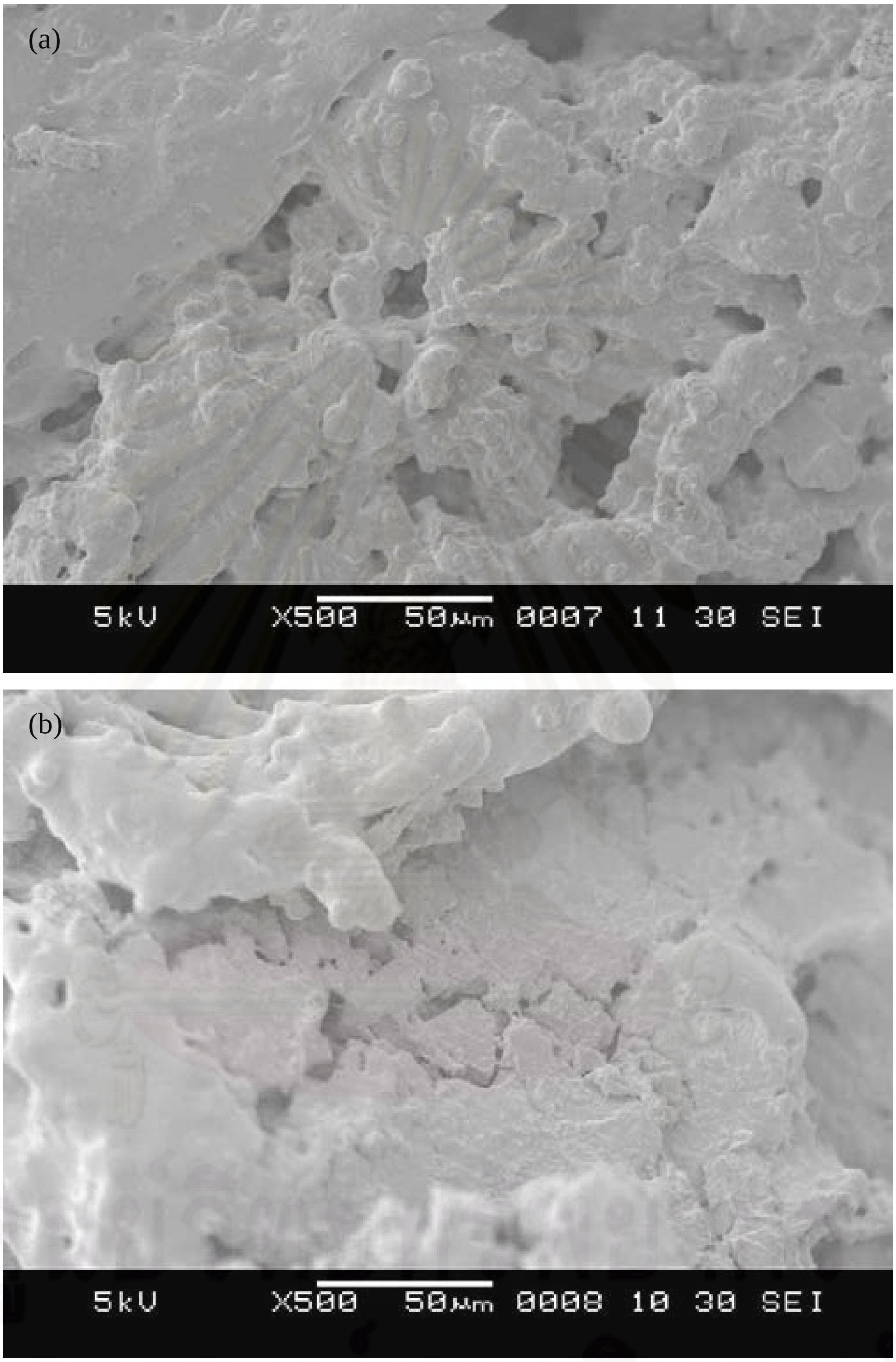

Figure 4.14 SEM micrographs of LLDPE/ZnO nanocomposites synthesized using: (a) ZnO/Al; and (b) ZnO/Al/Zr

CHAPTER V

CONCLUSIONS AND RECOMMENDATIONS

5.1 Conclusions

- The synthesis of LLDPE/ZnO nanocomposites can be achieved via the in situ polymerization of ethylene/1- octene with zirconocene/MAO catalyst.

- The initial content of comonomer greatly affected polymerization activity. The enhancement in the catalyst activity was related to better monomer diffusion. However, at higher comonomer content, polymerization activity decreased because the excess comonomer led to a decrease in the propagation rate.

- The in situ-immobilized catalytic system exhibited higher activities compared with the ex situ system because, for the in situ method, MAO or zirconocene can be present in the bulk enable it similar to homogeneous system.

- The in situ impregnation exhibited LLDPE/ZnO with the highest insertion of 1-octene due to less steric hindrance than the ex situ system.

- For the ex situ impregnation system, the catalytic activities were in the order of ZnO/Al > ZnO/Al/Zr > ZnO/Zr (n.o.).

5.2 Recommendations

- LLDPE/ZnO nanocomposites should be further characterized using TEM to determine the dispersion of ZnO nanoparticles within polymer matrix.

- LLDPE/ZnO nanocomposites should be further characterized using DSC to determine thermal properties.

- Copolymerization reaction should be scaled up to synthesize enough polymer nanocomposites for testing other properties such as mechanical properties.

REFERENCES

Awudza, J.A.M., Tait, P.J.T. The comonomer effect in ethylene/α-olefin copolymerization using homogeneous and silica-supported Cp_2ZrCl_2/MAO catalyst systems: some insights from the kinetics of polymerization, active center studies, and polymerization temperature. Journal of Polymer Science Part A: Polymer Chemistry 46 (2008): 267–277.

Bochmann, M. Kinetic and mechanistic aspects of metallocene polymerization catalysts. Journal of Organometallic Chemistry 689 (2004): 3982–3998.

Carrión, F.J., Sanes, J., Bermúdes, M.D. Influence of ZnO nanoparticle filler on the properties and wear resistance of polycarbonate. Wear 262 (2007): 1504–1510.

Chien, J.C.W. Supported metallocene polymerization catalysis. Topic in Catalysis 7 (1999): 23–36.

Chien, J.C.W., He, D. Olefin copolymerization with metallocene catalysts. II. Kinetics, cocatalyst, and additives. Journal Polymer Science Part A: Polymer Chemistry 29 (1991): 1595–1601.

Chien, J.C.W., Wang, B.P. Metallocene-methylaluminoxane catalysts for olefin polymerizations. IV. Active site determinations and limitation of the ^{14}CO radiolabeling technique. Journal of Polymer Science Part A: Polymer Chemistry 27 (1989): 1539–1557.

Coates, G. W. Precise control of polyolefin stereo chemistry using single-site metal catalysts. Chemical Reviews 100 (2000): 1223–1252.

Desharun, C., Jongsomjit, B., Praserthdam, P. Study of LLDPE/alumina nanocomposites synthesized by *in situ* polymerization with zirconocene/d-MMAO catalyst. Catalysis Communications 9 (2008): 522–528.

Dos Santos, J.H.Z., Krug, C., Da Rosa, M.B., Stedile, F.C., Dupont, J., Forte, M.D.C. The effect of silica dehydroxylation temperature on the activity of SiO_2-supported zirconocene catalysts. Journal of Molecular Catalysis A: Chemical 139 (1999):199–207.

Ewen, J.A. Symmetry rules and reaction mechanisms of Ziegler-Natta catalysts. Journal of Molecular Catalysis A: Chemistry 128 (1998): 103–109.

Ewen, J.A., Jones, R.L., Razavi, A. Syndiospecific propylene polymerizations with group 4 metallocenes. Journal of American Chemical Society 110 (1988): 6255–6256.

Gauthier, W.J., Tian, J., Rauscher, D., Henry, S. US Patent Appl 2003/0236365 (2003).

Guimarães, R., Stedile, F.C., Dos Santos, J.H.Z. Ethylene polymerization with catalyst systems based on supported metallocenes with varying steric hindrance. Journal of Molecular Catalysis A: Chemical 206 (2003): 353–362.

Hamielec, A.E., Soares, J.B.P. Polymerization reaction engineering – Metallocene catalysts. Progress in Polymer Science (Oxford) 21 (1996): 651–706.

Herfert, N., Fink, G. Copolymerization of ethene and α-olefins with stereorigid metallocene/MAO Ziegler catalysts: kinetic and mechanistic insight. Polymeric Materials Science and Engineering, Proceedings of the ACS Division of Polymeric Materials Science and Engineering 67 (1992): 31–32.

Huang, J., Rempel, G.L. Ziegler-Natta catalysts for olefin polymerization: mechanistic insights from metallocene systems. Progress in Polymer Science (Oxford) 20 (1995): 459–526.

Jongsomjit, B., Panpranot, J., Okada, M., Shiono, T., Praserthdam, P. Characteristics of LLDPE/ZrO_2 nanocomposite synthesized by in-situ polymerization using a zirconocene/MAO catalyst. Iranian Polymer Journal 15 (2006): 433–439.

Kale, R.B., Hsu, Y.-J., Lin, Y.-F., Lu, S.-Y. Synthesis of stoichiometric flowerlike ZnO nanorods with hundred percent morphological yield. Solid State Communications 142 (2007): 302–305.

Kaminsky, W. The discovery of metallocene catalysts and their present state of the art. Journal Polymer Science Part A: Polymer Chemistry 42 (2004): 3911–3921.

Kaminsky, W., Arndt, M. Metallocenes for polymer catalysis. Advances in Polymer Science 127 (1996) 143–187.

Kaminsky, W., Laban, A. Metallocene catalysis. Applied Catalysis A: General 222 (2001): 47–61.

Li, K.T., Dai, C.L., Kuo, C.W. Ethylene polymerization over a nano-sized silica supported Cp_2ZrCl_2/MAO catalyst. Catalysis Communications 8 (2007): 1209–1213.

Long, N.J. Metallocenes: An introduction to sandwich complexs, London, Blackwell Science Ltd., 1998.

Olabisi, O., Atiqullah, M., Kaminsky, W. Group 4 metallocenes: Supported and unsupported. Polymer Reviews 37 (1997): 519–554.

Owpradit, W., Jongsomjit, B. A comparative study on synthesis of LLDPE/TiO_2 nanocomposites using different TiO_2 by *in situ* polymerization with zirconocene/dMMAO catalyst. Materials Chemistry and Physics 112 (2008): 954–961.

Paredes, B., Soares, J.B.P., Van Grieken, R., Carrero, A., Suarez, I. Characterization of ethylene-1-hexene copolymers made with supported metallocene catalysts: Influence of support type. Macromolecular Symposia 257 (2007) 103–111.

Park, H.W., Chung, J.S., Lim, S.S., Song, I.K., Chemical composition distributions and microstructures of ethylene–hexene copolymers produced by a *rac*-$Et(Ind)_2ZrCl_2/TiCl_4$/MAO/SMB catalyst. Journal of Molecular Catalysis A: Chemical 264 (2007): 202–207.

Pédeutour, J.-N., Radhakrishnan, K., Cramail, H., Deffieux, A. Reactivity of metallocene catalysts for olefin polymerization: Influence of activator nature and structure. Macromolecular Rapid Communications 22 (2001): 1095–1123.

Peng, G., Li, Q., Yang, Y., Wang, H., Li, W. Effects of nano ZnO on strength and stability of unsaturated polyester composites. Polymers for Advanced Technologies 19 (2008): 1629–1634.

Piel, C., Starck, P., Seppälä, J.V., Kaminsky, W. Thermal and mechanical analysis of metallocene-catalyzed ethene-α-olefin copolymers: The influence of the length and number of the crystallizing side chains. Journal of Polymer Science Part A: Polymer Chemistry 44 (2006): 1600–1612.

Razavi, A. Metallocene catalysts technology and environment. Comptes Rendus de l'Academie des Sciences - Series IIc: Chemistry 3 (2000): 615–625.

Razavi, A., Debras, G.L.G. US Patent 5719241 (1998).

Reddy, C.S., Ratna, D., Das, C.K. Polyethylene nanocomposites by gas-phase polymerization of ethylene in the presence of a nanosilica-supported zirconocene catalyst system. Polymer International 57 (2008): 282–291.

Reddy, S.S., Sivaram, S. Homogeneous metallocene - Methylaluminoxane catalyst system for ethylene polymerization. Progress in Polymer Science (Oxford) 20 (1995): 309–367.

Ribeiro, M.R., Deffieux, A., Portela, M.F. Supported metallocene complexs for ethylene and propylene polymerizations: preparation and activity. Industrial and Engineering Chemistry Research 36 (1997): 1224–1237.

Schupfner, G., Kaminsky, W. Microstructure of polypropene samples produced with different homogeneous bridged indenyl zirconium catalysts. Clues on the structure and reactivity relation. Journal of Molecular Catalysis A: Chemical 102 (1995): 59–65.

Severn, J.R., Chadwick, J.C. Tailor-made polymers via immobilization of alpha-olefin polymerization catalysts, Weinheim, WILEY-VCH Verlag GmbH & Co., 2008.

Sinn, H., Kaminsky, W. Ziegler-Natta catalyst. Advances in Organometallic Chemistry 18 (1980): 99–149.

Smit, M., Zheng. X., Brüll, R., Loos, J., Chadwick, J.C., Koning, C.E. Effect of 1-hexene comonomer on polyethylene particle growth and copolymer chemical composition distribution. Journal of Polymer Science Part A: Polymer Chemistry 44 (2006): 2883–2890.

Somwangthanaroj, A., Suwanchatchai, K., Ando, S., Tanthapanichakoon, W. Effect of zinc precursor on thermal and light emission properties of ZnO nanoparticles embedded in polyimide films. Materials Chemistry and Physics 114 (2009): 751–755.

Somwangthanaroj, A., Phanthawonge, C., Ando, S., Tanthapanichakoon, W. Effect of the origin of ZnO nanoparticles dispersed in polyimide films on their photoluminescence and thermal stability. Journal of Applied Polymer Science 110 (2008): 1921–1928.

Stadler, F.J., Piel, C., Klimke, K., Kaschta, J., Parkinson, M., Wilhelm, M., Kaminsky, W., Münstedt, H. Influence of type and content of various comonomers on long-chain branching of ethene/α-olefin copolymers. Macromolecules 39 (2006): 1474–1482.

Takahashi, T. US Patent 5026797 (1991).

Tang, L., Zhou, B., Zhao, J., Lv, X., Sun, F., Wang, Z. Synthesis of morphological ZnO particles by a facile solution-based chemical method. Colloids and Surfaces A: Physicochemical and Engineering Aspects 332 (2009): 43–49.

Tjong, S.C., Liang, G.D. Electrical properties of low-density polyethylene/ZnO nanocomposites. Materials Chemistry and Physics 100 (2006): 1–5.

Van Grieken, R., Carrero, A., Suarez, I., Paredes, B. Effect of 1-hexene comonomer on polyethylene particle growth and kinetic profiles. Macromolecular Symposia 259 (2007): 243–252.

Welborn, H.C. US Patent 4808561 (1989).

Yang, R., Li, Y., Yu, J. Photo-stabilization of linear low density polyethylene by inorganic nano-particles. Polymer Degradation and Stability 88 (2005): 168–174.

Zhao, H., Li, R.K.Y. A study on the photo-degradation of zinc oxide (ZnO) filled polypropylene nanocomposites. Polymer 47 (2006): 3207–3217.

Zou, H., Wu, S., Shen, J. Polymer/silica nanocomposites: preparation, characterization, properties, and applications. Chemical Reviews 108 (2008): 3893–3957.

APPENDICES

APPENDIX A

(NUCLEAR MAGNETIC RESONANCE)

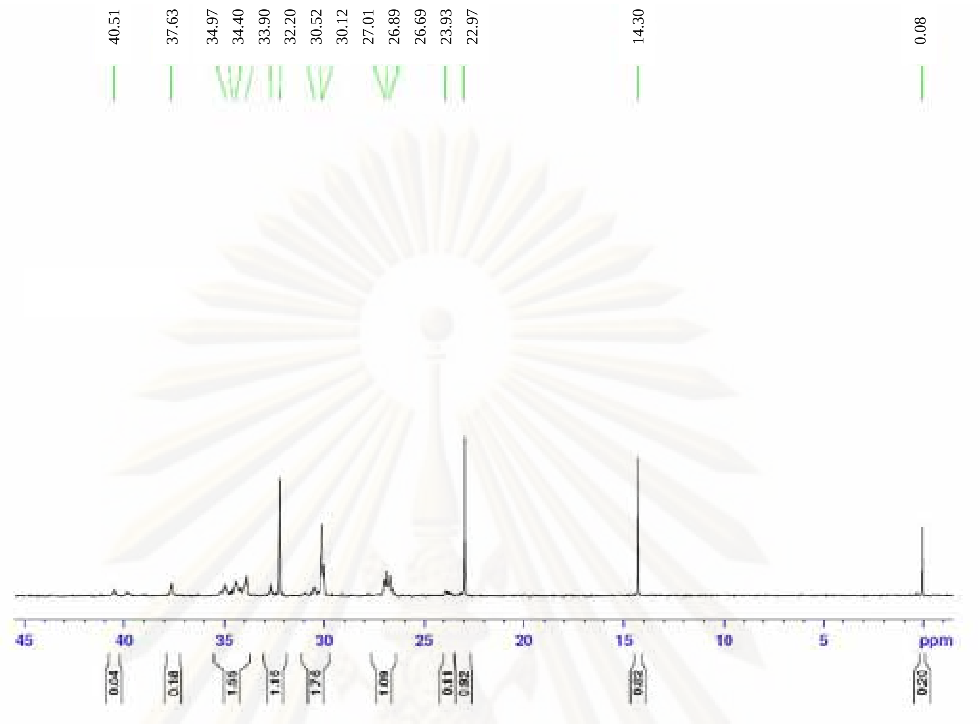

Figure A-1 ^{13}C NMR spectrum of LLDPE/ZnO nanocomposite synthesized with in situ impregnation system using initial 1-octene content of 0.0045 mol

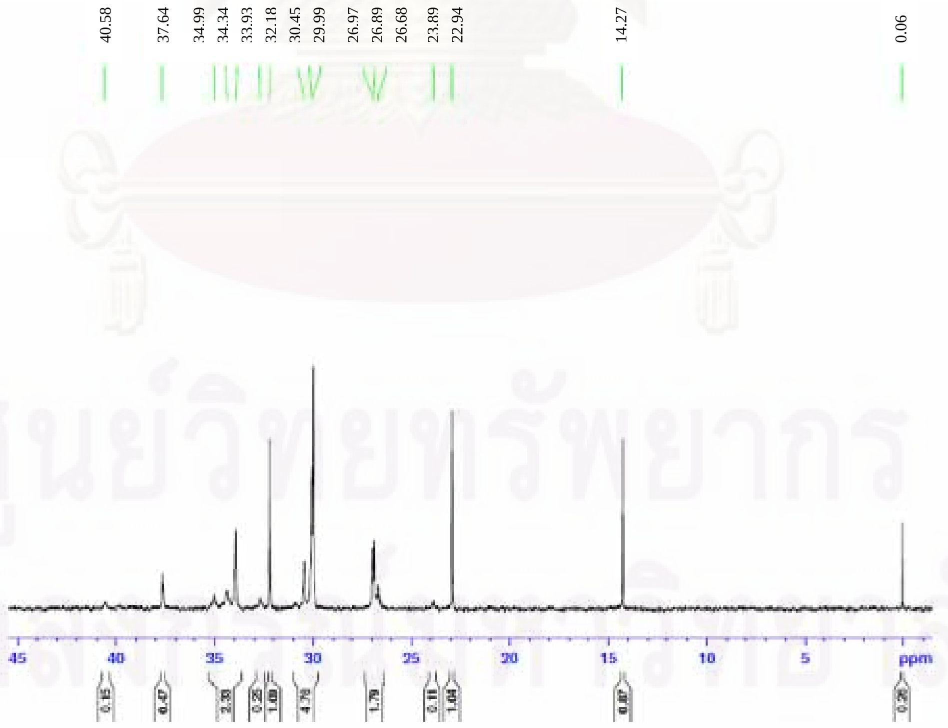

Figure A-2 ^{13}C NMR spectrum of LLDPE/ZnO nanocomposite synthesized with in situ impregnation system using initial 1-octene content of 0.009 mol

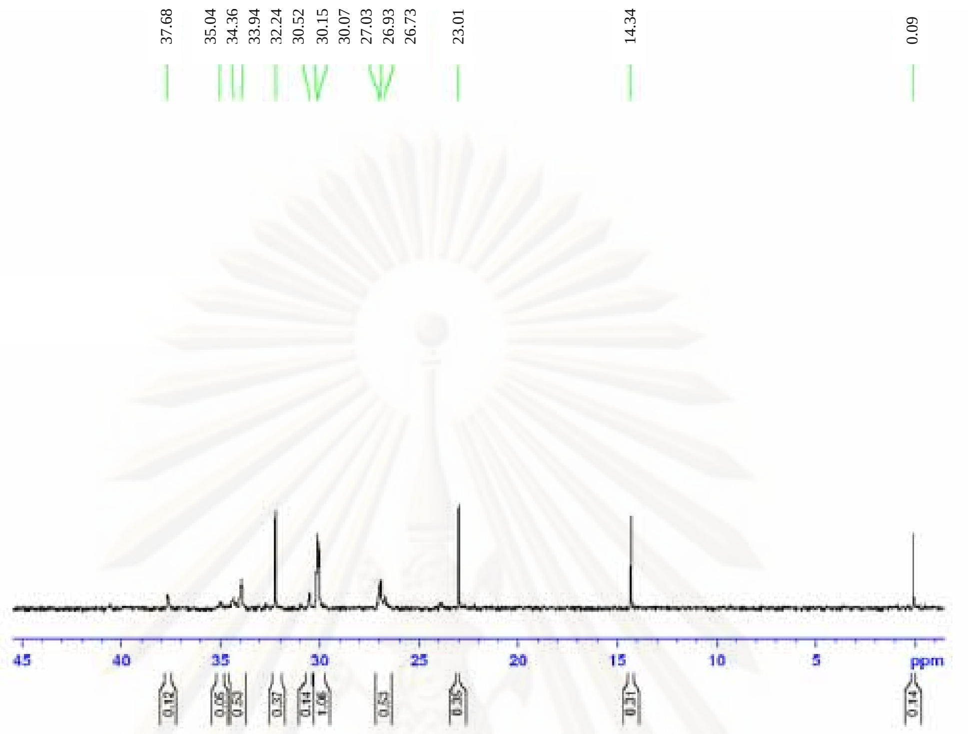

Figure A-3 ^{13}C NMR spectrum of LLDPE/ZnO nanocomposite synthesized with in situ impregnation system using initial 1-octene content of 0.0135 mol

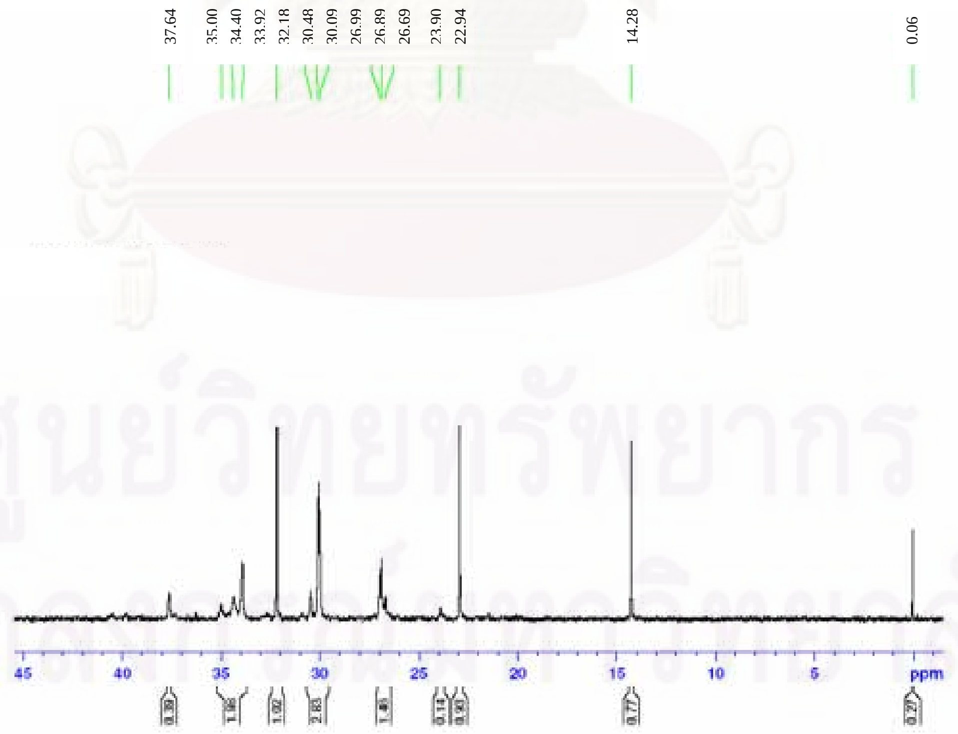

Figure A-4 ^{13}C NMR spectrum of LLDPE/ZnO nanocomposite synthesized with in situ impregnation system using initial 1-octene content of 0.018 mol

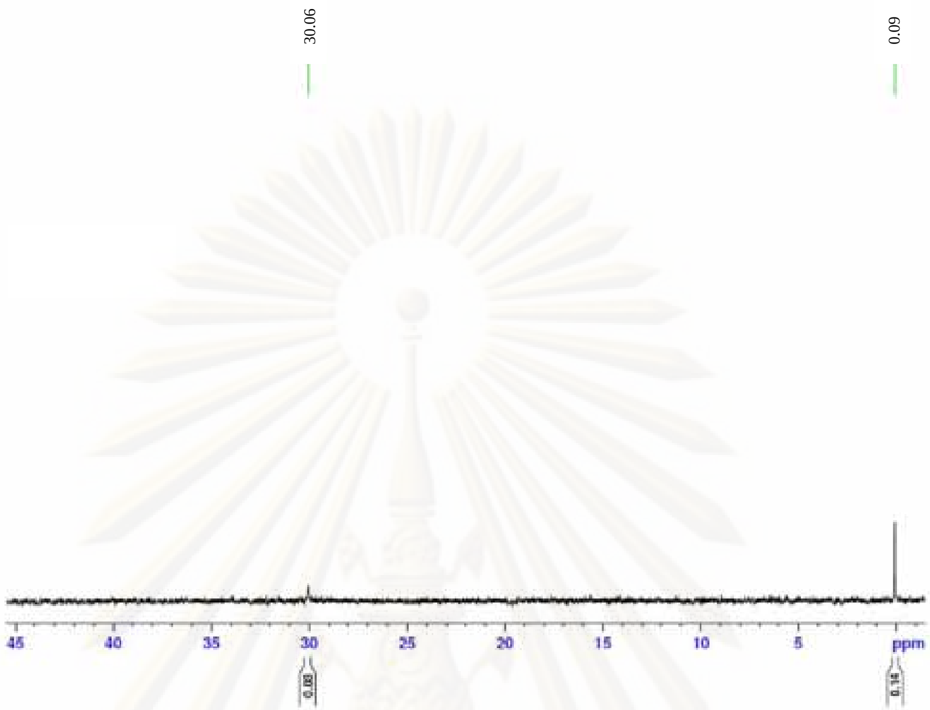

Figure A-5 ^{13}C NMR spectrum of LLDPE/ZnO nanocomposite synthesized using ZnO/Al with initial 1-octene content of 0.0045 mol

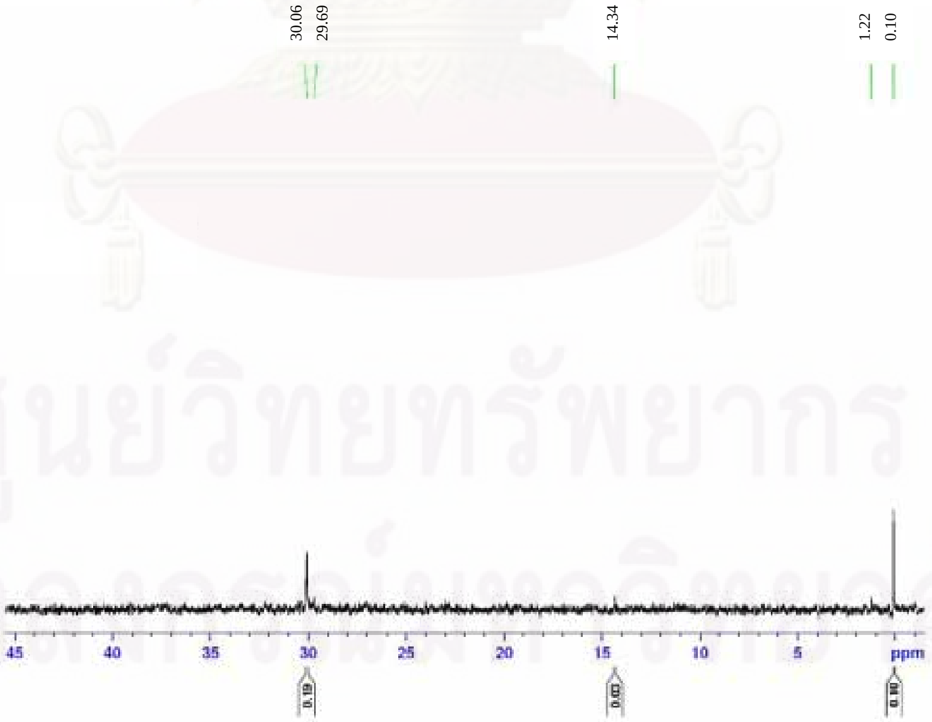

Figure A-6 ^{13}C NMR spectrum of LLDPE/ZnO nanocomposite synthesized using ZnO/Al with initial 1-octene content of 0.009 mol

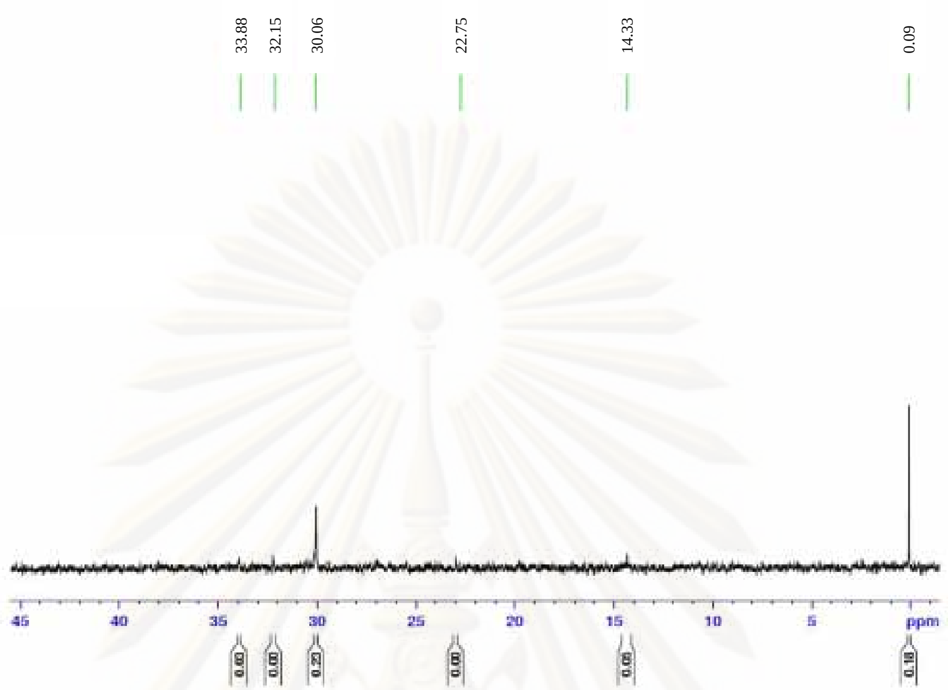

Figure A-7 ^{13}C NMR spectrum of LLDPE/ZnO nanocomposite synthesized using ZnO/Al with initial 1-octene content of 0.0135 mol

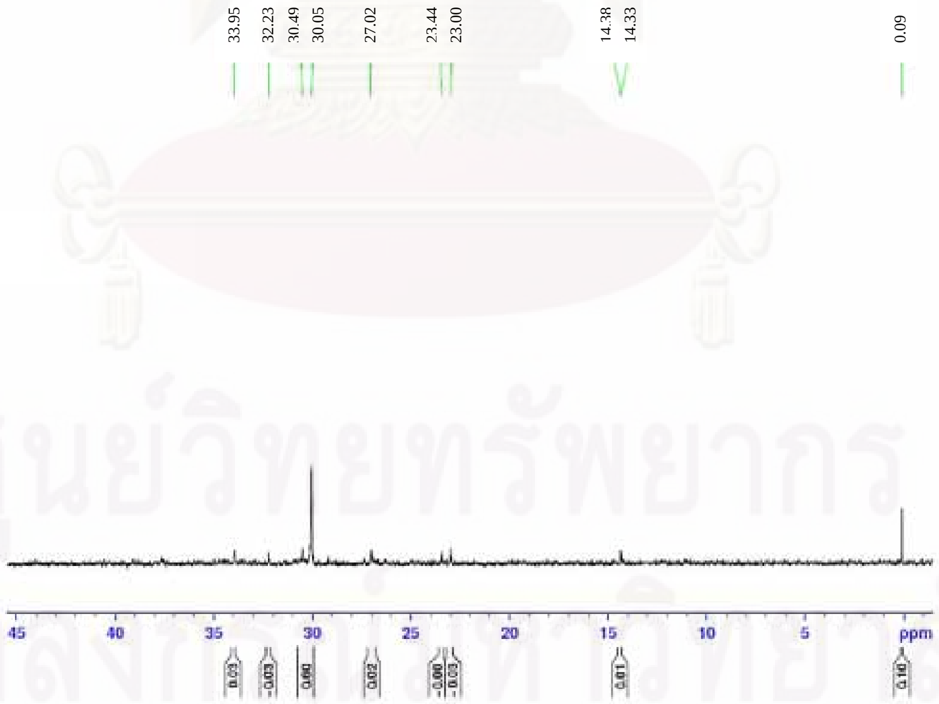

Figure A-8 ^{13}C NMR spectrum of LLDPE/ZnO nanocomposite synthesized using ZnO/Al with initial 1-octene content of 0.018 mol

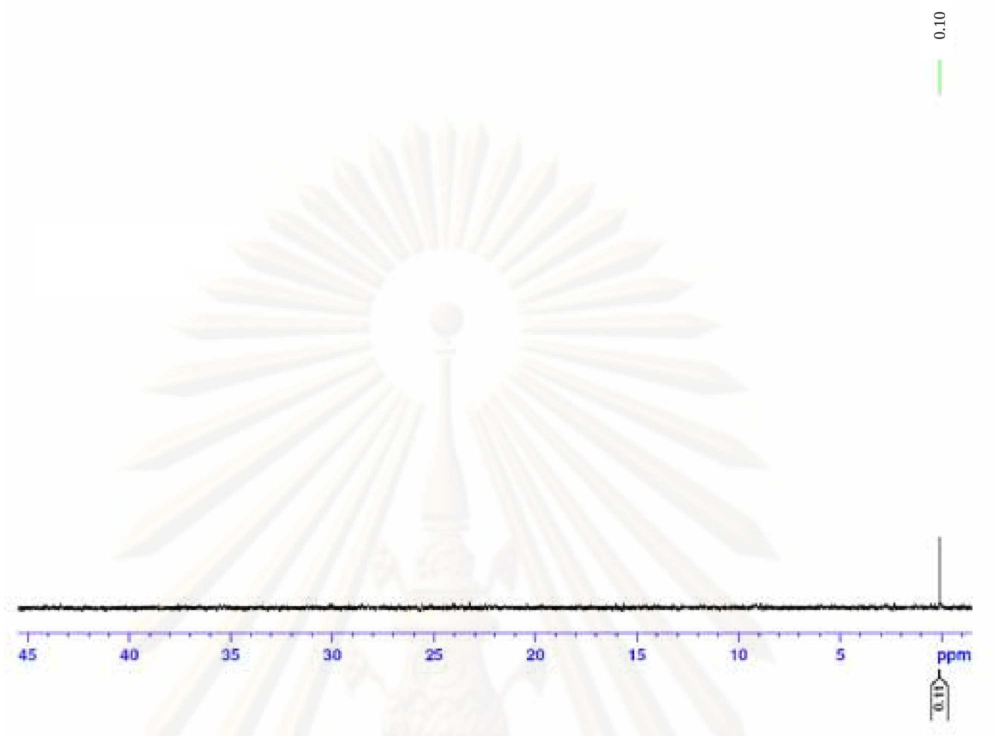

Figure A-9 ^{13}C NMR spectrum of LLDPE/ZnO nanocomposite synthesized using ZnO/Al/Zr with initial 1-octene content of 0.0045 mol

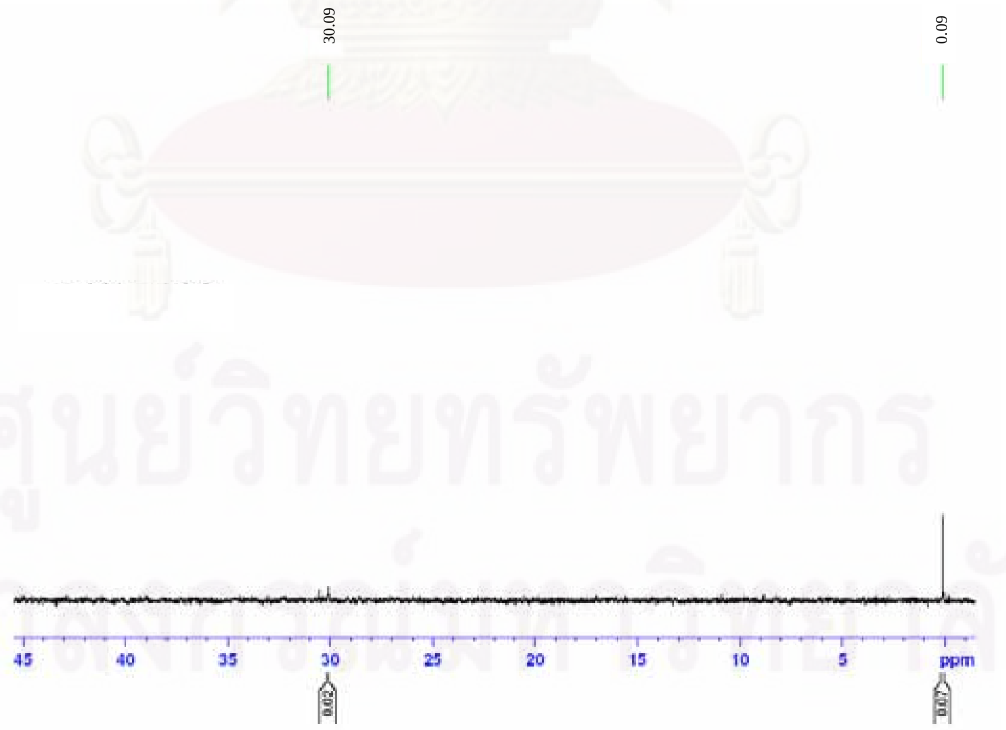

Figure A-10 ^{13}C NMR spectrum of LLDPE/ZnO nanocomposite synthesized using ZnO/Al/Zr with initial 1-octene content of 0.009 mol

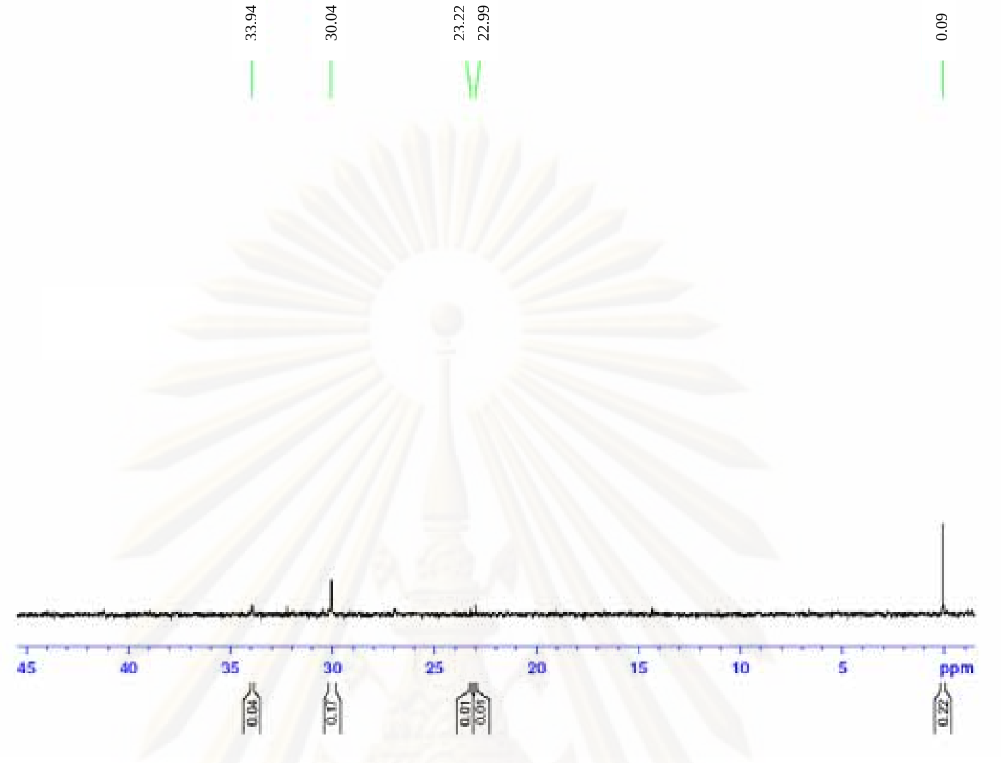

Figure A-11 ^{13}C NMR spectrum of LLDPE/ZnO nanocomposite synthesized using ZnO/Al with initial 1-octene content of 0.0135 mol

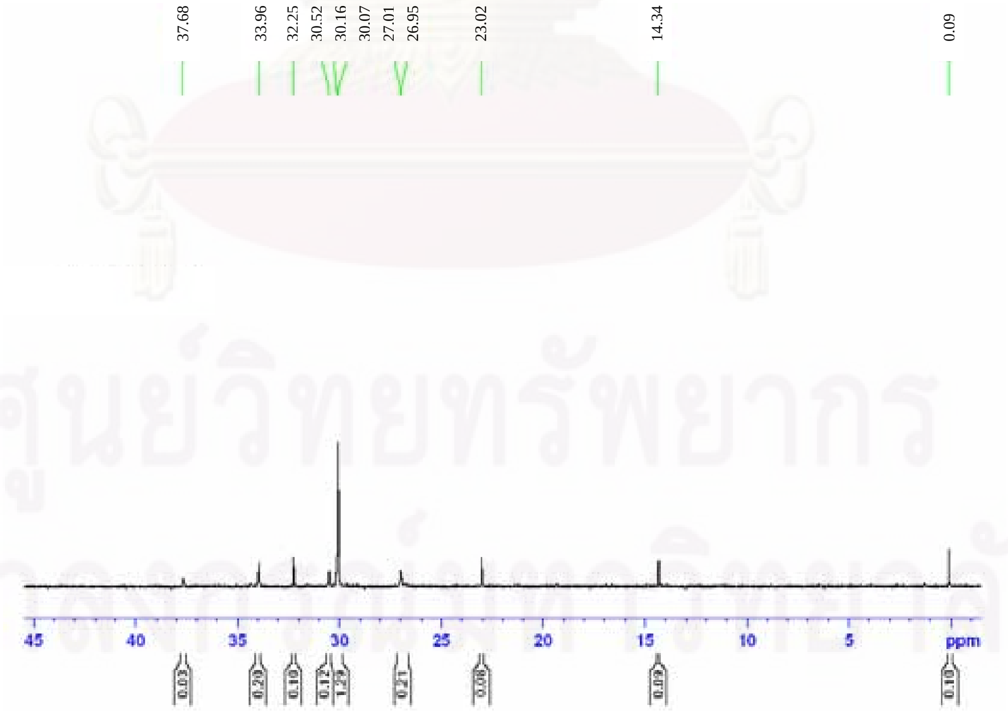

Figure A-12 ^{13}C NMR spectrum of LLDPE/ZnO nanocomposite synthesized using ZnO/Al with initial 1-octene content of 0.018 mol

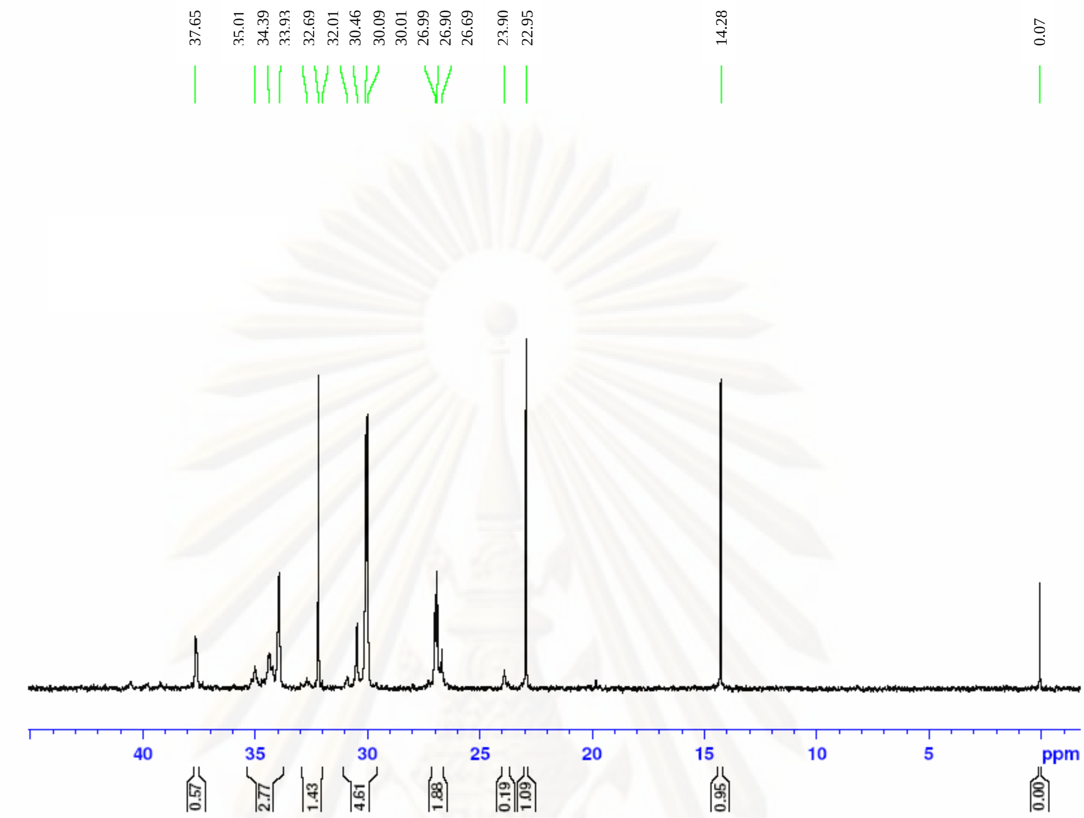

Figure A-13 ^{13}C NMR spectrum of LLDPE/ZnO nanocomposite synthesized via homogeeous system with initial 1-octene content of 0.018 mol

APPENDIX B

(X-RAY PHOTOELECTRON SPECRTOSCOPY)

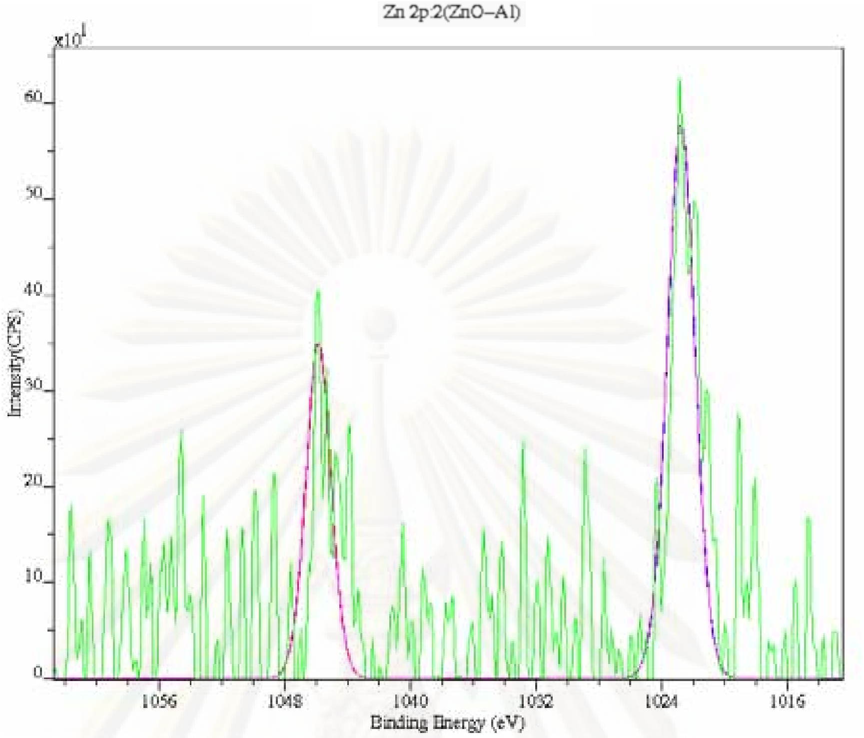

Figure B-1 XPS spectrum of Zn 2p of ZnO/Al

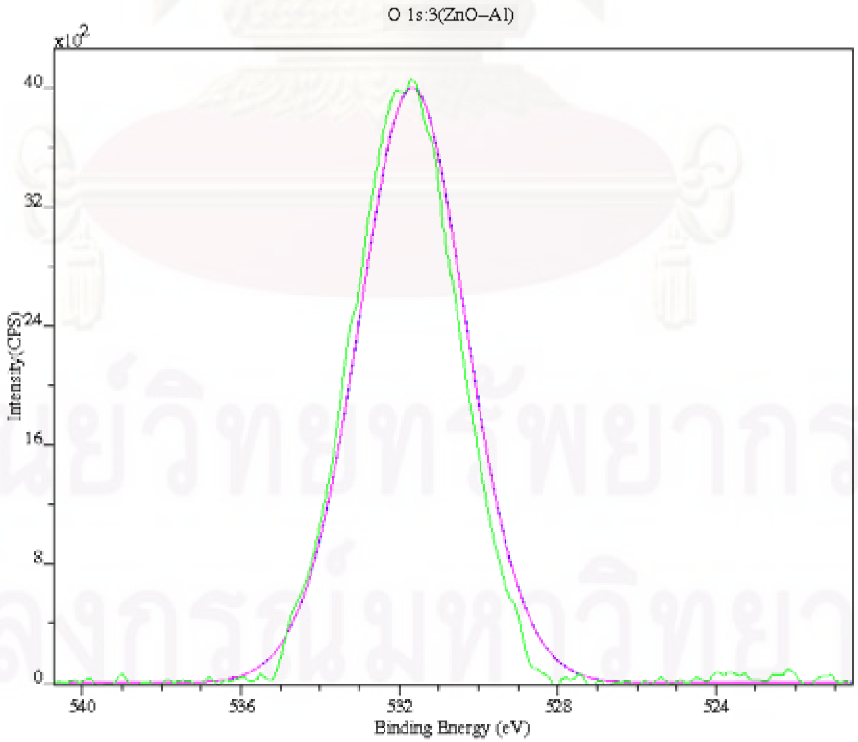

Figure B-2 XPS spectrum of O 1s of ZnO/Al

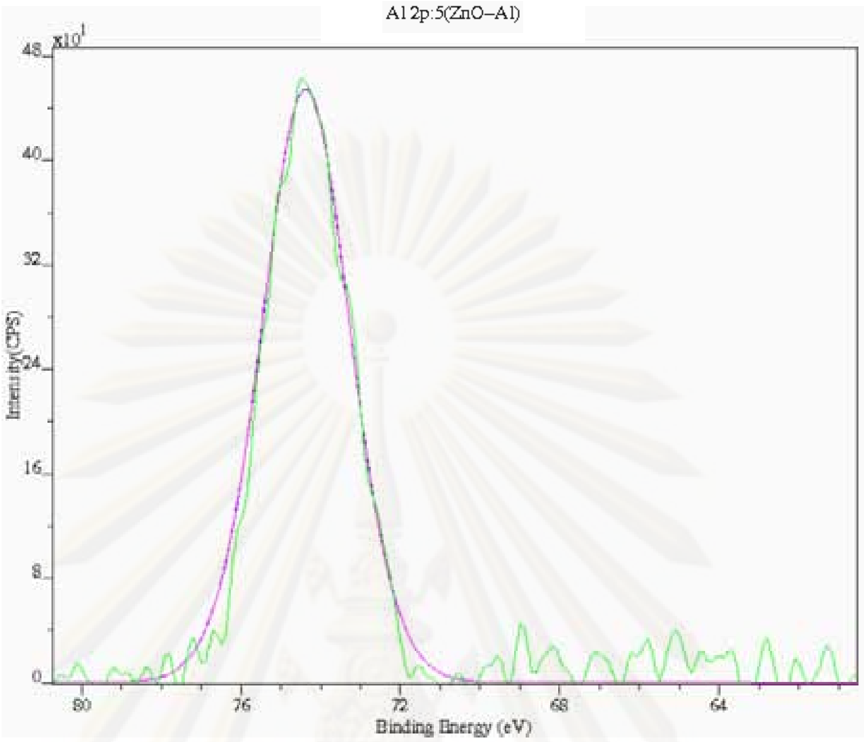

Figure B-3 XPS spectrum of Al 2p of ZnO/Al

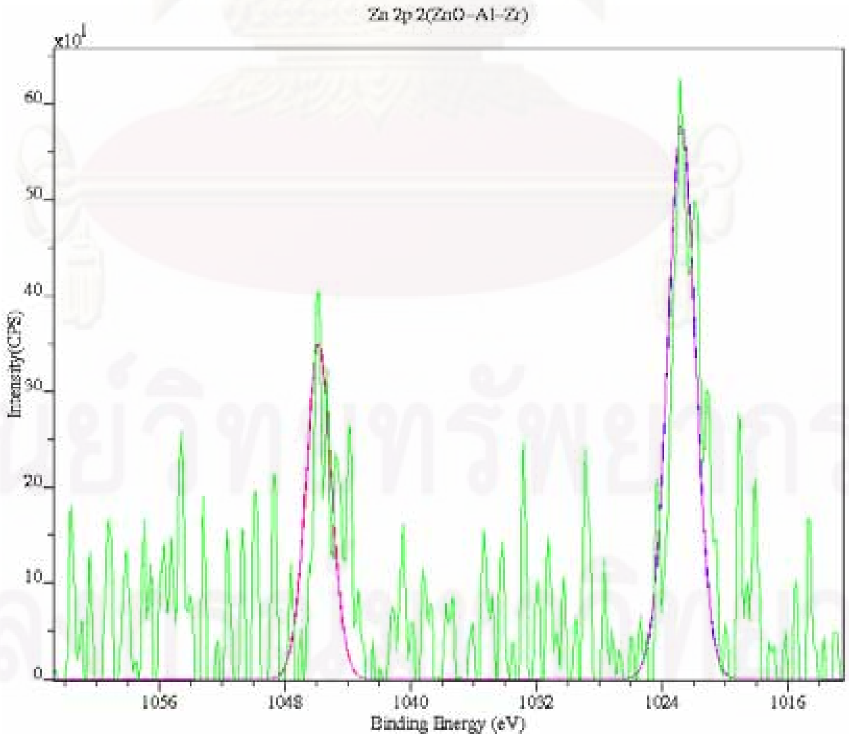

Figure B-4 XPS spectrum of Zn 2p of ZnO/Al/Zr

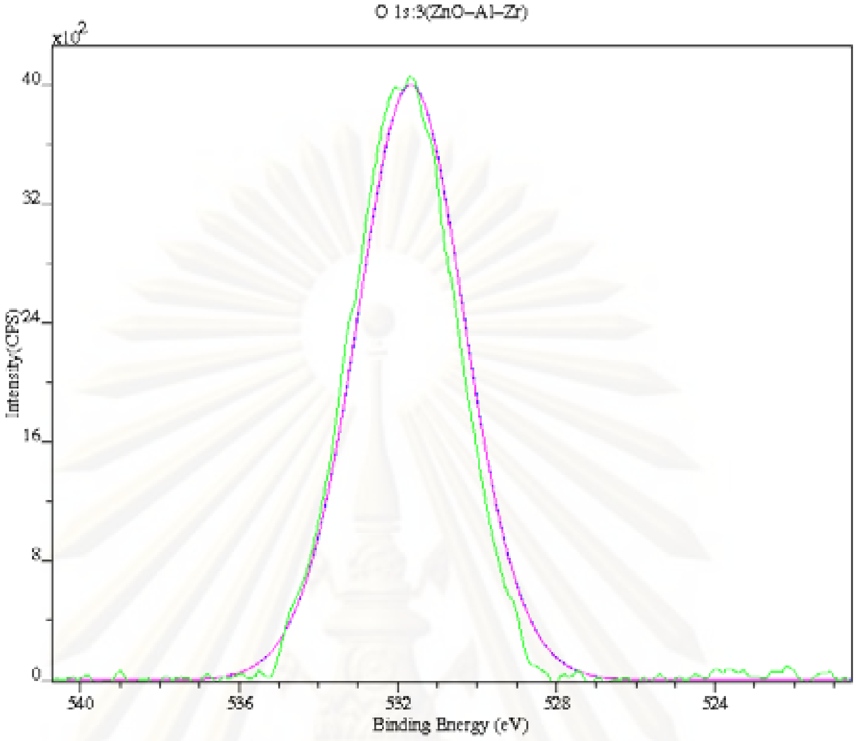

Figure B-5 XPS spectrum of O 1s of ZnO/Al/Zr

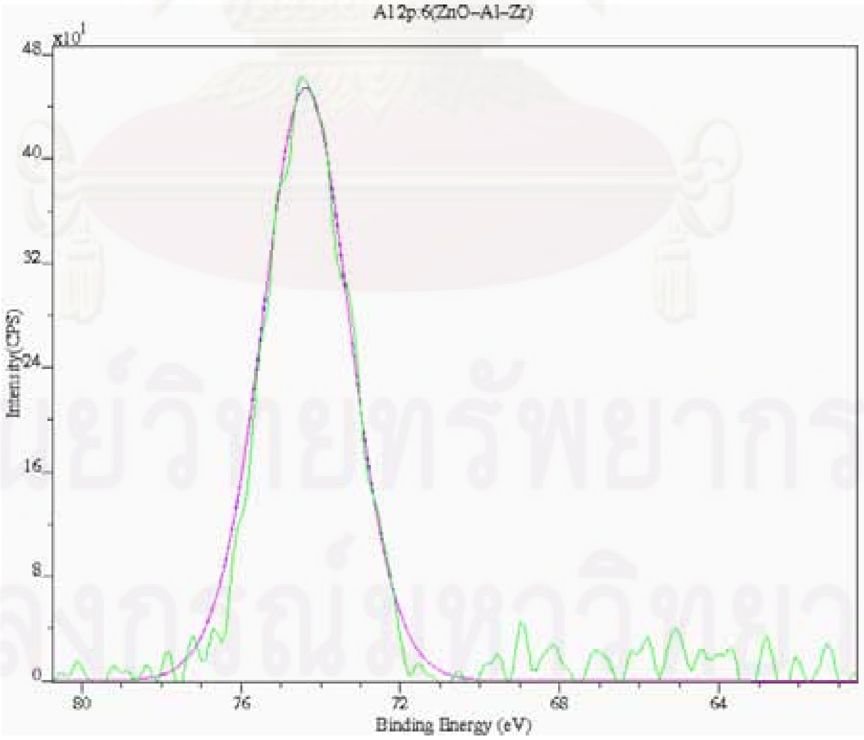

Figure B-6 XPS spectrum of Al 2p of ZnO/Al/Zr

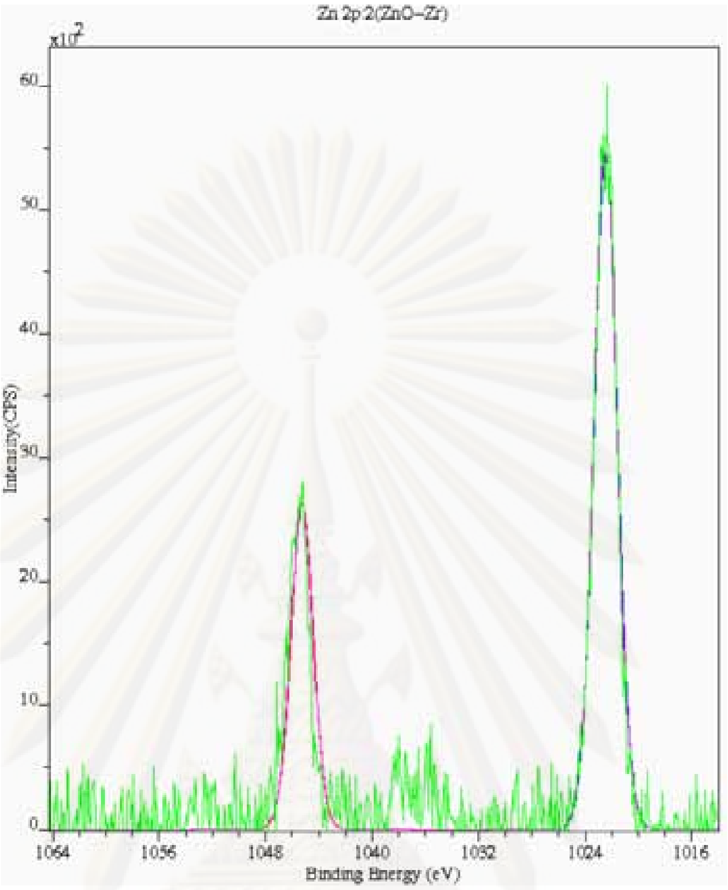

Figure B-7 XPS spectrum of Zn 2p of ZnO/Zr

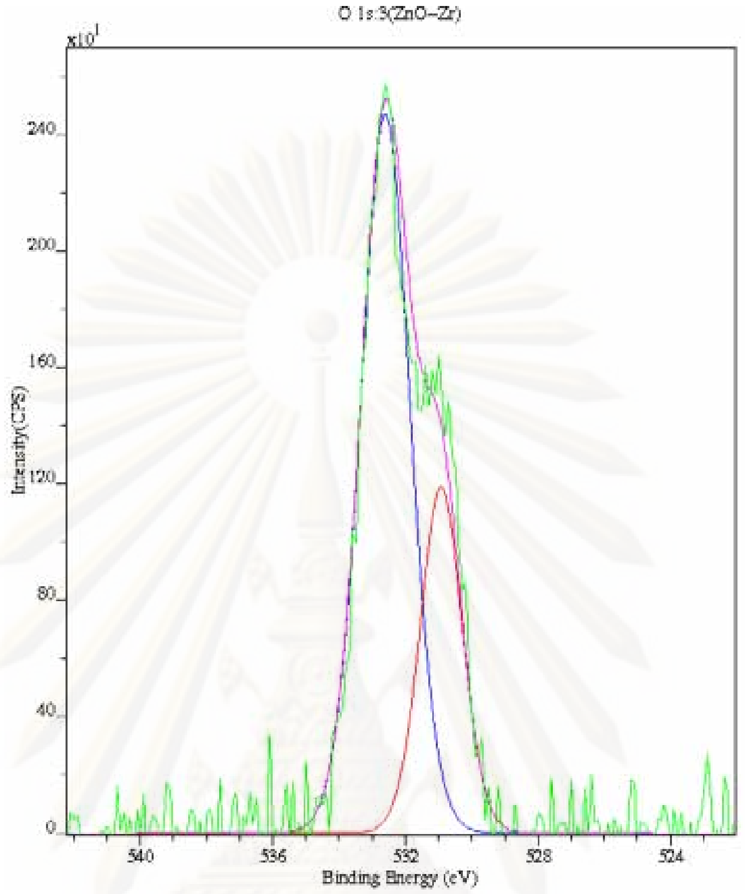

Figure B-8 XPS spectrum of O 1s of ZnO/Zr

APPENDIX C
(SYNTHESIS OF LLDPE/ZnO POLYMER NANOCOMPOSITES VIA HOMOGENEOUS METALLOCENE SYSTEM)

In situ polymerization of ethylene/1-octene with homogeneous metallocene system

Homogeneous metallocene system was developed to synthesize LLDPE/ZnO polymer nanocomposites for comparative study. The polymerization activities obtained with various initial amounts of 1-octene are shown in Table 4.3.

Table C-1 Polymerization activities of LLDPE/ZnO nanocomposites synthesized by homogeneous metallocene system with various 1-octene contents

Initial content of 1-octene (mol)	Time[a] (s)	Polymer yield[b] (g)	Catalytic activity (kg of polymer/ mol Zr.h)
0.009	158	0.7155	10868
0.0135	147	1.6384	26749
0.018	101	1.9503	46343

[a] A period of time used for ethylene comsumption of 0.018 mol

[b] Measured at polymerization temperature of 70 °C; ethylene consumption = 0.018 mol; $[Al]_{TMA}/[Zr]_{zirconocene} = 2500$; in toluene with total volume = 30 ml; and $[Zr]_{zirconocene} = 5\times10^{-5}$ M

APPENDIX D
(PARTICLE SIZE DISTRIBUTION OF ZnO NANOPARTICLES)

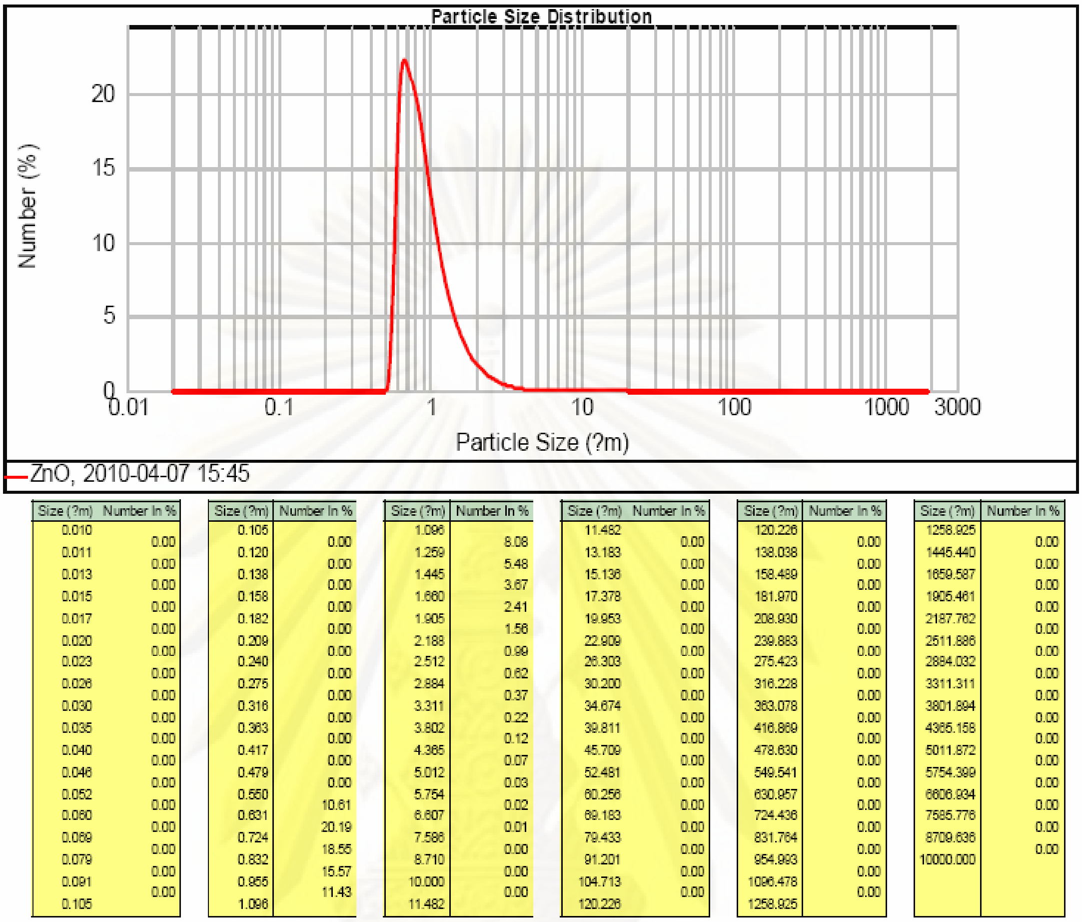

Size (?m)	Number In %	Size (?m)	Number In %	Size (?m)	Number In %	Size (?m)	Number In %	Size (?m)	Number In %	Size (?m)	Number In %
0.010	0.00	0.105	0.00	1.096	8.08	11.482	0.00	120.226	0.00	1258.925	0.00
0.011	0.00	0.120	0.00	1.259	5.48	13.183	0.00	138.038	0.00	1445.440	0.00
0.013	0.00	0.138	0.00	1.445	3.67	15.136	0.00	158.489	0.00	1659.587	0.00
0.015	0.00	0.158	0.00	1.660	2.41	17.378	0.00	181.970	0.00	1905.461	0.00
0.017	0.00	0.182	0.00	1.905	1.56	19.953	0.00	208.930	0.00	2187.762	0.00
0.020	0.00	0.209	0.00	2.188	0.99	22.909	0.00	239.883	0.00	2511.886	0.00
0.023	0.00	0.240	0.00	2.512	0.62	26.303	0.00	275.423	0.00	2884.032	0.00
0.026	0.00	0.275	0.00	2.884	0.37	30.200	0.00	316.228	0.00	3311.311	0.00
0.030	0.00	0.316	0.00	3.311	0.22	34.674	0.00	363.078	0.00	3801.894	0.00
0.035	0.00	0.363	0.00	3.802	0.12	39.811	0.00	416.869	0.00	4365.158	0.00
0.040	0.00	0.417	0.00	4.365	0.07	45.709	0.00	478.630	0.00	5011.872	0.00
0.046	0.00	0.479	0.00	5.012	0.03	52.481	0.00	549.541	0.00	5754.399	0.00
0.052	0.00	0.550	10.61	5.754	0.02	60.256	0.00	630.957	0.00	6606.934	0.00
0.060	0.00	0.631	20.19	6.607	0.01	69.183	0.00	724.436	0.00	7585.776	0.00
0.069	0.00	0.724	18.55	7.586	0.00	79.433	0.00	831.764	0.00	8709.636	0.00
0.079	0.00	0.832	15.57	8.710	0.00	91.201	0.00	954.993	0.00	10000.000	
0.091	0.00	0.955	11.43	10.000	0.00	104.713	0.00	1096.478	0.00		
0.105		1.096		11.482		120.226		1258.925			

Figure D-1 Particle size distribution of ZnO nanoparticles (the 1st measurement)

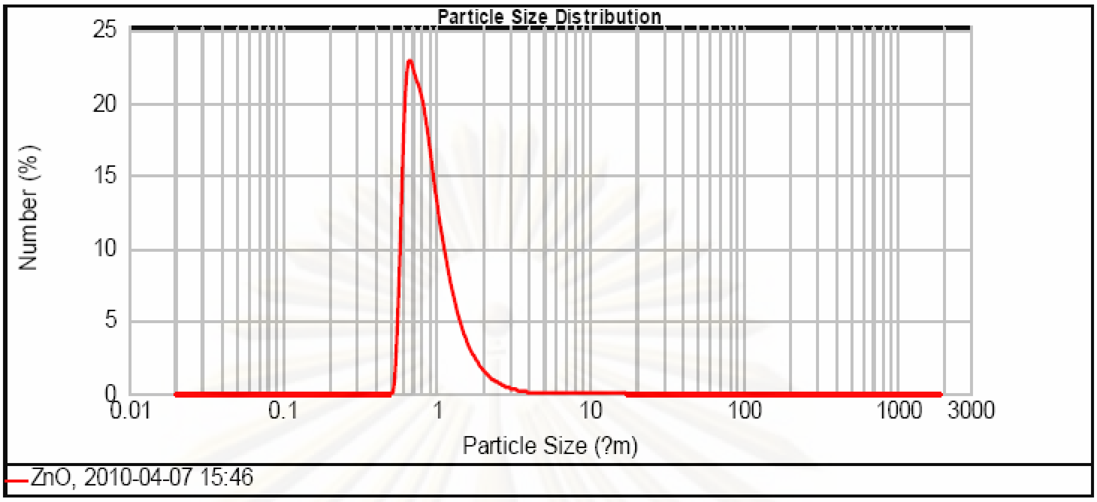

Size (?m)	Number In %	Size (?m)	Number In %	Size (?m)	Number In %	Size (?m)	Number In %	Size (?m)	Number In %	Size (?m)	Number In %
0.010	0.00	0.105	0.00	1.096	7.92	11.482	0.00	120.226	0.00	1258.925	0.00
0.011	0.00	0.120	0.00	1.259	5.26	13.183	0.00	138.038	0.00	1445.440	0.00
0.013	0.00	0.138	0.00	1.445	3.43	15.136	0.00	158.489	0.00	1659.587	0.00
0.015	0.00	0.158	0.00	1.660	2.19	17.378	0.00	181.970	0.00	1905.461	0.00
0.017	0.00	0.182	0.00	1.905	1.38	19.953	0.00	208.930	0.00	2187.762	0.00
0.020	0.00	0.209	0.00	2.188	0.86	22.909	0.00	239.883	0.00	2511.886	0.00
0.023	0.00	0.240	0.00	2.512	0.52	26.303	0.00	275.423	0.00	2884.032	0.00
0.026	0.00	0.275	0.00	2.884	0.31	30.200	0.00	316.228	0.00	3311.311	0.00
0.030	0.00	0.316	0.00	3.311	0.18	34.674	0.00	363.078	0.00	3801.894	0.00
0.035	0.00	0.363	0.00	3.802	0.09	39.811	0.00	416.869	0.00	4365.158	0.00
0.040	0.00	0.417	0.00	4.365	0.05	45.709	0.00	478.630	0.00	5011.872	0.00
0.046	0.00	0.479	0.00	5.012	0.03	52.481	0.00	549.541	0.00	5754.399	0.00
0.052	0.00	0.550	10.93	5.754	0.01	60.256	0.00	630.957	0.00	6606.934	0.00
0.060	0.00	0.631	20.74	6.607	0.01	69.183	0.00	724.436	0.00	7585.776	0.00
0.069	0.00	0.724	18.94	7.586	0.00	79.433	0.00	831.764	0.00	8709.636	0.00
0.079	0.00	0.832	15.74	8.710	0.00	91.201	0.00	954.993	0.00	10000.000	
0.091	0.00	0.955	11.40	10.000	0.00	104.713	0.00	1096.478	0.00		
0.105		1.096		11.482		120.226		1258.925			

Figure D-2 Particle size distribution of ZnO nanoparticles (the 2nd measurement)

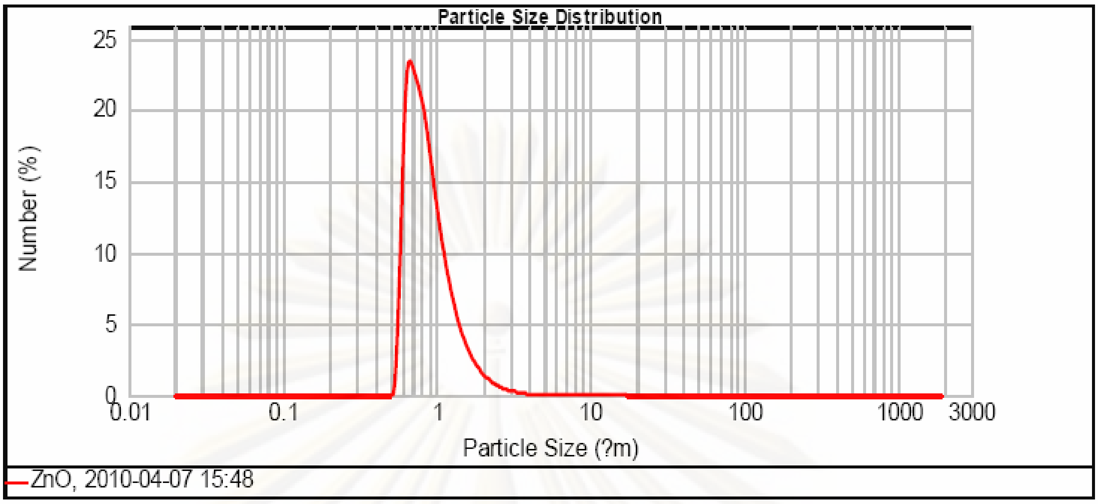

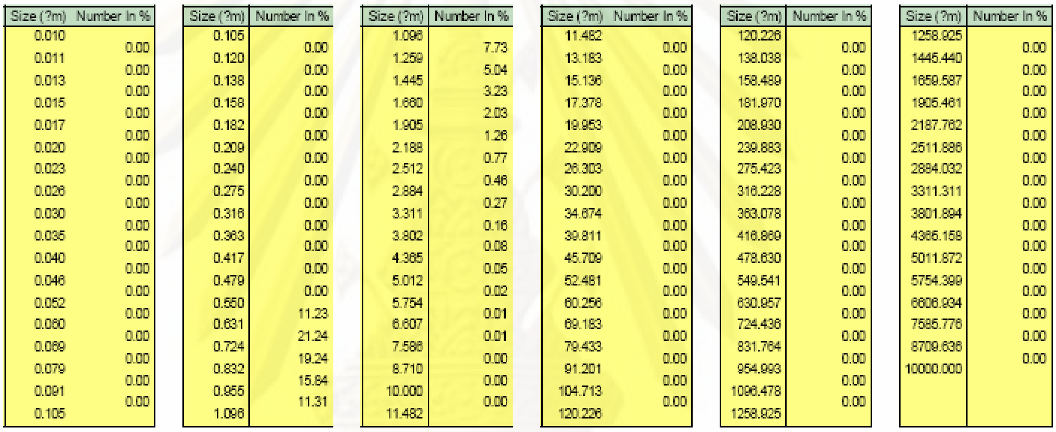

Size (?m)	Number In %	Size (?m)	Number In %	Size (?m)	Number In %	Size (?m)	Number In %	Size (?m)	Number In %	Size (?m)	Number In %
0.010	0.00	0.105	0.00	1.096	7.73	11.482	0.00	120.226	0.00	1258.925	0.00
0.011	0.00	0.120	0.00	1.259	5.04	13.183	0.00	138.038	0.00	1445.440	0.00
0.013	0.00	0.138	0.00	1.445	3.23	15.136	0.00	158.489	0.00	1659.587	0.00
0.015	0.00	0.158	0.00	1.660	2.03	17.378	0.00	181.970	0.00	1905.461	0.00
0.017	0.00	0.182	0.00	1.905	1.26	19.953	0.00	208.930	0.00	2187.762	0.00
0.020	0.00	0.209	0.00	2.188	0.77	22.909	0.00	239.883	0.00	2511.886	0.00
0.023	0.00	0.240	0.00	2.512	0.46	26.303	0.00	275.423	0.00	2884.032	0.00
0.026	0.00	0.275	0.00	2.884	0.27	30.200	0.00	316.228	0.00	3311.311	0.00
0.030	0.00	0.316	0.00	3.311	0.16	34.674	0.00	363.078	0.00	3801.894	0.00
0.035	0.00	0.363	0.00	3.802	0.08	39.811	0.00	416.869	0.00	4365.158	0.00
0.040	0.00	0.417	0.00	4.365	0.05	45.709	0.00	478.630	0.00	5011.872	0.00
0.046	0.00	0.479	0.00	5.012	0.02	52.481	0.00	549.541	0.00	5754.399	0.00
0.052	0.00	0.550	11.23	5.754	0.01	60.256	0.00	630.957	0.00	6606.934	0.00
0.060	0.00	0.631	21.24	6.607	0.01	69.183	0.00	724.436	0.00	7585.776	0.00
0.069	0.00	0.724	19.24	7.586	0.00	79.433	0.00	831.764	0.00	8709.636	0.00
0.079	0.00	0.832	15.84	8.710	0.00	91.201	0.00	954.993	0.00	10000.000	
0.091	0.00	0.955	11.31	10.000	0.00	104.713	0.00	1096.478	0.00		
0.105		1.096		11.482		120.226		1258.925			

Figure D-3 Particle size distribution of ZnO nanoparticles (the 3rd measurement)

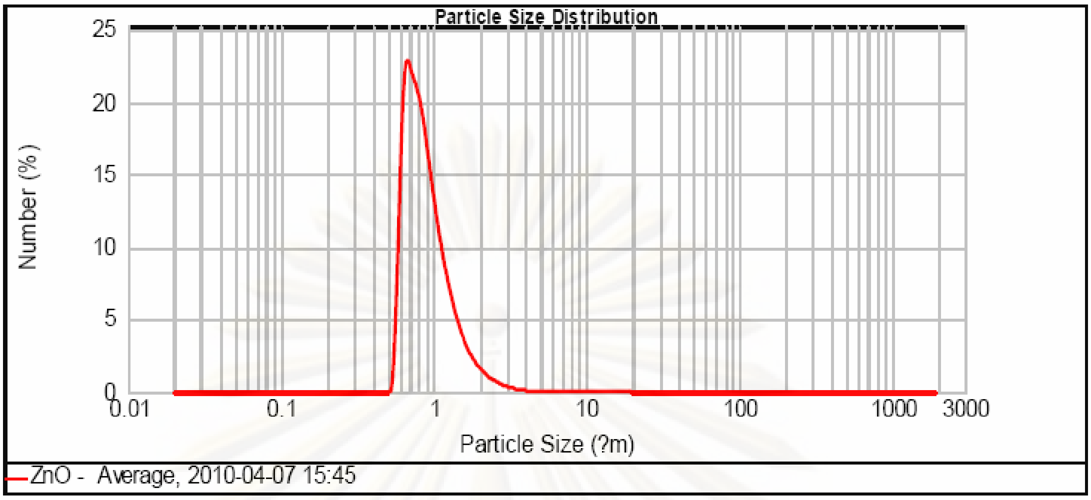

Size (?m)	Number In %	Size (?m)	Number In %	Size (?m)	Number In %	Size (?m)	Number In %	Size (?m)	Number In %	Size (?m)	Number In %
0.010	0.00	0.105	0.00	1.096	7.90	11.482	0.00	120.226	0.00	1258.925	0.00
0.011	0.00	0.120	0.00	1.259	5.25	13.183	0.00	138.038	0.00	1445.440	0.00
0.013	0.00	0.138	0.00	1.445	3.43	15.136	0.00	158.489	0.00	1659.587	0.00
0.015	0.00	0.158	0.00	1.660	2.20	17.378	0.00	181.970	0.00	1905.461	0.00
0.017	0.00	0.182	0.00	1.905	1.39	19.953	0.00	208.930	0.00	2187.762	0.00
0.020	0.00	0.209	0.00	2.188	0.87	22.909	0.00	239.883	0.00	2511.886	0.00
0.023	0.00	0.240	0.00	2.512	0.53	26.303	0.00	275.423	0.00	2884.032	0.00
0.026	0.00	0.275	0.00	2.884	0.31	30.200	0.00	316.228	0.00	3311.311	0.00
0.030	0.00	0.316	0.00	3.311	0.18	34.674	0.00	363.078	0.00	3801.894	0.00
0.035	0.00	0.363	0.00	3.802	0.10	39.811	0.00	416.869	0.00	4365.158	0.00
0.040	0.00	0.417	0.00	4.365	0.06	45.709	0.00	478.630	0.00	5011.872	0.00
0.046	0.00	0.479	0.00	5.012	0.03	52.481	0.00	549.541	0.00	5754.399	0.00
0.052	0.00	0.550	10.94	5.754	0.01	60.256	0.00	630.957	0.00	6606.934	0.00
0.060	0.00	0.631	20.76	6.607	0.01	69.183	0.00	724.436	0.00	7585.776	0.00
0.069	0.00	0.724	18.93	7.586	0.00	79.433	0.00	831.764	0.00	8709.636	0.00
0.079	0.00	0.832	15.72	8.710	0.00	91.201	0.00	954.993	0.00	10000.000	
0.091	0.00	0.955	11.38	10.000	0.00	104.713	0.00	1096.478	0.00		
0.105		1.096		11.482		120.226		1258.925			

Figure D-4 Particle size distribution of ZnO nanoparticles (the average values)

APPENDIX E

(CALCULATION OF POLYMER PROPERTIES)

E-1 Calculation of polymer microstructure

Polymer microstructure and triad distribution of monomer can be calculated according to Randall (1989). The detail of calculation for ethylene/1-octene copolymer is shown as follows.

The integral area of ^{13}C NMR spectrum in the specified range is listed.

T_A = 39.5 - 42 ppm
T_B = 38.1 ppm
T_C = 36.4 ppm
T_D = 33 - 36 ppm
T_E = 32.2 ppm
T_F = 28.5 - 31 ppm
T_G = 25.5 - 27.5 ppm
T_H = 24 - 25 ppm
T_I = 22 - 23 ppm
T_J = 14 – 15 ppm

Triad distribution was calculated as the followed formula.

$k[OOO] = T_A - 0.5T_C$
$k[EOO] = T_C$
$k[EOE] = T_B$
$k[EEE] = 0.5T_F - 0.25T_E - 0.25T_G$
$k[OEO] = T_H$
$k[OEE] = T_G - T_E$

All copolymer was calculated for the relative comonomer reactivity (r_E for ethylene and r_C for the comonomer) and monomer insertion by using the general formula below.

$$r_E = 2[EE]/([EC]X) \qquad r_C = 2[CC]X/[EC]$$

where r_E = ethylene reactivity ratio

r_C = comonomer (α -olefin) reactivity ratio

$[EE]$ = $[EEE] + 0.5[CEE]$

$[EC]$ = $[CEC] + 0.5[CEE] + [ECE] + 0.5[ECC]$

$[CC]$ = $[CCC] + 0.5[ECC]$

X = [E]/[C] in the feed = concentration of ethylene (mol/L) / concentration of comonomer (mol/L) in the feed.

%E = $[EEE] + [EEC] + [CEC]$

%C = $[CCC] + [CCE] + [ECE]$

E-2 Calculation of crystallinity of copolymer

The crystallinities of copolymers were determined by differential scanning calorimeter (DSC). The %crystallinity of copolymers is calculated from the following equation.

$$\chi(\%) = \frac{\Delta Hm}{\Delta H_{mo}} \times 100$$

Where $\chi(\%)$ = %crystallinity

ΔHm = Heat of fusion of sample (J/g)

ΔHm_0 = Heat of fusion of perfectly crystalline polyethylene (286 J/g)

APPENDIX F

(ENERGY DISPERSIVE X-RAY SPECTROSCOPY)

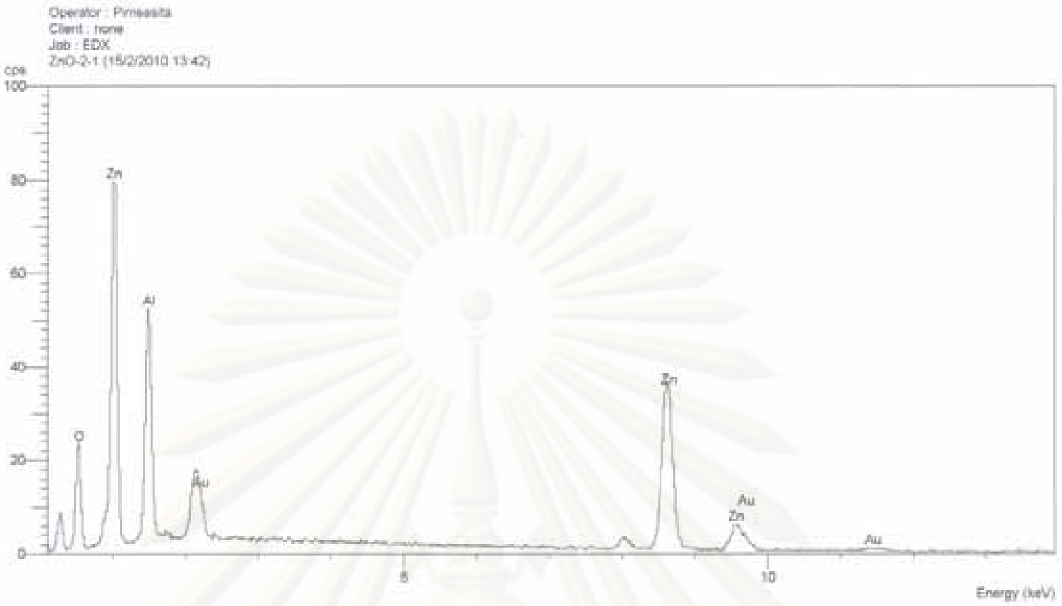

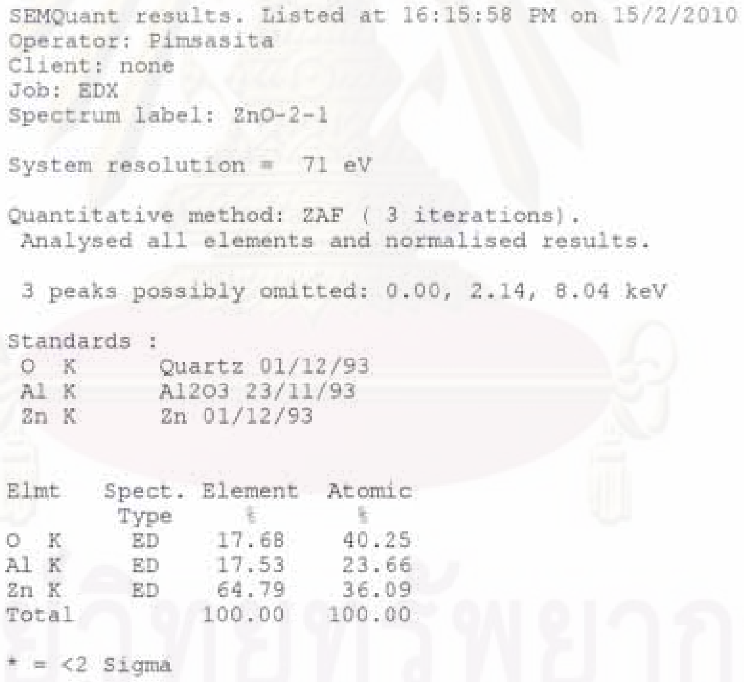

```
SEMQuant results. Listed at 16:15:58 PM on 15/2/2010
Operator: Pimsasita
Client: none
Job: EDX
Spectrum label: ZnO-2-1

System resolution =  71 eV

Quantitative method: ZAF ( 3 iterations).
 Analysed all elements and normalised results.

 3 peaks possibly omitted: 0.00, 2.14, 8.04 keV

Standards :
 O  K      Quartz 01/12/93
 Al K      Al2O3 23/11/93
 Zn K      Zn 01/12/93


Elmt   Spect. Element  Atomic
        Type     %        %
O  K     ED    17.68    40.25
Al K     ED    17.53    23.66
Zn K     ED    64.79    36.09
Total         100.00   100.00

* = <2 Sigma
```

Figure F-1 EDX analysis of ZnO/Al (the 1st measurement)

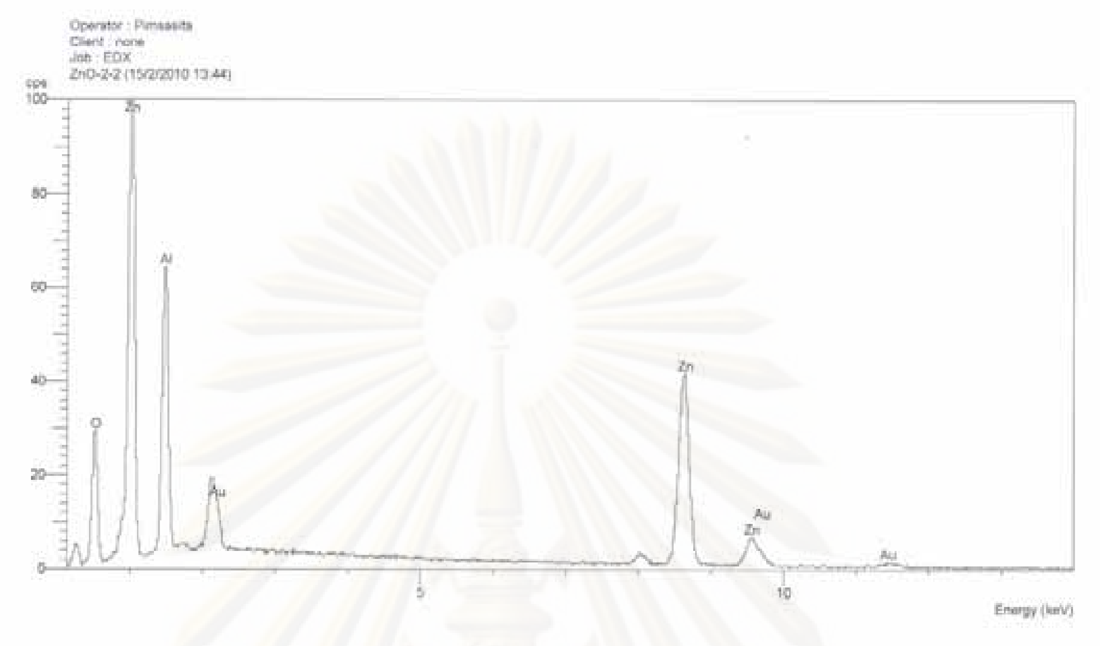

```
SEMQuant results. Listed at 16:16:31 PM on 15/2/2010
Operator: Pimsasita
Client: none
Job: EDX
Spectrum label: ZnO-2-2

System resolution =  71 eV

Quantitative method: ZAF ( 4 iterations).
 Analysed all elements and normalised results.

 4 peaks possibly omitted: 0.00, 2.14, 8.04,
 11.46 keV

Standards :
 O  K      Quartz 01/12/93
 Al K      Al2O3 23/11/93
 Zn K      Zn 01/12/93

Elmt   Spect. Element  Atomic
        Type     %        %
O  K     ED     19.24    42.32
Al K     ED     18.54    24.18
Zn K     ED     62.23    33.50
Total          100.00   100.00

* = <2 Sigma
```

Figure F-2 EDX analysis of ZnO/Al (the 2nd measurement)

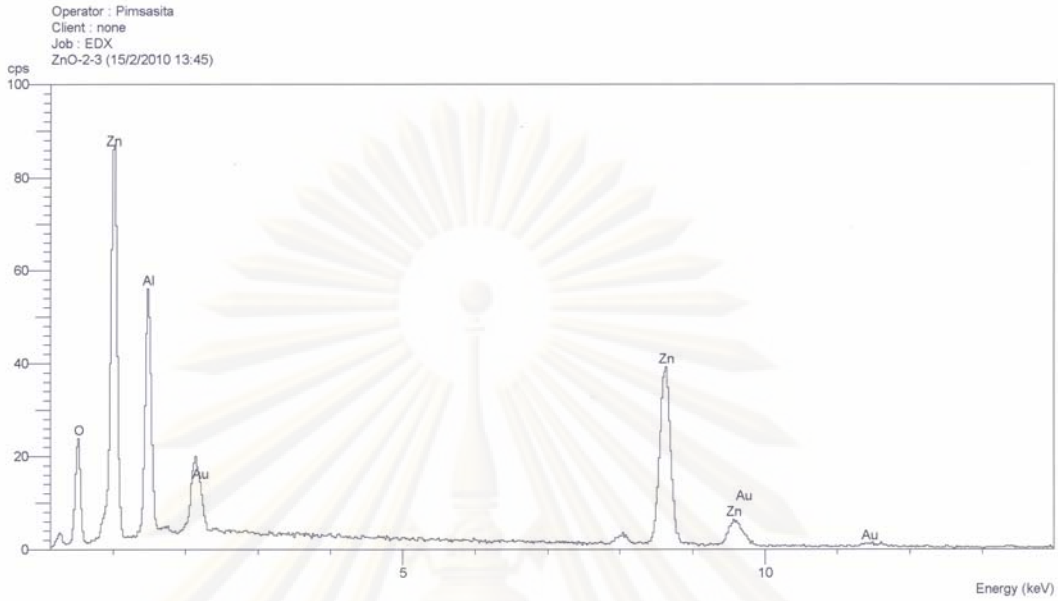

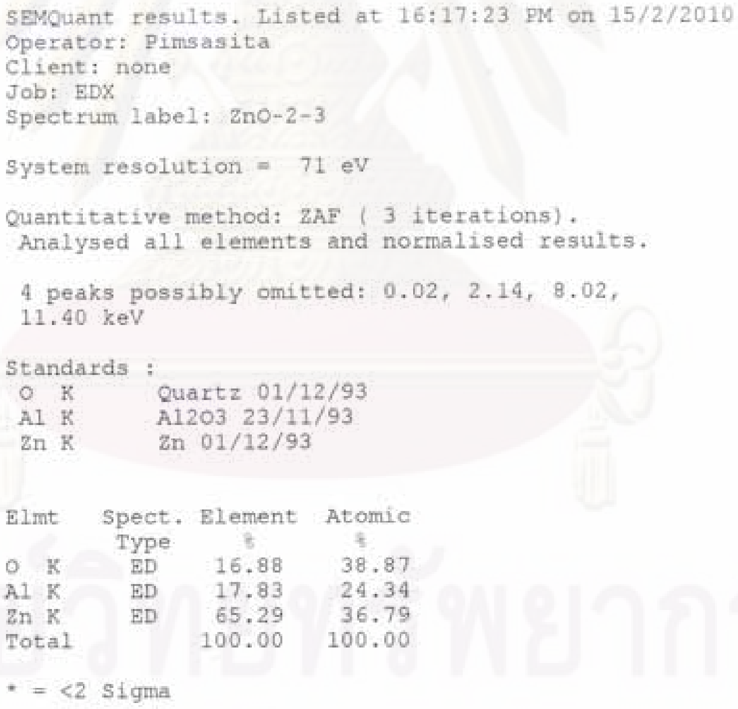

```
SEMQuant results. Listed at 16:17:23 PM on 15/2/2010
Operator: Pimsasita
Client: none
Job: EDX
Spectrum label: ZnO-2-3

System resolution =  71 eV

Quantitative method: ZAF ( 3 iterations).
 Analysed all elements and normalised results.

 4 peaks possibly omitted: 0.02, 2.14, 8.02,
 11.40 keV

Standards :
 O  K      Quartz 01/12/93
 Al K      Al2O3 23/11/93
 Zn K      Zn 01/12/93


Elmt   Spect. Element  Atomic
        Type     %       %
O  K     ED    16.88    38.87
Al K     ED    17.83    24.34
Zn K     ED    65.29    36.79
Total         100.00   100.00

* = <2 Sigma
```

Figure F-3 EDX analysis of ZnO/Al (the 3rd measurement)

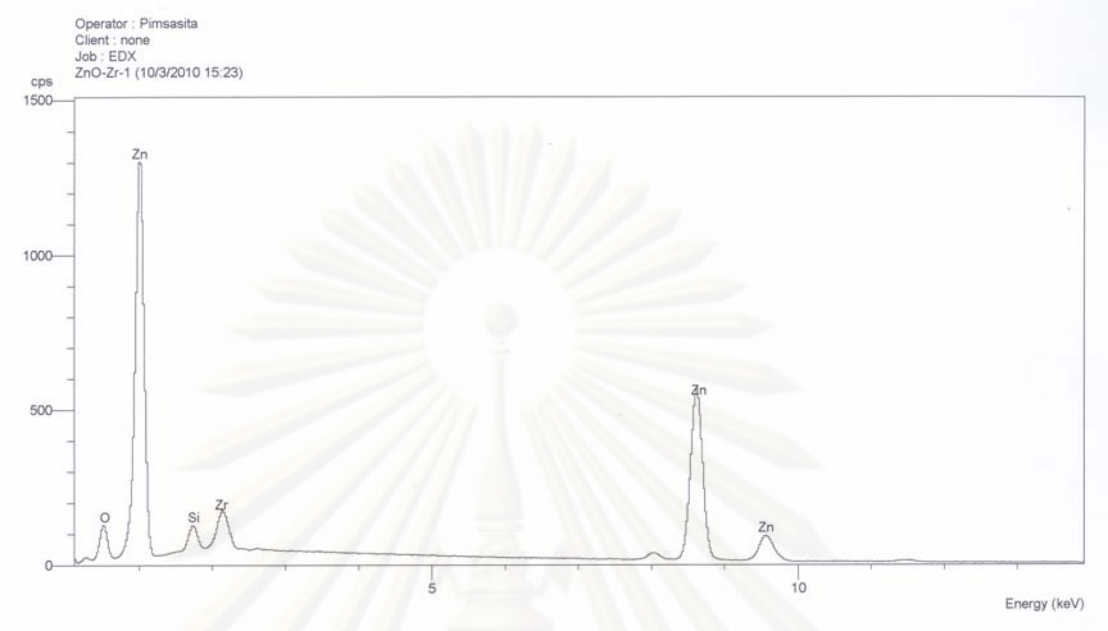

Operator : Pimsasita
Client : none
Job : EDX
ZnO-Zr-1 (10/3/2010 15:23)

```
SEMQuant results. Listed at 12:58:04 PM on 11/3/2010
Operator: Pimsasita
Client: none
Job: EDX
Spectrum label: ZnO-Zr-1

System resolution =  112 eV

Quantitative method: ZAF ( 4 iterations).
 Analysed all elements and normalised results.

 3 peaks possibly omitted: 0.00, 8.02, 11.46 keV

Standards :
 O  K      Quartz 01/12/93
 Si K      Quartz 01/12/93
 Zn K      Zn 01/12/93
 Zr L      Zr 01/12/93


Elmt    Spect. Element  Atomic
         Type     %        %
O  K      ED     10.00    30.48
Si K      ED      2.90     5.03
Zn K      ED     84.86    63.30
Zr L      ED      2.24     1.20
Total           100.00   100.00

* = <2 Sigma
```

Figure F-4 EDX analysis of ZnO/Zr (the 1st measurement)

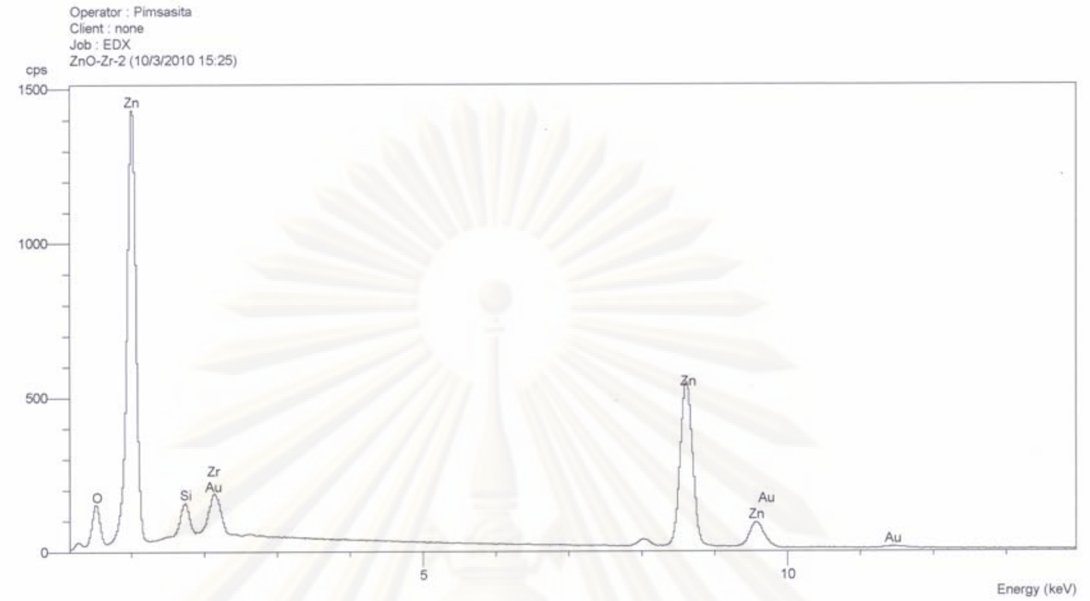

```
SEMQuant results. Listed at 12:58:34 PM on 11/3/2010
Operator: Pimsasita
Client: none
Job: EDX
Spectrum label: ZnO-Zr-2

System resolution =  112 eV

Quantitative method: ZAF ( 4 iterations).
 Analysed all elements and normalised results.

 3 peaks possibly omitted: 0.00, 8.02, 11.46 keV

Standards :
 O  K      Quartz 01/12/93
 Si K      Quartz 01/12/93
 Zn K      Zn 01/12/93
 Zr L      Zr 01/12/93


Elmt   Spect. Element  Atomic
        Type     %        %
O  K     ED    11.72    34.13
Si K     ED     3.61     5.99
Zn K     ED    82.35    58.70
Zr L     ED     2.32     1.19
Total         100.00   100.00

* = <2 Sigma
```

Figure F-5 EDX analysis of ZnO/Zr (the 2nd measurement)

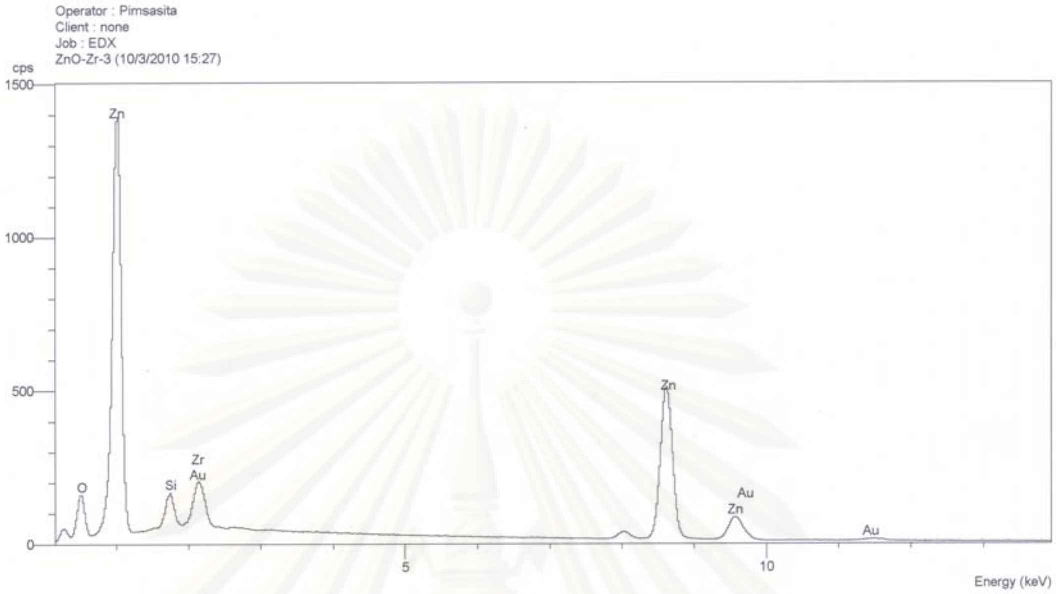

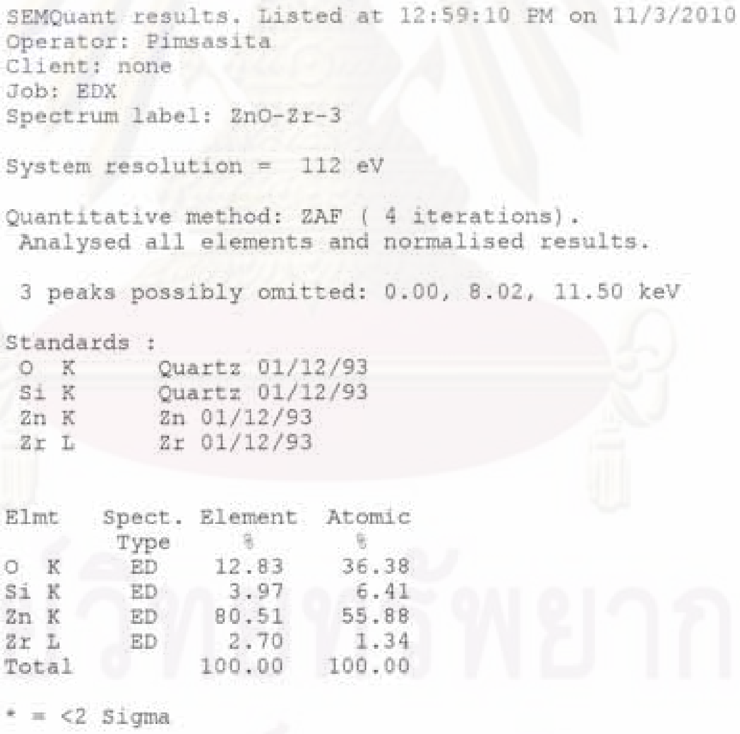

```
SEMQuant results. Listed at 12:59:10 PM on 11/3/2010
Operator: Pimsasita
Client: none
Job: EDX
Spectrum label: ZnO-Zr-3

System resolution =  112 eV

Quantitative method: ZAF ( 4 iterations).
 Analysed all elements and normalised results.

 3 peaks possibly omitted: 0.00, 8.02, 11.50 keV

Standards :
 O  K      Quartz 01/12/93
 Si K      Quartz 01/12/93
 Zn K      Zn 01/12/93
 Zr L      Zr 01/12/93


Elmt   Spect. Element  Atomic
        Type     %        %
O  K     ED    12.83    36.38
Si K     ED     3.97     6.41
Zn K     ED    80.51    55.88
Zr L     ED     2.70     1.34
Total         100.00   100.00

* = <2 Sigma
```

Figure F-6 EDX analysis of ZnO/Zr (the 3rd measurement)

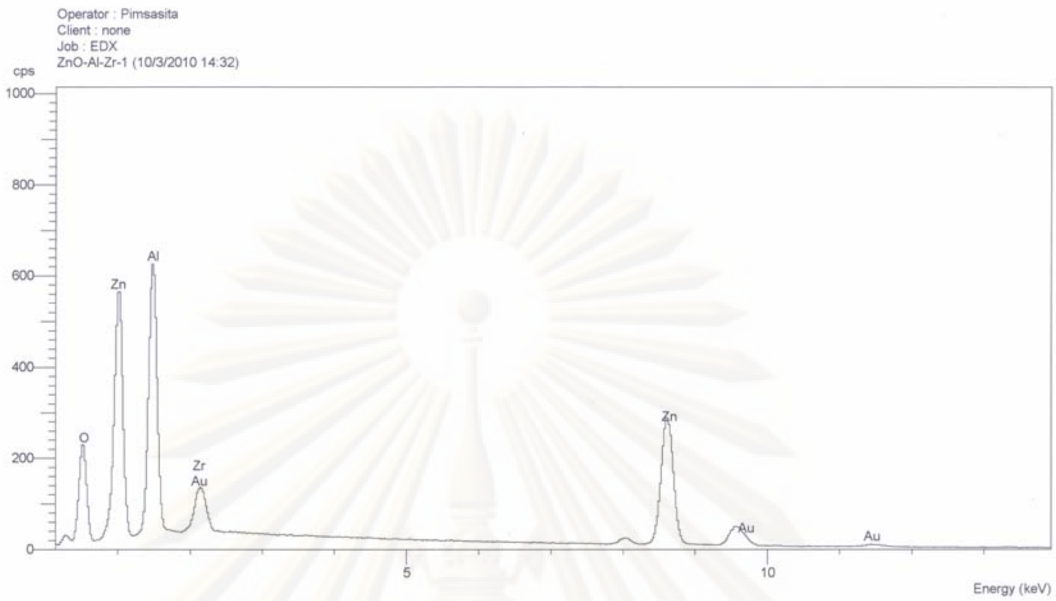

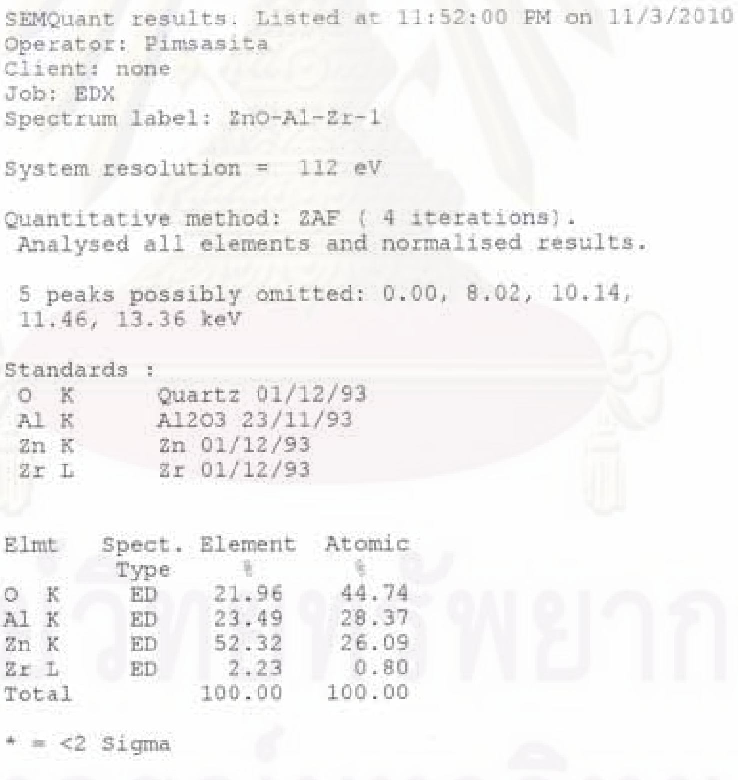

```
SEMQuant results. Listed at 11:52:00 PM on 11/3/2010
Operator: Pimsasita
Client: none
Job: EDX
Spectrum label: ZnO-Al-Zr-1

System resolution =  112 eV

Quantitative method: ZAF ( 4 iterations).
 Analysed all elements and normalised results.

 5 peaks possibly omitted: 0.00, 8.02, 10.14,
 11.46, 13.36 keV

Standards :
 O  K      Quartz 01/12/93
 Al K      Al2O3 23/11/93
 Zn K      Zn 01/12/93
 Zr L      Zr 01/12/93

Elmt   Spect. Element  Atomic
        Type     %        %
O  K     ED     21.96    44.74
Al K     ED     23.49    28.37
Zn K     ED     52.32    26.09
Zr L     ED      2.23     0.80
Total          100.00   100.00

* = <2 Sigma
```

Figure F-7 EDX analysis of ZnO/Al/Zr (the 1st measurement)

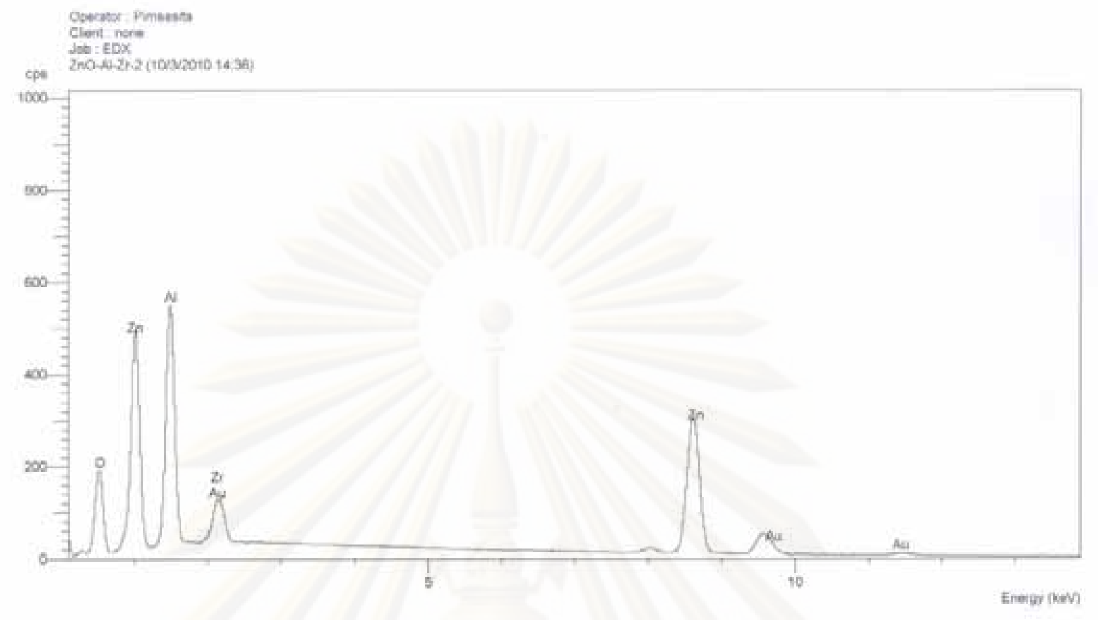

```
SEMQuant results. Listed at 11:52:37 PM on 11/3/2010
Operator: Pimsasita
Client: none
Job: EDX
Spectrum label: ZnO-Al-Zr-2

System resolution =  112 eV

Quantitative method: ZAF ( 4 iterations).
 Analysed all elements and normalised results.

 3 peaks possibly omitted: 0.00, 8.02, 11.46 keV

Standards :
 O  K      Quartz 01/12/93
 Al K      Al2O3 23/11/93
 Zn K      Zn 01/12/93
 Zr L      Zr 01/12/93


Elmt   Spect. Element  Atomic
        Type     %        %
O  K     ED    19.10    41.15
Al K     ED    21.99    28.09
Zn K     ED    56.84    29.97
Zr L     ED     2.08     0.78
Total         100.00   100.00

* = <2 Sigma
```

Figure F-8 EDX analysis of ZnO/Al/Zr (the 2nd measurement)

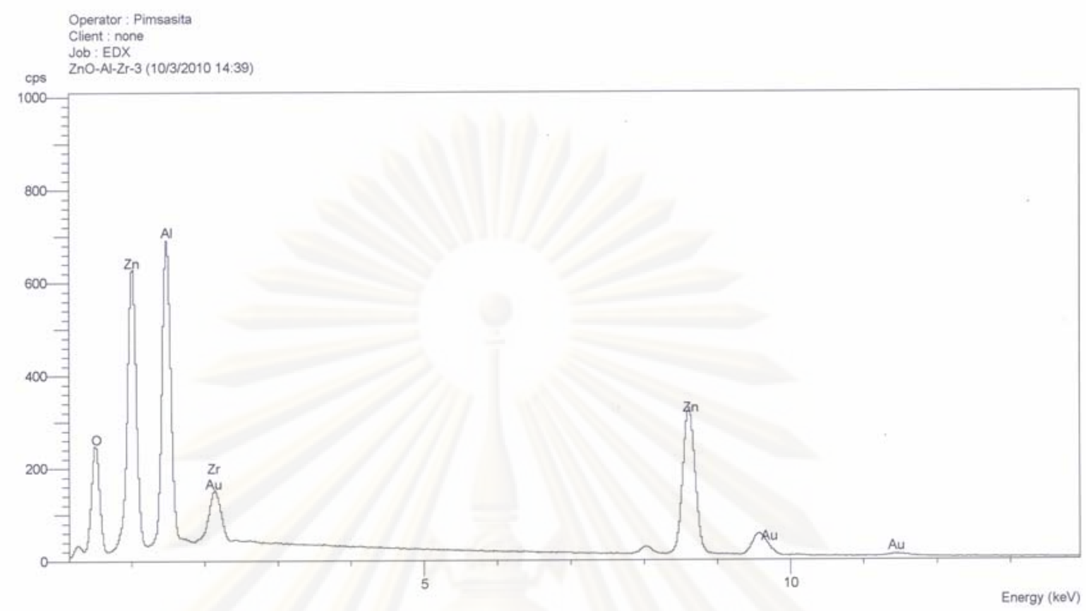

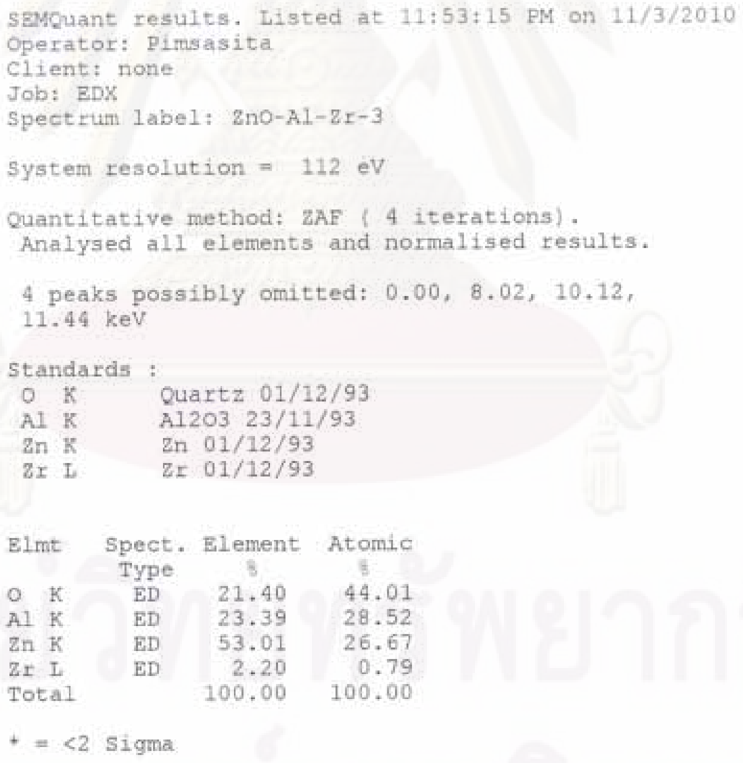

```
SEMQuant results. Listed at 11:53:15 PM on 11/3/2010
Operator: Pimsasita
Client: none
Job: EDX
Spectrum label: ZnO-Al-Zr-3

System resolution =  112 eV

Quantitative method: ZAF ( 4 iterations).
 Analysed all elements and normalised results.

 4 peaks possibly omitted: 0.00, 8.02, 10.12,
 11.44 keV

Standards :
 O  K      Quartz 01/12/93
 Al K      Al2O3 23/11/93
 Zn K      Zn 01/12/93
 Zr L      Zr 01/12/93


Elmt    Spect. Element  Atomic
         Type     %        %
O  K      ED     21.40    44.01
Al K      ED     23.39    28.52
Zn K      ED     53.01    26.67
Zr L      ED      2.20     0.79
Total           100.00   100.00

* = <2 Sigma
```

Figure F-9 EDX analysis of ZnO/Al/Zr (the 3rd measurement)

APPENDIX G

(DIFFERENTIAL SCANNING CALORIMETRY)

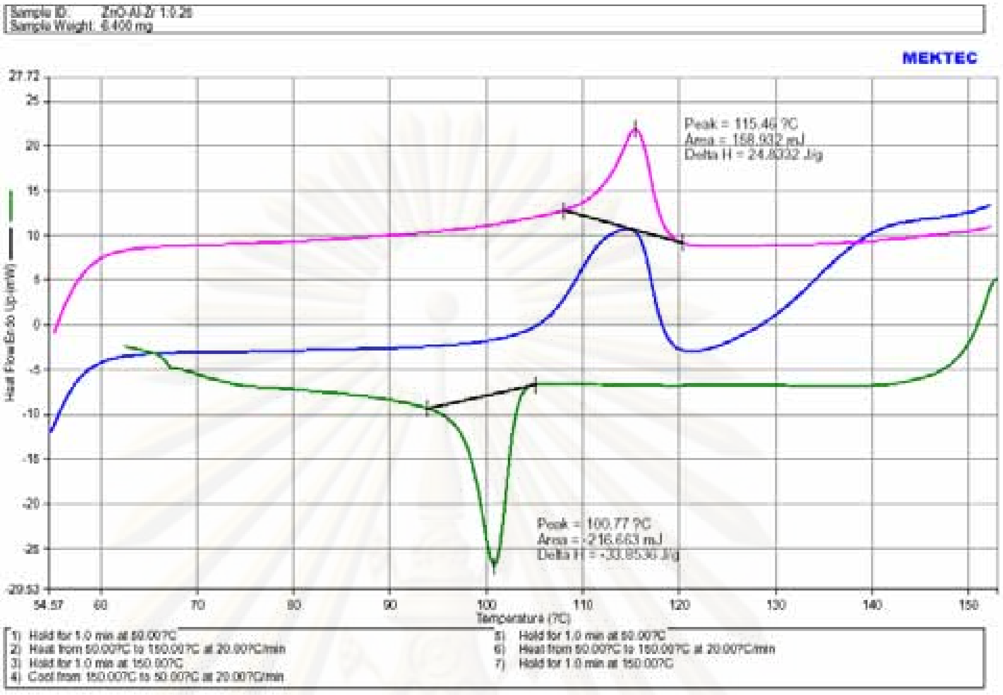

Figure G-1 DSC analysis of LLDPE/ZnO nanocomposites synthesized using ZnO/Al/Zr with 1-octene content of 0.0045 mol

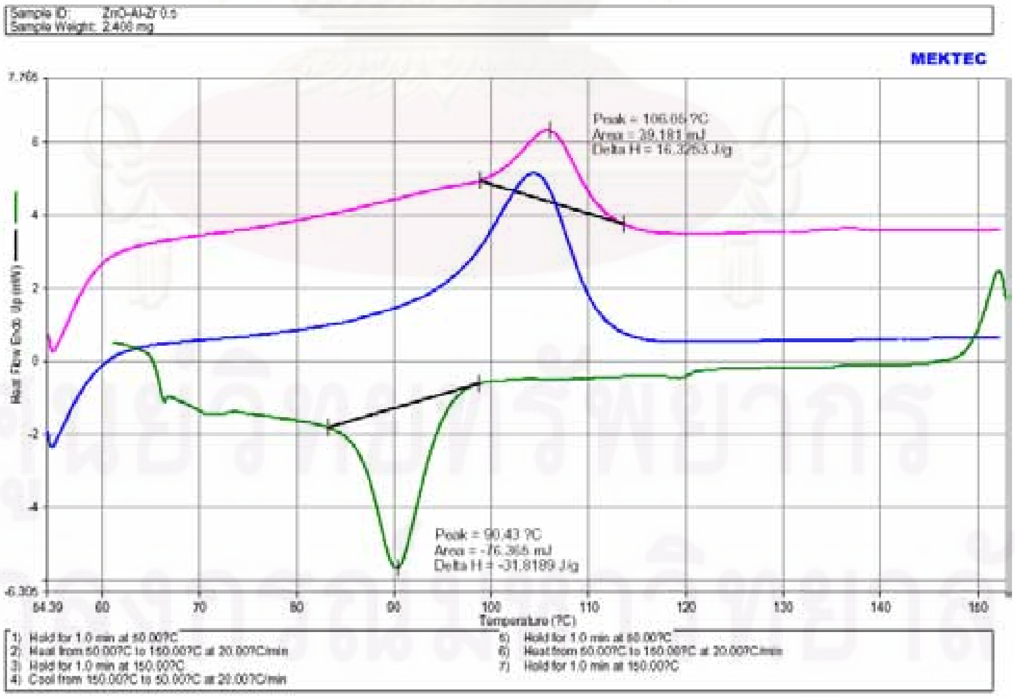

Figure G-2 DSC analysis of LLDPE/ZnO nanocomposites synthesized using ZnO/Al/Zr with 1-octene content of 0.009 mol

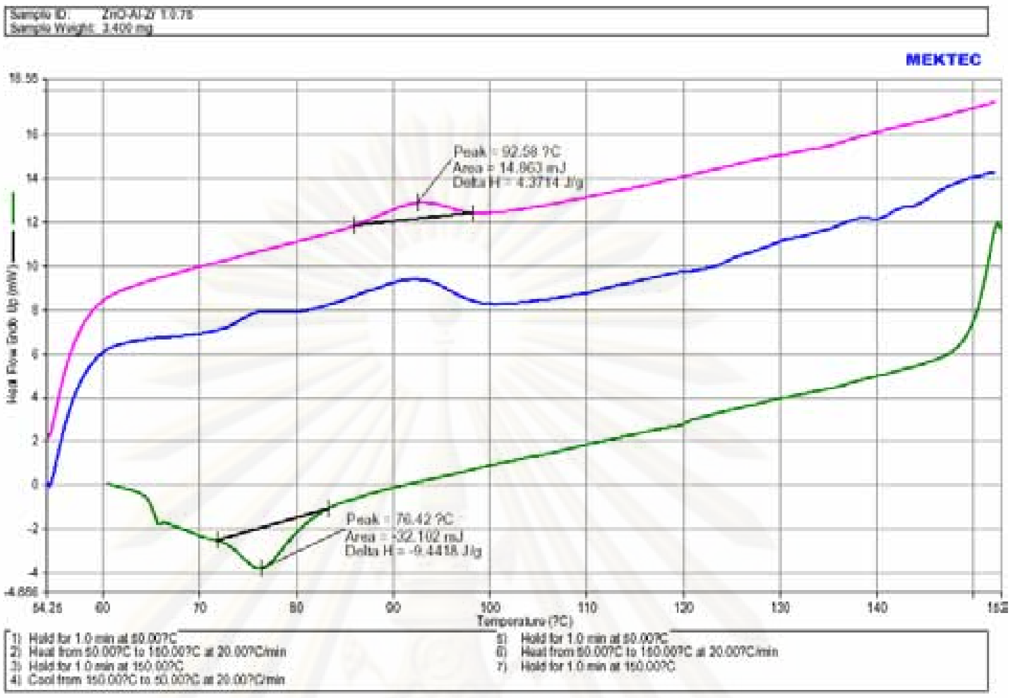

Figure G-3 DSC analysis of LLDPE/ZnO nanocomposites synthesized using ZnO/Al/Zr with 1-octene content of 0.0135 mol

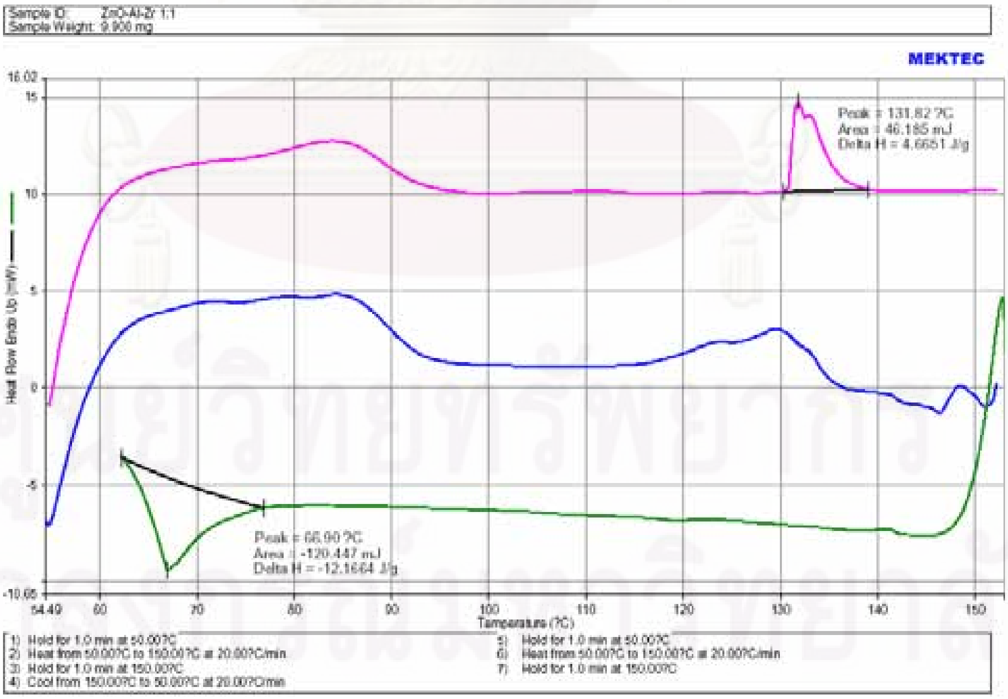

Figure G-4 DSC analysis of LLDPE/ZnO nanocomposites synthesized using ZnO/Al/Zr with 1-octene content of 0.018 mol

APPENDIX H
(LIST OF PUBLICATION)

Ngowthanawat, A.; Jongsomjit, B. “Synthesis of LLDPE/ZnO nanocomposites via in situ polymerization of ethylene/1-octene with zirconocene/MAO catalyst” (The Proceeding of 19th Thailand Chemical Engineering and Applied Chemistry Conference, TIChE 2009, Kanchanaburi)

VITA

Mr.Apiwat Ngowthanawat was born on February 23rd, 1984 in Nakhon Pathom, Thailand. He finished high school level from Suankularb Wittayalia School, Bangkok. He received the Bachelor’s Degree of Chemical Engineering from the Department of Chemical Engineering, Faculty of Engineering, Chulalongkorn University in March 2006. He continued graduate study at Chulalongkorn University in June, 2008.